Evaluation of Geologic Dust Entrainment, Removal, and Transport Mechanisms

Final Report
Contract No. 99-717

California Air Resources Board
Planning and Technical Support Division
1001 I Street
Sacramento, CA 95814

Prepared by:

Dennis R. Fitz
Center for Environmental Research and Technology
College of Engineering
University of California
Riverside, CA 92521
(909) 781-5781
(909) 781-5790 fax

And

C. Russell Philbrick
Department of Electrical Engineering
Pennsylvania State University
University Park, PA 16802
(814) 865-2975

November 2004

Disclaimer

The statements and conclusions in this report are those of the contractor and not necessarily those of the California Air Resources Board. The mention of commercial products, their source or test use in connection with the materials reported herein is not to be construed as either an actual or implied endorsement of such products.

Acknowledgments

This report was submitted in fulfillment of ARB Contract, "Evaluation of Geologic Dust Entrainment, Removal, and Transport Mechanisms" with project oversight by Patrick Gaffney.

The lidar measurements were performed by a research team from Penn State University led by Guangkun (Homer) Li, who served as Project Engineer for the lidar and optical measurements, and was assisted by Gregg O'Marr and Praveen Atreya. The analysis of the lidar data and the optical imaging data, as well as all of the modeling simulations and analyses of the field measurements were carried out by Guangkun Li as part of his research for completion of the Ph.D. degree in Electrical Engineering at Penn State University. Professor C. Russell Philbrick served as the Principle Investigator for the Penn State University effort. Several CE-CERT staff members also contributed this study, including David Pankratz, Kurt Bumiller, Tony Taliaferro, and Charles Bufalino.

Table of Contents

Disclaimer ii

Acknowledgments iii

List of Figures vi

List of Tables viii

Abstract ix

Executive Summary x

Glossary xii

1. Introduction and Objectives 1
- 1.1 Background 1
- 1.2 Objectives 1

2. Approach 2
- 2.1 Literature Search 2
- 2.2 Pilot Study 3
  - 2.2.1 Test Location 4
  - 2.2.2 Measurement Methods 10
    - 2.2.2.1 Meteorological Measurements 10
    - 2.2.2.2 Dust Generation 10
    - 2.2.2.3 Lidar Measurements 11
    - 2.2.2.4 Real-Time Particulate Matter Measurements 12
    - 2.2.2.5 Integrated (Filter) Particulate Matter Measurements 12
    - 2.2.2.6 Sulfur Hexafluoride Tracer Release System 12
    - 2.2.2.7 Sulfur Hexafluoride Tracer Measurement System 12
    - 2.2.2.8 Laboratory Analyses of Filer Samples 12
    - 2.2.2.9 High Resolution Photography 13
    - 2.2.2.10 Silt and Soil Moisture Measurements 13
- 2.3 Main Study 14
  - 2.3.1 Test Location 14
    - 2.3.1.1 Site Layout 14
    - 2.3.1.2 Soils Tested 15
  - 2.3.2 Measurement Methods 16
    - 2.3.2.1 Meteorological Measurements 16
    - 2.3.2.2 Dust Generation 17
    - 2.3.2.3 Lidar Measurements 17
    - 2.3.2.4 Real-Time Particulate Measurements 17
    - 2.3.2.5 Integrated Filter Sampler 17
    - 2.3.2.6 Laboratory Analysis Filter Samples 17
    - 2.3.2.7 High Resolution Photography 17
    - 2.3.2.8 Silt and Soil Measurements 17
    - 2.3.2.9 Outdoor Field Calibration Chamber 17

3.0 Results **21**
3.1 Literature Search **21**
3.1.1 Search Results **21**
3.1.2 Journal Articles **23**
3.1.3 Industrial References (Designated C1 – C5) **25**
3.1.4 Discussion **26**
3.2 Pilot Study Results **28**
3.2.1 Study Period **28**
3.2.2 Dust Generation Tests **28**
3.2.3 Hourly Meteorological Data **32**
3.2.4 10-Second Meteorological, Particulate Matter, Tracer Data **34**
3.2.5 Soil Sample Analysis **34**
3.2.6 Collocated DustTrak Quality Control Procedures **35**
3.2.7 Lidar Results **41**
3.2.7.1 Imaging Analysis of Dust Plumes **41**
3.2.7.2 Lidar Measurements of the Generation and Evolution of Dust Plumes **45**
3.2.7.3 Lidar Model Simulations **53**
3.2.8 Conclusions and Recommendations from the Pilot Study **56**
3.3 Main Study Results **57**
3.3.1 Study Period **57**
3.3.2 Meteorological Data **58**
3.3.3 Resuspension Chamber Calibrations **58**
3.3.3.1 DustTrak Calibration **59**
3.3.3.2 Lidar Calibration **60**
3.3.4 Soil Sample Analysis **64**
3.3.5 Lidar Field Measurements **65**
3.3.6 Model Simulations of Plumes **67**

4. Conclusions **70**

5. References **72**

Appendices
Appendix A - Details form Pilot Study
Appendix B - Description of the 10-Second Meteorological, DustTrak, and SF_6 Files
Appendix C - Description of Hourly Meteorological Data Files
Appendix D - Details from Model Simulations
Appendix E - Details from Main Study
Appendix F - Copies of Manuscripts Prepared for Conference Proceedings

List of Figures

Figure 2-1. Map of study area showing the UCR Field Station.
Figure 2-2. Site map of Moreno Valley Agricultural Field Station with the testing area indicated.
Figure 2-3. Plot of testing area showing measurement equipment layout.
Figure 2-4. The test arrangement and generation of a dust plume is shown in the upper panel and lidar instrument is shown in the lower panel.
Figure 2-5. Photograph of downwind particulate matter and meteorological monitoring equipment.
Figure 2-6. The pictures show the centrifugal blower and the motor vehicle used to generate the dust plumes that were measured.
Figure 2-7. Photographs of generation of dust plumes using indigenous soil and $CaCO_3$ crushed powder.
Figure 2-8. Layout of the field site for Main Study.
Figure 2-9. Photograph of the dust generator.
Figure 2-10. Lidar calibration box diagram.
Figure 2-11. Soil resuspension blower.
Figure 2-12. Photograph of particle entrainment system chamber (a) View of the east side of 10-meter chamber, (b) Front (west) and north sides of test chamber where samples are injected and measurements made, the chamber is shown with instrumented meteorological tower, (c) DustTrak optical scatter instruments and Climet particle spectrometer (16 channels - 0.5 to 10 μm).
Figure 3.1. Time series plot of real time PM data and filter PM data for Test #2 on 12/13/2000.
Figure 3-2. Time series plot of real time PM data and filter PM data for Test #5 on 12/14/2000.
Figure 3-3. Time series plot of real time PM data and filter PM data for Test #22 on 12/16/2000.
Figure 3-4. Time series of SF_6 tracer data for 12/14/2000.
Figure 3-5. Time Series of collocated DustTrak data obtained on 12/15/2000.
Figure 3-6. Time Series of collocated DustTrak data obtained on 12/16/2000.
Figure 3-7. Plot of real time PM_{10} sampler QC data normalized to the background PM_{10} sampler.
Figure 3-8. Plot of real time $PM_{2.5}$ sampler QC data normalized to the background $PM_{2.5}$ sampler.
Figure 3-9. The lidar with digital camera observed in foreground scans dust cloud generated by a blower, a 10 m tower is located directly behind the generator and the target board can be seen in front of trees on the far left.
Figure 3-10. A set of the digital images selected from Test #2 to illustrate the growth of a dust cloud using the imaging data.
Figure 3-11. Test 18 (12/15/2000 14:30) generate dust with vehicle, this is time sequence of CCD images along with the corresponding background removed images. (a)14:31:37 (b) 14:32:36 (c) 14:32:49 (d) 14:33:14.
Figure 3-12. Vertical profile (elevation angle 70°) during period fo afternoon convection shows the top of the boundary layer near 1300 m.
Figure 3-13. Examples of the raw data profiles from the lidar at the VIS and NIR wavelengths during Test #4 on 14 December 2000 show the variation in backscatter and extinction associated with a dust plume at a range of about 500 meters.
Figure 3-14. The backscatter and extinction for both visible and NIR wavelengths resulting from vehicle generated dust between 14:32:00 and 14:32:45 during Test #18 on 15 December 2000.

Figure 3-15. An example shows the mesh plot approach for display of the distribution of plume materials. Left frames show the log of the relative scatter intensity on the vertical axis for signal ranges to 1 km and angle scans of $\pm 5^{o}$. The right hand frames show the look down at contours of plume scattering intensity.
Figure 3-16. Vertical profiles show that most of the material in the dust plumes is distributed between surface and 700 m. The raw signals have only been range corrected (the red channel shows an instrument artifact near 300 m).
Figure 3-17. Horizontal scan profiles of raw data plots showing dust plumes were generated by the large wind shear at the surface during the Santa Anna on 18 Dec 2000.
Figure 3-18. Simulation model of scattering intensity shows the difference between the two laser wavelengths and the scattering dependence on number density.
Figure 3-19. Model simulation of scattering intensity shows the difference between changing the particle density and scattering dependence on particle size.
Figure 3-20. Scatter plots of the response of DustTraks UCR #2 and UCR #3 relative to UCR #1 during collocated sampling.
Figure 3-21. Plot of the filter mass concentration measurements compared to the mean DustTrak response (four-analyzer mean).
Figure 3-22. The chamber test measurements from Tests #10, #11, #12 on 19 December 2001 are shown. The upper panel shows the raw signal returns from the lidar at the range intervals corresponding to the chamber and the target board. The lower panel shows the signal from the DustTrak instruments and the normalized lidar return on a logarithmic scale.
Figure 3-23. The log-normal distributions for a two components are fit to the Climet instrument measured curve for the 0.7 :m sample of $CaCO_3$.
Figure 3-24. The Climet spectrum of the particle counts versus particle size for the several samples of $CaCO_3$ power that were used during the testing. Notice that the 0.7 µm case is an anomaly (see text), however the other samples do show changes that generally agree with the increasing size of the samples.
Figure 3-25. The Climet spectrum for the 0.7 µm sample of the $CaCO_3$ dust is shown for the measurements in Figure 3-25 converted to number density and to mass density
Figure 3-26. The Climet particle size spectrum for the several different types of soil and powder during the test are compared.
Figure 3-27. The open-air measurement sequence shows the lidar backscatter peak values and extinction values for profiles during Test #44 on 19 December 2001 that used a 0.7 µm $CaCO_3$ 600 g sample.
Figure 3-28. The expected settling velocity versus particle diameter from standard text (Seinfeld and Pandis[8]).
Figure 3-29. Sequence of pictures shows a puff plume of local soil that was tracked by scanning lidar.
Figure 3-30. The results from Test #44 on 19 December 2001 show several of the lidar profiles that show the time variation in the backscatter and the extinction measured by the lidar. These range profiles are from the same data set that is shown in Figure 3-28.
Figure 3-31. The results from a calculation of the backscatter and extinction expected when one sequentially removes the larger end of the spectrum of the scattering particles. The calculation is performed for the spectrum shown in Figure 3-26 and corresponds to the measurements shown in Figure 3-31.

List of Tables

Table 2-1. Portable digital lidar (dual wavelength and scanner) system specifications.
Table 2-2. Description of Soils and Surrogate Soils.
Table 3-1. CDL literature search of the Current Contents Data Base.
Table 3-2. CDL literature search of Melvyl Catalog.
Table 3-3. Internet Search using Google as Search Engine.
Table 3-4. Literature search of the SPIE Database.
Table 3-5. Test activities log.
Table 3-6. Summary of hourly meteorological data.
Table 3-7. Analysis of soils used for dust generation.
Table 3.8. Summary of meteorological conditions during the testing period.
Table 3-9. Comparison of filter with the DustTrak response.
Table 3-10. Particle size analysis of various soil types used.

Abstract

Ambient measurements suggest that the contribution of geologic dust sources to emission inventories of PM_{10} are overestimated by 50 percent or more. The objective of this research was to characterize the deposition of PM_{10} components so that more accurate emission inventories of PM_{10} from geologic sources could be constructed. Point-based sampling using conventional measurement methods and a two-wavelength scanning backscatter lidar were used to characterize the deposition of particles generated from test aerosols, resuspended soils, unpaved roadways, and a tilling operation. The lidar could remotely track dust plumes for many kilometers. The lidar measurements and model simulations demonstrated that the optical backscatter is more strongly dependant on the concentration of particles, and the optical extinction is more strongly dependant on the particle size. Lidar results showed that the larger particles, which contain most of the PM mass, settled out of the air fairly quickly, however, the fine particles contribute primarily to the backscatter, and remained suspended aloft much longer. The particle settling velocities observed were more rapid than those reported for static systems. The effective settling velocity is apparently changed by turbulent motions and increases the migration for particles in a range of aerodynamic sizes.

Executive Summary

The PM_{10} concentrations in the San Joaquin Valley often exceed both the State and Federal ambient air quality standards. In order to apply effective control strategies it is necessary to know the contributions from the various sources. Estimating emission inventories of PM_{10} from geologic sources is difficult since these emissions come from open areas and not ducts where the emission rates may be measured. Inventories of such sources are therefore subject to considerable and largely unquantifiable error. Ambient measurements suggest that the contribution of geologic dust sources to emission inventories of PM_{10} are overestimated by 50 percent or more. This discrepancy may be due to inaccurate emission calculations and/or due to the rapid deposition of PM_{10} after entrainment into the atmosphere. The objective of this research was to characterize the deposition of PM_{10} components so that more accurate emission inventories of PM_{10} from geologic sources could be constructed.

The approach used was to characterize dust plumes using both point-based sampling using conventional measurement methods and a two-wavelength scanning backscatter lidar. Lidar is an acronym for Light Detection and Ranging and is based on sending out a pulse of light and the measuring the amount of light that is scattered back. The amount of scattered light depends on the frequency of light and the size and concentration of particles. A primary advantage of this technique is that it detects particles remotely and has a range of many kilometers. By scanning both horizontally and vertically it is possible to “map” a dust plume. Since the scattered light cannot be directly converted to concentration units, we calibrated it by characterizing the response in a test chamber where particles were suspended and measured using conventional techniques. Dust was generated using vehicles on unpaved roads, tilling operations, and from a blower fan, that dispersed known amounts of finely ground calcium carbonate or sieved soils, both native and from three areas of the San Joaquin Valley.

The optical scattering from the lidar was used to monitor changes in the size and concentration of the resulting dust plumes for up to a half-hour and distances of several kilometers. The changes in these dust plumes’ characteristics with time are depicted using a lidar to measure the relationship between backscatter and extinction at two wavelengths. The results were compared with model simulations based on the optical properties of aerosol particles. These model simulations described the dependence of optical backscatter and extinction upon the size, number density and refractive index of the particles. Thus, simultaneous measurements of the backscatter and extinction at two different wavelengths permitted an examination of settling rates of dust particles as a function of size.

The pilot study for this project showed that point sampling was not useful in characterizing the deposition from a dust plume and that the lidar would need to be the primary measurement tool. Lidar showed that the larger particles, which contain most of the PM mass, settled out of the air fairly quickly, however, the fine particles contribute primarily to the backscatter, and remained suspended aloft much longer. The measurements and model simulations demonstrated that the optical backscatter is more strongly dependant on the concentration of particles, and the optical extinction is more strongly dependant on the particle size. This leads to a situation that a dust plume generated from tilling a field appears to visually change relatively slowly, while the larger particles, which possess most of the mass, are rapidly settling out of a dust plume. Since most of the mass in a dust plume is contained in the larger particles, the observed optical scattering does not represent the mass in the plume.

The particle settling velocities in standard texts indicate longer residence times than those found in these experiments. The effective settling velocity is apparently changed by turbulent motions and increases the migration for particles in a range of aerodynamic sizes. Gravitational effects dominate motion of heavy particles and very light particles are controlled by diffusion. Both are

affected by turbulence cells are present from generation by wind shears and by turbulent convection from surface heating.

Although we obtained qualitative evidence of the larger particles settling out faster than smaller ones, we were unable, however, to answer was how fast particles of a specific size range settled. This was primarily due to the limited wavelength resolution of the lidar and the inability to generated monodisperse particles for calibration. A great deal of data was generated and more useful information could be obtained by a detailed analysis of the optical properties and comparison with particle scattering theory. Such a detailed analysis was beyond the scope of this study; the approach was far more complex than originally envisioned.

Glossary

ARB or CARB .....California Air Resources Board

CE-CERT.....College of Engineering-Center for Environmental Research and Technology, University of California, Riverside

DAS.....Data acquisition system

DIAL …… Differential Absorption Lidar

DT……..DustTrak

L .....Liter

NIR ……. Near Infrared

$\mu g/m^3$.....Micrograms per meter cubed

prf …… pulse repetition frequency

PSU ……...Penn State University

RH.....Relative humidity

RSD.....Relative standard deviation

SD……..Standard Deviation

SJV ……...San Joaquin Valley

TMP……..Temperature

UV ……Ultraviolet

VIS …….. Visible

VWS……..Vertical wind speed

WD.....Wind direction

WS.....Wind speed

1.0 Introduction and Objectives

1.1 Background

Many areas in the State of California consistently exceed both the State and Federal PM_{10} air quality standards, and they are expected to exceed the new $PM_{2.5}$ standards. Geologic material is a major component of the airborne particulate matter in the western United States. Airborne particulate matter is an air quality concern because:

1. Recent studies have associated increases in airborne particulate matter with increased morbidity and mortality, particularly in elderly and respiratory impaired individuals.
2. Reduced visibility due to airborne particulate matter has both degraded the aesthetic beauty of natural views and affects activities such as the scheduled air traffic operations.
3. The changes in optical transmission of the atmosphere due to suspended airborne particulate matter alters the radiative energy balance of the Earth's environment.

Source emission inventories for PM_{10} and $PM_{2.5}$ show that geologic dust should contribute approximately 50% of the $PM_{2.5}$ in the Western United States. Ambient measurements show that the materials of geologic origin typically contribute approximately 10% to the mass concentration (Watson and Chow, 1999). There are several possible reasons for this discrepancy, the primary ones being inaccurate algorithms, input data used to calculate emission inventories, and uncertainties of the lifetime of PM in the atmosphere.

1.2 Objectives

The primary objective of the research activity was to characterize the fate (deposition and transport) of PM emissions originating from mechanical disturbance of the soil. The results from the measurements were to provide data for evaluating the algorithms used to compute emission inventories from airborne particulate sources. The study focused on the problems of PM generated from unpaved roads and agricultural tilling in the San Joaquin Valley of California. The tests used locally generated dust clouds of various materials, some with known size distribution, to provide measurements that could provide a validation of the analysis of the optical scattering properties, and information on the distribution and settling of airborne particulate matter. Meeting these objectives would permit more accurate assessment of such source contributions to the regional PM concentrations. These assessments would then aid the formulation of cost-effective PM control strategies.

2.0 Approach

The overall approach was to fully characterize several types of dust generation processes that are expected to be significant sources of geologic material contributing to the PM in the San Joaquin Valley. The work was done in a test area at an agricultural field site belonging to the University of California, Riverside, where the generation conditions could be controlled and where backscatter lidar could be safely and unobtrusively used in the scanning mode. Tests were conducted on artificially generated dust plumes representing PM emissions by using particles of known size distributions and soils from the San Joaquin Valley, from the local field, and crushed $CaCO_3$ powders. The lidar response to particle concentration was investigated by generating test aerosols in a 10-meter long chamber, while monitoring the concentrations with DustTrak optical scattering instruments and a Climet optical particle size spectrometer. Tests were also performed using the dust clouds from vehicular travel on a dirt road and from soil tilling operations in an agricultural field.

The primary instrument selected for these investigations is lidar. Lidar is an acronym for LIght Detection and Ranging. Lidar systems operate on similar principles as radar (RAdio Detection and Ranging) systems, but use a pulsed laser to measure atmospheric properties over a desired range of directions and elevations. A lidar system uses laser pulses to measure optical scattering and thereby determine the distribution and profiles of atmospheric properties and composition, such as aerosols, ice crystals, water vapor and some trace gases (ozone for example). Profiles of these parameters measured as a function of time and location can be used for weather forecasting, modeling, and environmental monitoring.

A lidar transmits short pulses of laser light into the atmosphere. The laser beam light is scattered as it passes through the atmosphere. At each range, some of the light is backscattered into a detector. Because the light takes longer to return from the more distant ranges, the time delay of the return pulses can be converted to the corresponding distance between the atmospheric scattering volume and the lidar. The end result is a profile of atmospheric scattering versus distance. Analysis of this signal can yield information about the distribution of aerosols in the atmosphere. The amount of backscatter depends on density, size and type of the scattering particles, and the signal can be used to measure cloud base or track plumes of pollution.

Other properties of the atmosphere can also be deduced from the lidar return signals. A frequency shift in the light because of the Doppler effect permits measurement of wind speeds. By detecting the amount of depolarization, one can discriminate between spherical liquid droplets and irregular ice particles. DIfferential Absorption Lidar (DIAL) techniques use two laser wavelengths to measure the absorption specific to a chosen chemical species and are used to determine the concentration of atmospheric gases. A Raman lidar detects particular atmospheric components (such as water vapor) by measuring the signal from vibrational Raman shifted wavelengths of selected molecules.

2.1 Literature Search

A detailed survey of the pertinent literature was necessary to guide the approach to be taken. This ensured that work was not unnecessarily duplicated and that the methods chosen were likely to meet the project objectives. Although we were very familiar with the research that has been done, the related work that has been or is being conducted was summarized to maximize the achievement of the project objectives. Two extensive compilations of references compiled by Watson and Chow (1999) and the California Digital Library (CDL) were a focus for the review. The objective of this task was to obtain and review literature relative to the potential use of lidar based methods for the evaluation of airborne particulate matter measurements.

The primary effort involved a literature search to determine what had been published. This was done using the California Digital Library (CDL) to search the UC library (MELVYL) and Current Contents databases. The former contains all types of books, periodicals, and reports while the latter focuses on journal articles published within the past 15 years. Also since lidar is an optical technique, a similar technique was employed using the International Society for Optical Engineering (SPIE) database. Keywords for the search, such as lidar, were combined with others such as dust, fugitive, plumes, aerosols, and emissions. Titles found by the databases were reviewed and either abstracts or full papers of applicable titles were obtained. These references were reviewed and applicable references cited were added to the literature compiled. Applicable references involved measurement of fugitive dust. This approach was the primary technique to find references that were published prior to the start of the electronic data base compilation. Additional references were obtained from personal contacts with staff and colleagues. A synopsis of the relevant literature is presented. A general search into the applications of companies that fabricate lidar-based equipment was also conducted using the Google search engine. Applicable references of these companies and their websites are also included, as well as a brief description of their instrumentation and relevant work.

2.2 Pilot Study

The Pilot Study was the first of two field measurement programs. The goal was to use the results of this study to plan the Main Study. The first set of field measurements were planned to obtain initial data for initial investigations using a lidar to measure the optical scattering properties associated with a dust plume. Our objective was to use these properties to map the distribution and evolution of the airborne dust plumes. The selection of the techniques and instruments included consideration of the following factors:

(1) Use of lidar provides a very sensitive way of detecting airborne particles in the size range between 0.1 and 10 μm.
(2) Rapid scanning with a high prf laser provides a capability for mapping the time evolution of a dust plume.
(3) A micro-pulse lidar is necessary for horizontally scanning a lidar that uses visible wavelengths because of eye-safety requirements (pulse energy densities must be limited to $< 5x10^{-7}$ J/cm^2 – less for multiple pulse operations).
(4) High spatial resolution is needed to define the volume, thus requiring short laser pulses and narrow bin widths for the detector electronics.
(5) Two laser wavelengths are needed to provide information on variations in the particle size distribution.
(6) Our idea was to use a new approach for analysis of a plume that would result in measurements of both the backscatter and extinction, simultaneously. Past analysis of simple lidar measurements has shown that backscatter results are only useful for interpretation of qualitative properties in the lower atmosphere. However, in the case when the backscatter profile is available before and after the plume region, we expected that it may be possible to measure both the backscatter <u>and</u> the extinction signals simultaneously. The combined backscatter and extinction measurement has provided a very useful way to analyze the relative effects of variations in the number density and size distribution that both contribute to the measured profiles of scattered intensity.

2.2.1 Test Location

The criteria for site selection included:

- Large open area (preferably 40 acres or more),
- No significant nearby sources of PM and no significant variations in background, PM during the course of a test,
- Power availability,
- Reasonable security,
- Close proximity to UCR,
- Site permission, and
- Cost.

Based on these criteria, the UCR Agricultural Field Station in Moreno Valley (12 miles from the main UCR campus) was selected for the pilot field study. Figure 2-1 is a map showing the location of the field site. The UCR Agricultural Field Station is an approximately 720-acre facility. As shown in Figure 2-2, the facility is subdivided into twelve fields; each field is between 40 and 80 acres in size. The entire facility is relatively level, except for some raised dirt roads (~10 foot width) that sub-divide the area into rectangular fields. Field K was provided for use in this study. The fields adjacent to Field K (Fields H, J and L) remained furrowed during the December dust entrainment pilot study. There were no significant sources of PM around the facility. The project team coordinated with the UCR field site staff regarding any planned field plowing to avoid that activity during periods that tests were performed.

Since the prevailing daytime winds are typically from the west during December, the chosen arrangement located the lidar generally upwind from the area for plume generation. The site has power at the west end of Field K. Figures 2-3 through 2-6 show the layout for the equipment and the arrangement at the site. A background (upwind) site included measurements of real-time PM and integrated filter samples of PM_{10} and $PM_{2.5}$. A meteorological station that included wind speed (WS), wind direction (WD), temperature (T) and dew point (DP) was also located at this site. The arrangement for the lidar, which was located 153 meters upwind of the main dust generator, and the lidar instrument hardware are shown in Figure 2-4. The distance of about 150 meters between the lidar and generation area was considered to be minimum for the experiment. The lidar uses a long focal length telescope, and thus suffers a loss of signal and a region of non-linearity for near field signals due to overfilling, or vignetting, at the detector. To avoid any effects from the telescope form factor would require that the measurements be conducted at a range greater than 800 meters; however, the 150 meters was considered to be an acceptable compromise. Most of the dust generation and tracer gas release were performed using a stationary dust generator (Figure 2-6) at the location shown in Figure 2-3. Limited testing was carried out using calcium carbonate (~10μ size) and a fogger (propylene glycol) of the type used for stage plays. For the remaining tests, dust generation was from automobile tire/loose soil contact from a vehicle (Figure 2-6) driving the line paths shown in Figure 2-3. Tracer gas was released from the vehicle during these tests.

The trailer-mounted tower shown in Figure 2-5 was used to monitor downwind PM and tracer gas. The tower included the following instruments at 2, 5, and 10 meters:

- Integrated (filter) PM_{10}
- Integrated (filter) $PM_{2.5}$
- Real-time PM_{10}

- Real-time $PM_{2.5}$
- WS/WD

This tower also included temperature measurements at 2 and 10 meters, net radiation measurements at 1.5 meters and tracer gas measurements at 2-meters. The tower was placed at the location shown in Figure 2-3.

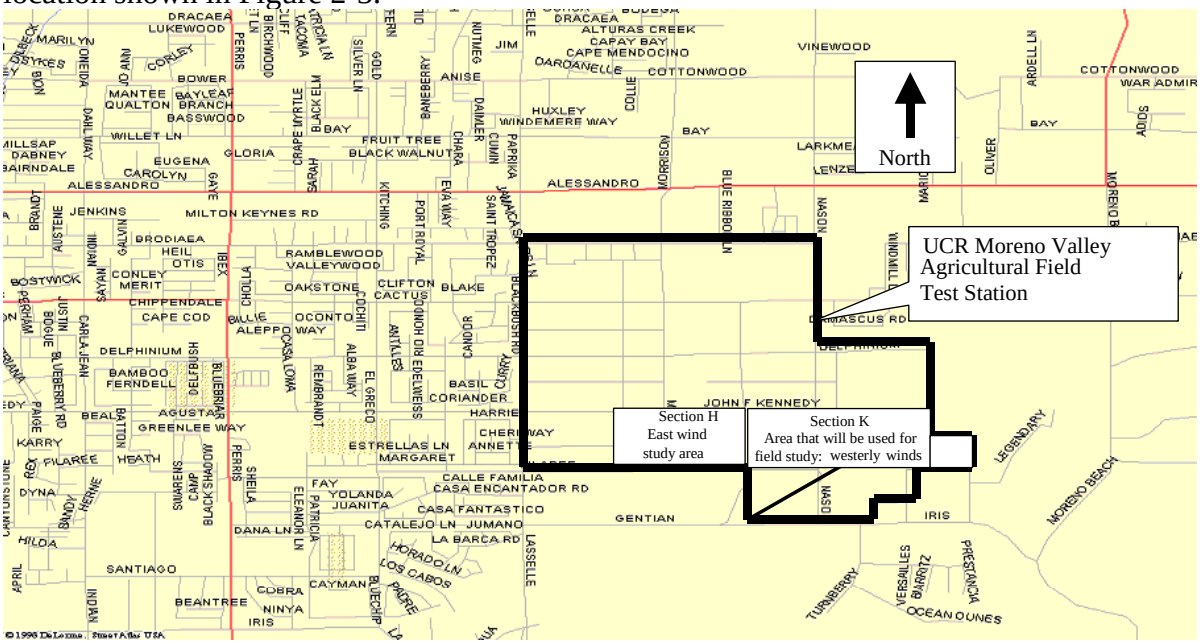

Figure 2-1. Map of study area showing the UCR Field Station.

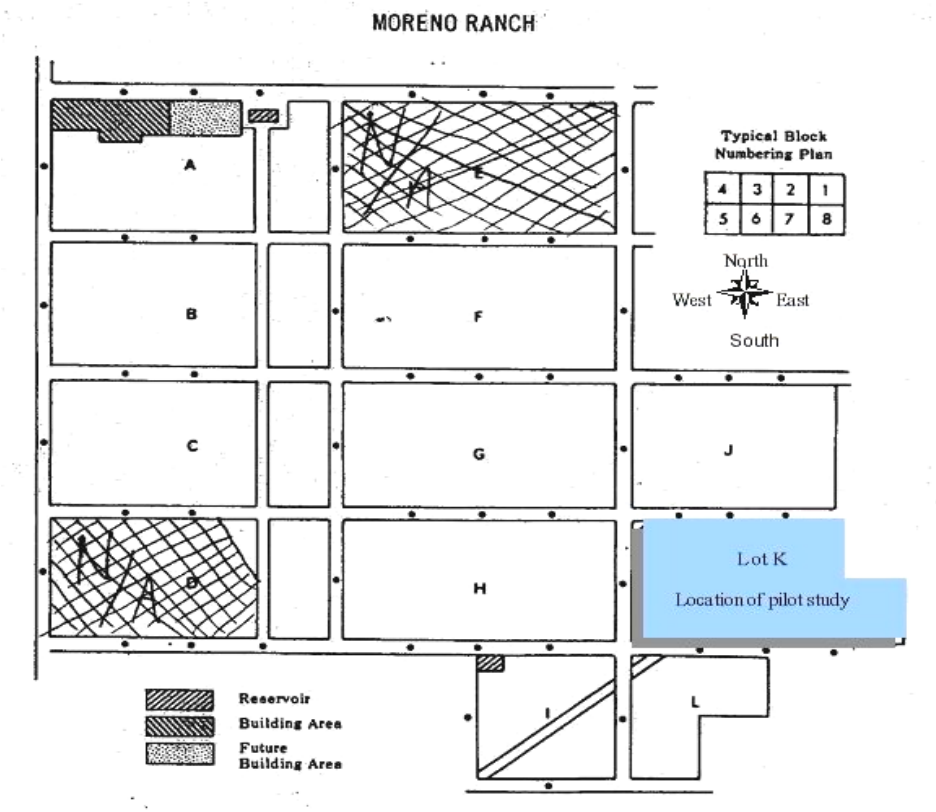

Figure 2-2. Site map of Moreno Valley Agricultural Field Station with the testing area indicated.

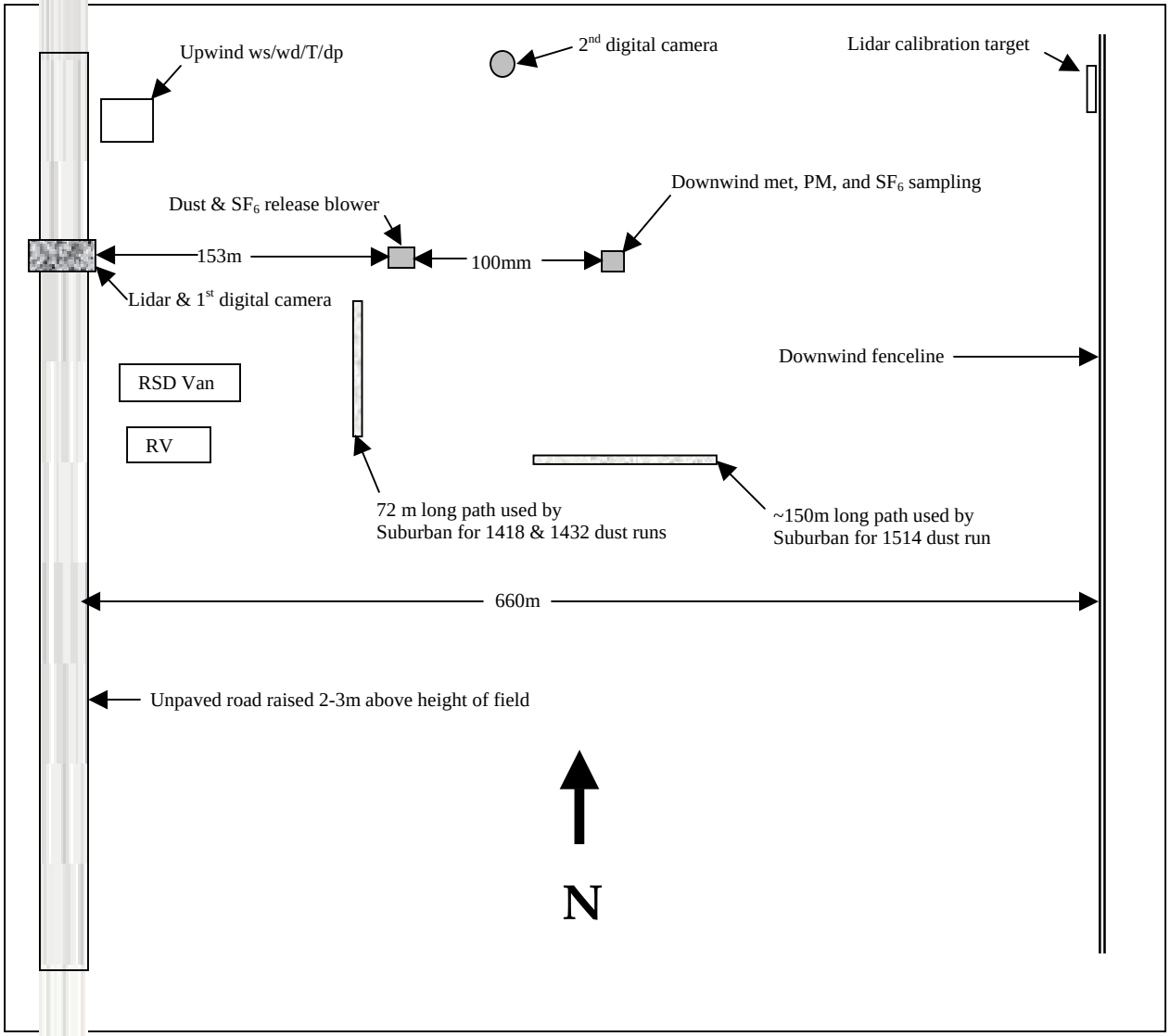

Fig 2-3. Plot of testing area showing measurement equipment layout (not to scale).

Figure 2-4. The test arrangement and generation of a dust plume is shown in the upper panel and lidar instrument is shown in the lower panel.

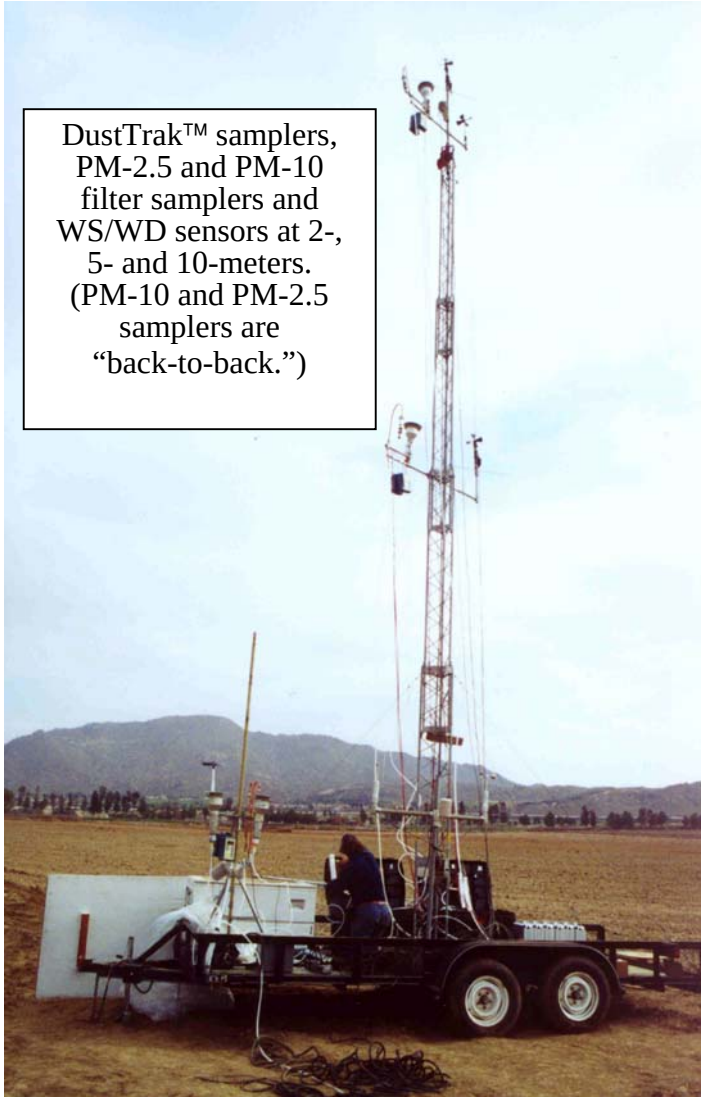

Figure 2-5. Photograph of downwind particulate matter and meteorological monitoring equipment.

Figure 2-6. The pictures show the centrifugal blower and the motor vehicle used to generate the dust plumes that were measured.

2.2.2 Measurement Methods

2.2.2.1 *Meteorological Measurements*

Measurements for wind speed, wind direction, temperature, dew point and solar radiation were performed at the background location. This system included a Climatronics F460 wind speed and wind direction sensor mounted at a height of 7 meters prior to 13 December 2000 and at 2 meters thereafter. This system included a cup anemometer and a wind vane. A Campbell CR10X data logger located at the base of the tower scanned the wind speed and direction signals once per second.

Temperature and dew point was measured using a Climatronics power aspirated system at a height of 5 meters prior to 13 December 2000 and at 2 meters thereafter. The Campbell CR10X data logger located at the base of the tower was also scanned the signals from these sensors once per second.

The Campbell data logger processed the scanned meteorological data into one-hour averages for the approximately one-month period it operated prior to the pilot study. During the pilot study, the data logger processed the collected data into ten-second averages.

Three additional sets of WS/WD sensors were located on the downwind trailer mounted tower. They were located at 2, 5, and 10 meters. Two of these sensors were RM Young Type AE wind speed and direction sensors. The third was a Climatronics F460. Temperature was measured at 2 and 10 meters using naturally aspirated Campbell temperature sensors. The signals from these sensors were scanned once per second by a Campbell CR10X data logger and processed into ten-second averages.

2.2.2.2 *Dust Generation*

Several dust generation methods were used for the pilot study. The primary dust generator used a 5 horsepower centrifugal blower. Weighed amounts of selected indigenous, presieved soils and materials of known particle sizes were introduced into the blower. The blower expelled these particles horizontally at a height of one meter. Figure 2-7 shows examples of the dust plumes generated for the presieved soil, and a crushed power of $CaCO_3$, which was purported to contain particles distributed with a peak near 10 μm.
A second method of dust generation was to drive a vehicle in straight lines on the dirt field. Figure 2-6 shows an example of a line source dust plume created from the vehicle driving along an approximately 150 meter long path.

A third method used commercially available “fog” generators, similar to those used for control of film stage effects. Fogs of propylene glycol were generated.

Generation of indigenous dust particulate

Generation of white paint dust particulate

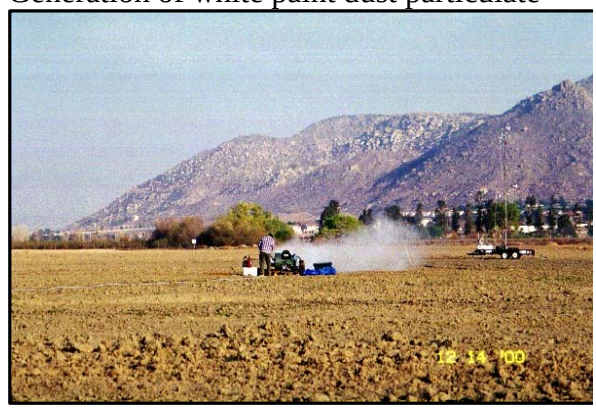

Figure 2-7. Photographs of generation of dust plumes using indigenous soil and $CaCO_3$ crushed powder.

2.2.2.3 ***Lidar Measurements***

The Scanning Micro-Pulse Lidar (MPL) used for these investigations was leased from Science and Engineering Services Inc. (SESI) and operated by the Pennsylvania State University graduate students. The SESI MPL instrument provides the backscatter coefficient at two wavelengths and has several features that make it the ideal instrument for mapping the dust cloud plumes that were investigated in this program. The instrument provides a backscatter signal at two wavelengths and has a scanning platform, which can be used to provide a mapping of the airborne particulate matter. The instrument is eye-safe but maintains high sensitivity by using a high average power, obtained because of operating at a high prf (several kHz), and by expanding the beam to produce lower energy flux per unit area. Two Nd:YLF lasers are used at their fundamental and frequency doubled wavelengths of 1047 and 523.5 nm with energy outputs of approximately 10 and 5 μm, respectively. The beams are expanded and transmitted through a 20 cm diameter telescope, which is also used to receive the backscattered signal. An avalanche photo-diode detector is used in a pulse counting mode to measure the returned signal at each of the two wavelengths. The instrument has several operating modes, however we selected the highest range resolution (33 meter data bins) and used a two-second integration of the signals for each profile. The most useful results are obtained by averaging and comparing the returns backscattered from the dust plume, and from the ambient aerosols beyond the plume, with the ambient scattering from the clear atmospheric path before generating a dust plume on the path. The results obtained by forming ratios of the measured dust profiles to that of the clear path then provide a measure of the optical backscatter and extinction signals associated with the generated dust plume. The lidar measurements provide a most important data set for understanding the plume properties and processes associated with transport and remove the airborne dust. Table 2-1 provides the instrument's technical specifications.

The instrument measures the backscatter signal profiles at 1047 nm in the near infrared (NIR) and 523 nm in the mid-visible spectrum. These wavelengths are most sensitive to scattering from particle sizes in the size range between 0.1 and 10 μm, and they are separated sufficiently to provide some information on changes in the fine particle ($PM_{2.5}$) size distributions.

Table 2-1. Portable digital lidar (dual wavelength and scanner) system specifications.

Operating Environment Controlled Indoor
Detection Range 30 - 60 km
Laser (dual wavelength) DPSS:Nd:YLF (523.5 nm/1047 nm)
Laser Control Remote Set or RS232
Average Energy VIS: >5 µJ/pulse NIR: >10 µJ/pulse
Pulse Repetition Rate (pulse duration) 1 - 10 kHz (10 ns)
Cassegrain Telescope Diameter (F.O.V.) 0.2 m (- 100 :rad)
Detector APD Photon Counting Module
Scanning Mode Sweep or Stay and Stare
Horizontal Scanning (vertical swiveling) ± 90/ (0/ - 90/)
Scanning Speed per sec Variable from 0.1/ to 30/
Optical Transceiver Dimensions (weight) 33" x 14" x 12" (40 lbs)
Computer Desktop or Laptop PC
Software Windows 95/98 based software
Dual Multichannel Scaler (dimensions) Rack-mountable (19" x 14" x 7")
Data Averaging Time Adjustable from 1 sec to 1 hour
Range Resolution 30 m, 75 m, 150 m, 300 m

2.2.2.4 *Real-Time Particulate Matter Measurements*

Thermo Systems Inc. model 8520 DustTrak™ aerosol monitors were used to point measurements of the PM_{10} and $PM_{2.5}$ concentrations. This instrument measures PM concentrations from the light scattering intensity of the aerosol and provides data in ten-second intervals. Figure 3-5 shows the DustTraks™ at the downwind sampling location.

2.2.2.5 *Integrated (Filter) Particulate Matter Measurements*

Two different types of PM samplers were used, one for PM_{10} and the other for $PM_{2.5}$. For PM_{10} a Graseby-Andersen model 246B inlet is used, but modified such that a single filter could be directly attached to the inlet. The filter sampler operated at 16.7 L/min using a needle valve to control the flow. For $PM_{2.5}$, Sensidyne model 240 cyclones sampling at approximately 110 L/min were used to provide the cutpoint. Filters used for both were ringed “stretched” Teflon filters (47mm diameter, 2 micron pore size Gelman Teflo), selected for their low tare weight, mass stability and high collection efficiency at the sample flowrates planned for this program.

2.2.2.6 *Sulfur Hexafluoride Tracer Release System*

The goal of the SF_6 release system was to release and mix the tracer gas into the generated dust cloud. Pure SF_6 was metered from a cylinder using a mass flowmeter calibrated for SF_6. The SF_6 release rate was 400 grams per hour (g/hr) for the second study day and 200 g/hr for the subsequent days. The outlet of the mass flowmeter was fed to the inlet of the centrifugal blower (or adjacent to the vehicle generating dust or fogger, as appropriate).

2.2.2.7 *Sulfur Hexafluoride Tracer Measurement System*

SF_6 was measured using an AeroVironment Model CTA-1000 continuous tracer gas analyzer. The instrument uses an electron capture detector (ECD) to enable continuous detection of SF_6 from ambient air samples. The instrument has a dynamic range from one part per trillion (ppt) to over one part per million (ppm) concentrations of SF_6. A 0.5-inch diameter polyethylene sample line drew a sample from the downwind sample location to a van at the background location.

2.2.2.8 *Laboratory Analyses of Filer Samples*

Filter weighing was performed at CE-CERT’s filter weighing facility. The facility includes a room dedicated to filter weighing. A volume of approximately one cubic meter is humidity and temperature controlled for filter equilibration and storage. A Cahn Model C-35 balance is contained in a laminar flow hood. The temperature and humidity in the laminar flow hood and equilibration chamber are controlled to 25°C and approximately 40% RH. Filters were equilibrated for 24 hours or more prior to the “blank” (prefield use) weighing and also prior to

the "after" field use weighing. The balance used for filter weighing was calibrated with a 200 mg class M NIST-traceable weight before and after each weighing session.

2.2.2.9 *High Resolution Photography*

A high-resolution video camera (Sony Digital DCR-VX700) was mechanically coupled to the lidar to document the distribution of the dust generated and to verify the lidar position. Images were taken continuously as the lidar scanned through the dust plume. The camera followed the path of the laser beam to provide a clear picture of the area being scanned. The scanning lidar with the camera was located upwind of the generation point. The scan covered the region about 10-20° on either side of the centerline from the location of the lidar to the generation point. An inclinometer was mounted on the lidar to measure the elevation angle. A second video camera was used during the measurement periods to document the 3-demeinsional distribution of the plume. It was placed at the location shown in Figure 2-3. Running simultaneously, these two cameras provided a more complete visual representation of the spatial evolution of the dust clouds.

2.2.2.10 *Silt and Soil Moisture Measurements*

Aliquots from the indigenous soil used for the dust generation were collected and analyzed to determine the moisture content and the percent of silt. The amount of soil moisture was determined using EPA Method 160.3. This method included weighing an aliquot of each sample. The sample aliquots were then dried in an oven at 103 to 105°C, and reweighed. After adjusting for the weight of the weighing jar, the percentage of moisture was determined by the difference in weights divided by the dry weight of the sample.

The sand, silt and clay content were determined using American Society of Agronomy (ASA) Method 43-5. A ten-gram aliquot of each sample was placed into a sedimentation cylinder with a water and Calgon solution. The suspension was thoroughly mixed and hydrometer readings were taken at 0, 0.016, 0.033, 6 and 15 hours. The concentration and total suspended mass was determined for each of these measurements. The fraction of the mass that settled out during the first two minutes (0.033 hours) was defined as the "sand" fraction. The fraction of the mass that settled out between 2 minutes and 6 hours was defined as the silt fraction. The fraction of mass that settled out between 6 and 15 hours, or was still in suspension after 15 hours, was defined as the clay fraction. The method assumes that the particle density is between 2.5 and 2.8 grams/ml. Using the assumed particle densities and a relationship between sedimentation time and the "sedimentation parameter" provided in the method, the sand fraction are particles in the 25-50 μm and larger range, the silt fraction are particles in the 2-30 μm range and the clay fraction are particle less than about 2 μm.

2.3 Main Study

2.3.1 Test Location

The Main Study used the same site at the University of California, Riverside's Agricultural Field Station in Moreno Valley that was used in the Pilot Study. Figure 2-8 shows the layout of the site**.** The location of the equipment within the site was changed to provide a longer path to the lidar instrument measurement volume and to accommodate the location of the outdoor test chamber, while providing access to electrical power connections for both the chamber and the lidar.

2.3.1.1 *Site Layout*

The meteorological tower was located near the northwest corner of field K. This location kept it out of the planned beam path of the lidar during dust tracking, but the lidar scan path could easily be pointed to hit a target placed on the tower. The lidar was placed at about the middle of the southern end of field H. This location, about 400 meter northwest of that of the Pilot Study, was chosen because it provides a minimum of 400 meters to all targets and generated dust plumes, and power was readily available at the location.

The centrifugal dust generator was located about 500 meters west of the lidar, at the place shown in Figure 2-8. This is approximately the same location as used for the pilot field study. Dust was generated by a vehicle driving on a north-south road as shown in the figure. Tilling operations were conducted in section J to provide a dust cloud of local soil origin.

2.3.1.2 ***Soils Tested***

The soil used for the "disking" (plowing) and "dirt road" dust generation portions of this program are the indigenous soil at the UCR Moreno Valley Agricultural Station. The soils that were entrained into the atmosphere using the centrifugal blower fall into two categories. The first category includes soils that are typical of those encountered in agricultural activities, especially those in the San Joaquin Valley (SJV). In addition to using soil from the Moreno Valley Agricultural Station, soils from three other University of California Agricultural Stations located in different regions of the SJV and representing a cross section of soil types, were selected and obtained for use in this category. The second category included materials, which are reference "soils" used to characterize mixing, transport and fallout based predominantly on particle size. This reference category included eight essentially monodisperse "soils." The monodisperse "soils" were all calcium carbonate $CaCO_3$, which is widely used in the manufacturing of paper and paint pigments. $CaCO_3$ is ground to close tolerances for these manufacturing applications. $CaCO_3$ has a specific gravity of 2-7, which is similar to that of typical soils. During the Pilot Study a '10 µm' sample of $CaCO_3$ had been obtained and used for plume generation and so, for the main study, several different sizes of the material were obtained. For these reasons, using monodisperse $CaCO_3$ as a surrogate soil allowed the characterizing the mixing, transport and fallout of soil as a function of particle size. A description of these soils is included in Table 2-2.

Table 2-2 Description of Soils and Surrogate Soils

Soil #	Description
1	CaCO3 with median particle diameter of 0.7µm
2	CaCO3 with median particle diameter of 2µm
3	CaCO3 with median particle diameter of 4µm
4	CaCO3 with median particle diameter of 8µm
5	CaCO3 with median particle diameter of 10µm
6	CaCO3 with median particle diameter of 15um
7	CaCO3 with median particle diameter of 75µm
8	CaCO3 with median particle diameter of 150µm
9	Soil from UCR Moreno Valley Agricultural
10	Soil from UC Kearney Reseach Center, Parlier, CA; Hanford
11	Soil from UC Shafter Reseach Center, Shafter, CA; Wasco
12	Soil from UC West Side Reseach Center, Five Points, CA;

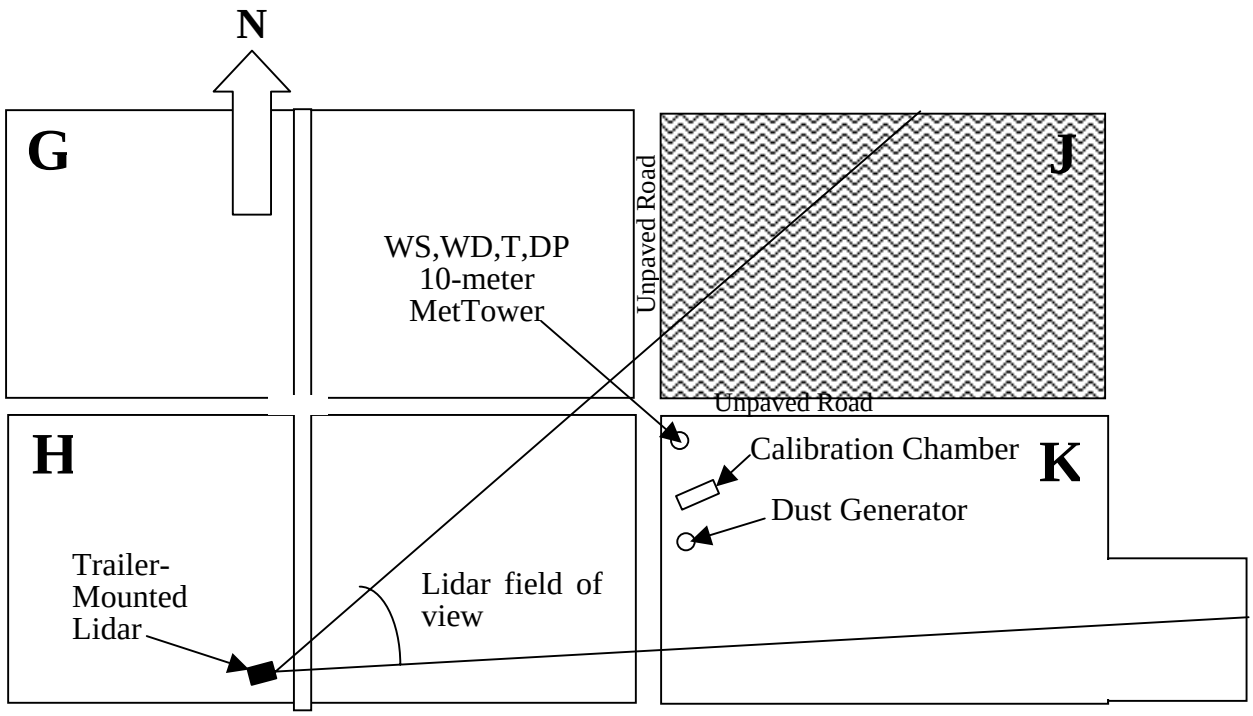

Figure 2-8. Layout of the field site for Main Study.

2.3.2 Measurement Methods

Many of the same measurement methods were the same as used in the pilot study. Please refer to section 2.2 for details of these methods. The following paragraphs describe the major differences from the Pilot Study.

2.3.2.1 ***Meteorological Measurements***
Unlike the pilot study meteorological measurements were made at a single height (10m) and location. Wind speed and direction were measured with a RM Young Type AQ propeller anemometer with a wind vane. Temperature and dew point were measured using a power aspirated Climatronics sensor system as in the pilot study. Solar radiation was monitored using an Eppley model PSP radiometer. In order to locate this sensor in a location where no shadows would pass over it, the radiometer was placed on a mast extending approximately 0.5 meters away from the tower at a height of three meters. A Campbell CR10 data logger was located at the base of the tower and logged as 1-minute averages of the output signals that were scanned once per second. The meteorological data was processed into one-hour averages for the approximately two-month period it operated prior to the main study.

2.3.2.2 *Dust Generation*
Three dust generation processes were used. Both soils and synthetic particles of known size were suspended in the air with a 10-inch diameter squirrel cage blower driven by a ½ hp motor. A round duct was added to the inlet to introduce material to be dispersed. Figure 2-9 is a photograph of the generator. The generator was operated on the top of a four-foot high ladder. The second method of dust generation was the operation of a car or truck on an unpaved road. The third source of dust generation was the disking of a field (Field J in Figure 2-8).

2.3.2.3 *Lidar Measurements*
The same lidar instrument that was used in the Pilot Study was used for the Main Study. The software used real-time data collection was upgraded before the second field campaign and several quick look analysis programs, which were prepared by PSU graduate students, were available for the field measurement program.

2.3.2.4 *Real-Time Particulate Measurements*
These analyzers were only used to measure concentrations in the calibration chamber for the lidar since the results of the pilot study showed that it was not feasible to sample dust plumes from a fixed site. TSI DustTrak samplers were again used to measure particulate mass concentrations. Only the PM_{10} inlets were used. To evaluate the particle size distribution a Climet, Model Spectro 0.3, optical particle counter was used. This instrument counts the particle number in 16 bins from 0.3 to 10 μm. It was set to update an output every minute, the minimum allowed.

2.3.2.5 *Integrated Filter Sampler*
Filter samples were also only collected from the calibration chamber. The samplers were of the Harvard design and used an impactor to remove particles greater than 10 μm aerodynamic diameter. They sample at 20 L/min with the flow monitored with a rotameter and controlled by a needle valve.

2.3.2.6 *Laboratory Analysis of Filter Samples*
Filter samples were weighed at the CE-CERT laboratory in the same manner as the pilot study.

2.3.2.7 *High Resolution Photography*
The same digital imaging equipment was used as the pilot study; however, the second camera, which provided a side view, was not included because it added little value.

2.3.2.8 *Silt and Soil Measurements*
The same methods and laboratory were used as in the Pilot Study.

2.3.2.9 *Outdoor Field Calibration Chamber*
A resuspension chamber was constructed to calibrate the lidar for response as a function of particle size and concentration. This chamber was a box four feet high and wide, and 24 feet long as shown in Figure 2-10. The box is fully closed except for the windows on each end to allow the lidar beam to pass through. These windows are covered while introducing the particles and while waiting for them to mix and achieve a steady concentration. Four fans were placed four inches above the floor of the chamber and evenly spaced along the length. These were used to mix the particles once they are introduced.

Particles were introduced as a “puff” by placing a weighed amount in the bottom of a plumbing “J” trap and blowing compressed air on one side of the trap. Figure 2-11 shows the configuration of this trap. The box was positioned such that the lidar beam was aimed down the center. The DustTraks sampled at position along the length of the box. The OPC inlet and the PM_{10} samplers were positioned in the center of the box. Figure 2-12 shows photographs of the chamber and the

instruments used to measure the properties of the particles inside. The resuspended material was allowed to mix for one minute with the ends of the chamber closed; the ends were then removed to allow the lidar beam to pass through the chamber.

Figure 2-9. Photograph of the dust generator.

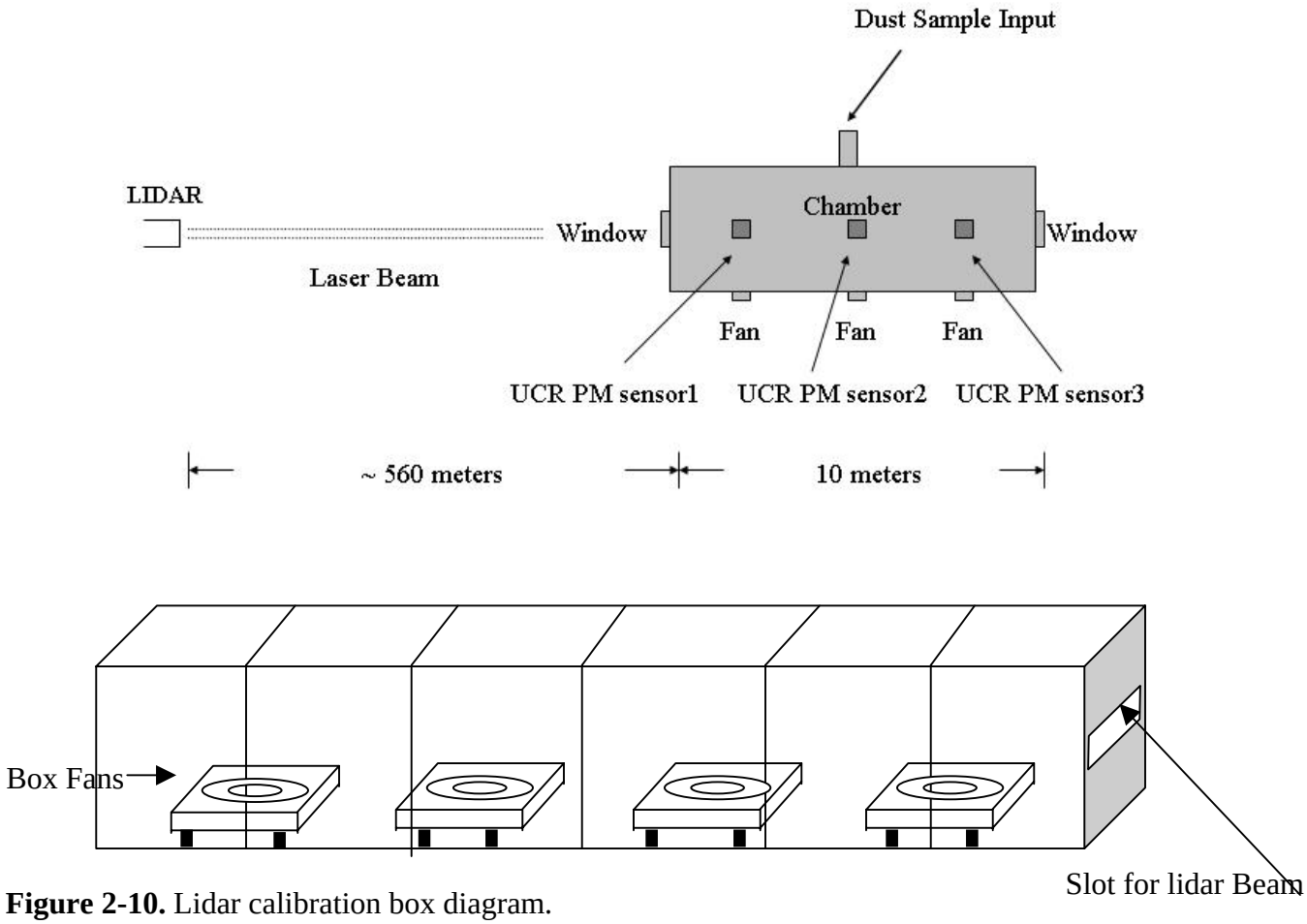

Figure 2-10. Lidar calibration box diagram.

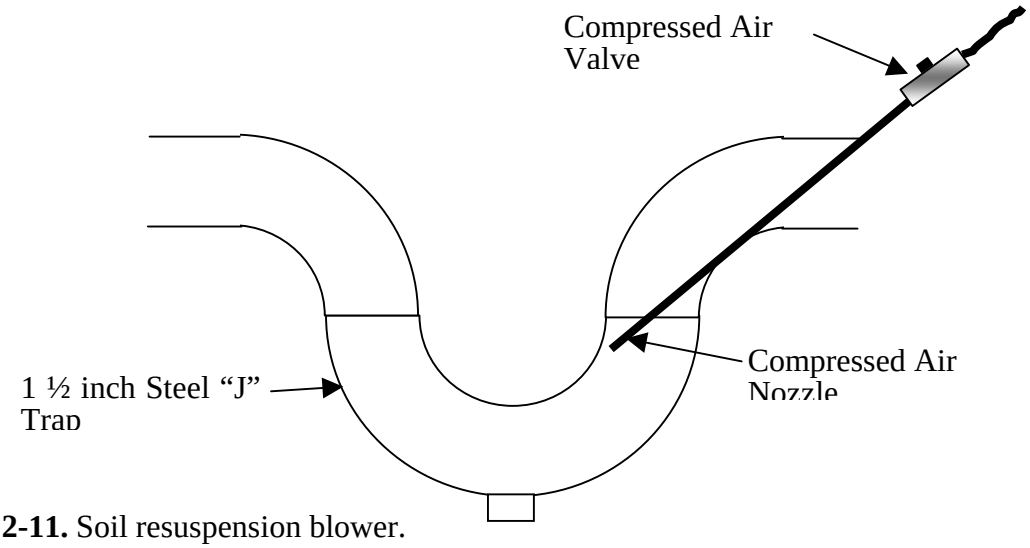

Figure 2-11. Soil resuspension blower.

Figure 2-12 Particle entrainment system chamber (a) View of the east side of 10-meter chamber, (b) Front (west) and north sides of test chamber where samples are injected and measurements made, the chamber is shown with instrumented meteorological tower, (c) DustTrak optical scatter instruments and Climet particle spectrometer (16 channels - 0.5 to 10 μm).

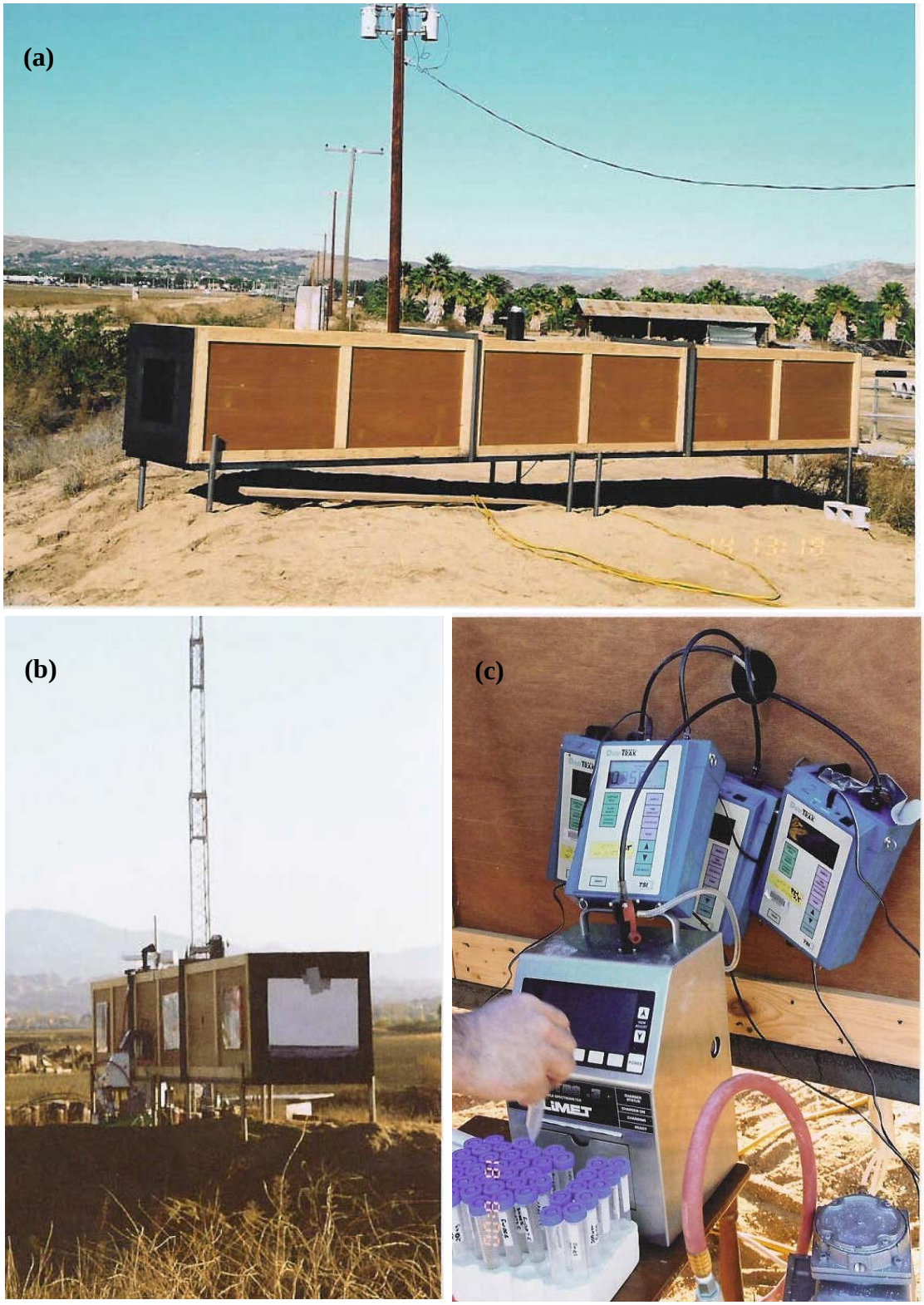

3.0 Results

3.1 Literature Search

3.1.1 Search Results

Tables 3-1 through 3-4 show the key words, database, number of references listed, and the number of applicable references for the respective search. The applicable references are listed below.

Table 3-1. CDL literature search of the Current Contents Data Base

Key Words	# Refs	# App Refs	Ref ID	Comments
Lidar	1266	?		Too large of category
Lidar + Aerosol	141	2	1,2	Local Areas
Lidar + Dust	4	4	1,3-5	Dust plume profiles
Lidar + Fugitive	0	0		
Lidar + Coal	0	0		
Lidar + Plumes	6	0		
Lidar + Particulates	0	0		
Lidar + Profiles	57	1	6	Model application
Lidar + Emissions	7	3	7-9	PM10 Measurements
Lidar + Modeling	11	1	6	Modeling fugitive dust

Table 3-2. CDL Literature search of Melvyl Catalog

Key Words	# Refs	# App Refs	Ref ID	Comments
Lidar	10	0		Too specific for this database

Table 3-3. Internet Search using Google as Search Engine

Key Words	# Refs	# App Refs	Ref ID	Comments
Lidar	142,000	?		Too large of category
Lidar + Aerosol	12,200	?		Too large of category
Lidar + Aerosol + Fugitive	75	3	C1-3	Company Profiles
Lidar + Fugitive + Dust	121	4	C4	Company Profiles
Lidar + Fugitive + Instrumentation	50	5	C1-5	Company profiles
Lidar + Fugitive + Coal	73	1	C4	Company profile

Table 3-4. Literature search of the SPIE Database

Key Words	# Refs	# App Refs	Ref ID	Comments
Lidar	1191	?		Too large of category
Lidar + Aerosol	236	?		Too large of category
Lidar + Dust	14	3	11-13	Applications
Lidar + Fugitive	3	1	11	Coal Dust
Lidar + CEM	1	0		
Lidar + Coal	4	1	11	Coal Dust
Lidar + Plumes	26	0		
Lidar + Particulates	12	8	14,15 20-25	
Lidar + Profiles	169	0		No new pertinent references
Lidar + Emissions	28	0		
Lidar + Modeling	50	0		No new pertinent references
Lidar + Instrumentation	25	1	16	
Lidar + Commercial	50	2	17-18	Commercial Applications

3.1.2 Journal Articles

The applicable references are listed below:

1. Barnaba, F; Gobbi, GP. Lidar Estimation Of Tropospheric Aerosol Extinction, Surface Area And Volume: Maritime And Desert-Dust Cases. *Journal Of Geophysical Research-Atmospheres, Feb 16, 2001, V106(Nd3):3005-3018.*

2. Hoff, RM; Harwood, M; Sheppard, A; Froude, F; Martin, JB; Strapp, W. Use Of Airborne Lidar To Determine Aerosol Sources And Movement In The Lower Fraser Valley (LFV), BC. *Atmospheric Environment, Jul, 1997, V31(N14):2123-2134.*

3. Di Sarra, A; Di Iorio, T; Cacciani, M; Fiocco, G; Fua, D. Saharan Dust Profiles Measured By Lidar At Lampedusa. *Journal Of Geophysical Research-Atmospheres, May 27, 2001, V106(Nd10):10335-10347.*

4. Murayama, T; Okamoto, H; Kaneyasu, N; Kamataki, H; Miura, K. Application Of Lidar Depolarization Measurement In The Atmospheric Boundary Layer: Effects Of Dust And Sea-Salt Particles. Journal Of Geophysical Research-Atmospheres, Dec 27, 1999, V104(Nd24):31781-31792.

5. Karyampudi, VM; Palm, SP; Reagen, JA; Fang, H; Grant, WB; Hoff, RM; Moulin, C; Pierce, HF; Torres, O; Browell, EV; Melfi, SH. Validation Of The Saharan Dust Plume Conceptual Model Using Lidar, Meteosat, And ECMWF Data. *Bulletin Of The American Meteorological Society, Jun, 1999, V80(N6):1045-1075.*

6. Kovalev Va; Moosmuller H. Distortion Of Particulate Extinction Profiles Measured With Lidar In A 2-Component Atmosphere. *Applied Optics, Sep 20, 1994, V33(N27):6499-6507.*

7. Holmen, BA; James, TA; Ashbaugh, LL; Flocchini, RG. Lidar-Assisted Measurement Of PM10 Emissions From Agricultural Tilling In California's San Joaquin Valley - Part I: Lidar. *Atmospheric Environment, Jul, 2001, V35 (N19): 3251-3264.*

8. Holmen, BA; James, TA; Ashbaugh, LL; Flocchini, RG. Lidar-Assisted Measurement Of PM10 Emissions From Agricultural Tilling In California's San Joaquin Valley - Part II: Emission Factors. *Atmospheric Environment, Jul, 2001, V35(N19):3265-3277.*

9. Holmen, BA; Eichinger, WE; Flocchini, RG. Application Of Elastic Lidar To PM10 Emissions From Agricultural Nonpoint Sources. *Environmental Science & Technology, Oct 15, 1998, V32(N20):3068-3076.*

10. Johns C., J., Holmen B.A., Niemeirer D.A., Shumway R.H. Nonlinear Regression For Modeling Censored One-Dimensional Concentration Profiles Of Fugitive Dust Plumes (submitted., *J. Agriculture, Biological, and Environmental Statistics).*

11. Dimarzio, C.A., Emmitt, G.D. Lidar For Continuous Monitoring Of Fugitive Dust *Proc. SPIE Vol. 3534, P. 393-398, Environmental Monitoring And Remediation Technologies, Tuan Vo-Dinh; Robert L. Spellicy; Eds. 2/1999.*

12. Grabowski, J., Skibinski, A. Backscattering lidar can be used in measurements of dust concentration profiles in the atmosphere: a simple procedure *Proc. SPIE Vol. 3104, p. 247-256, Lidar Atmospheric Monitoring, Jean-Pierre Wolf; Ed. 5/1997.*

13. Youmans, D.G., Garner, R., Petersen, K.R. Dust-Cloud Density Estimation Using A Single Wavelength Lidar *Proc. SPIE Vol. 2271, P. 13-28, Industrial Applications Of Laser Radar, Gary W. Kamerman; William E. Keicher; Eds. 9/1994.*

14. Belanger, B., Fougeres, A., Talbot, M. Industrial Site Particulate Pollution Monitoring With An Eye-Safe And Scanning Industrial Fiber Lidar *Proc. SPIE Vol. 4199, P. 67-76, Water, Ground, And Air Pollution Monitoring And Remediation, Tuan Vo-Dinh; Robert L. Spellicy; Eds. 2/2001.*

15. Grabowski, J., Latosinska, M. Evaluation Of A Backscattering Lidar For Measurements Of Air Pollution Concentration Profiles And Particulate Emissions From Single Stacks: Computer Simulations *proc. SPIE Vol. 2506, P. 695-706, Air Pollution And Visibility Measurements, Peter Fabian; Volker Klein; Marus Tacke; Konradin Weber; Christian Werner; Eds. 9/1995.*

16. Pershin, S.M. Trouble-Free Compact Lidar For In/Outdoor Atmosphere Monitoring *proc. SPIE Vol. 2506, P. 428-435, Air Pollution And Visibility Measurements, Peter Fabian; Volker Klein; Marus Tacke; Konradin Weber; Christian Werner; Eds. 9/1995.*

17. Pal, S.R., Hlaing, D., Carswell, A.I., Roy, G., Bastille, C. Scanning Lidar Application For Pollutant Sources In An Industrial Complex *Proc. SPIE Vol. 3504, P. 76-86, Optical Remote Sensing For Industry And Environmental Monitoring, Upendra N. Singh; Huanling Hu; Gengchen Wang; Eds. 8/1998.*

18. Moody, S.E. Commercial Applications Of Lidar: Review And Outlook *Proc. SPIE Vol. 3504, P. 41-44, Optical Remote Sensing For Industry And Environmental Monitoring, Upendra N. Singh; Huanling Hu; Gengchen Wang; Eds. 8/1998.*

19. Husar, R.B., Et.al. Asian Dust Events of April 1998 *J. Geophysical Research, August 27, 2001, V106(ND16):18,317-18,330.*

20. Tratt, D.M., Frouin, R.J. and Westphal, D.L. April 1998 Asian Dust Event: A Southern California Perspective *J. Geophysical Research, August 27, 2001, V106(ND16):18,371-18,379.*

21. Tratt, D.M. and Menzies, R.T. Evolution of the Pinatubo Volcanic Aerosol Column Above Pasadena, California Observed with a Mid-Infrared Backscatter Lidar *Geophysical Research Letters April 1, 1995, V22(N7):807-810.*

22. Philbrick, C.R., Investigations of Factors Determining the Occurrence of Ozone and Fine Particles in Northeastern USA, *Proceedings of Symposium on Measurement of Toxic and Related Air Pollutants,* Air &Waste Management Association, pp 248-260, 1999.

23. Mulik, G.L., G., and Philbrick, C.R. Raman Lidar Measurements of Ozone During Pollution Events, *Advances in Laser Remote Sensing*, Selected papers from 20th ILRC, 10-14 July 2000 in Vichy France, pp 443-446, 2001.

24. Philbrick, C.R. and Mulik, K.R. Application of Raman Lidar to Air Quality Measurements, *Proc. SPIE Conference on Laser Radar Technology and Applications V*, 22-33, 2000.

3.1.3 Industrial References (Designated C1-C5)

C1) ***CNL*** **Miniature Elastic Lidar**

website: http://crocker.ucdavis.edu/CNL/RESEARCH/lidar.html

Funded by the United States Department of Agriculture for studying fugitive dust emissions from agricultural operations (PI, Dr. Robert Flocchini), a new miniature elastic lidar instrument, designed by Dr. William Eichinger (University of Iowa), was hand-built by Drs. Holmén and Eichinger for application to air quality problems. In February 1997, the final stages of building the CNL miniature elastic lidar were completed, the first lidar scans were successfully collected, and hardware and software testing began. The CNL miniature elastic lidar is a compact, field portable instrument with full scanning capabilities.

C2) ***Spectral*** **Scanning Lidar**

website: http://www.spectral.ca/products/scanlidar/scanlidar.htm

Spectral is developing a mobile scanning lidar to map aerosol concentrations in the atmosphere in 3D. It will measure dust diffusion from demolition sites, track pollution plumes from smokestacks, and monitor air quality in residential areas. This self-contained system is mounted in a cube van for rapid deployment to your work site

C3) ***STC*** **Lidar**

website: http://users.erols.com/nbcgroup/science.htm

For the U.S. Army Chemical Biological Defense Command (CBDCOM), STC conducts the development and evaluation of standoff detection systems, including lidars and microbiological detection systems, for chemical and biological agents. This support involves test and evaluation (test planning, operations, analyses, and documentation), design and fabrication, simulation and modeling, tradeoff analyses, and effectiveness assessment. Since 1982, STC has supported the conduct of dust, smoke, and chemical field experiments using tracers, biological or chemical agent stimulants, military smokes/obscurants, and dust at test ranges in the Unites States (12 tests), NATO countries (two tests), and at sea (two ship cruises) in diverse natural environmental conditions

C4) ***SWA*** **Portable LAser for Coal Emissions Mapping (PLACEM)**

website: http://www.swa.com/coal/placem.htm

Since 1983, Simpson Weather Associates has been funded by many sources as NASA, NOAA, U.S. DoD, CNRS, Lockheed, and General Electric. These major sources provided funding to develop simulation models for space-based and airborne Doppler lidar wind measuring systems. This resulting in instrumentation, a Portable LAser for Coal Emissions Mapping (PLACEM), which is a scanning lidar for producing spatial images of airborne particulate concentrations in a continuous mode. It is a high power, eye-safe, scanning, pulsed laser with a highly sensitive detector measuring the reflected light from particulate matter in the air. PLACEM has a major application in the coal industry as an instrument to map fugitive dust emissions within a complex industrial setting. Data collected over a period of time is then used to prioritize control measures.

***C5) Optech* Scanning Lidar Systems**

website: http://www.optech.on.ca/aboutoptech.htm

Optech is a high-tech company specializing in manufacturing laser-based ranging and detection systems. They have been in business for 25 years, moving from a research and development base into a company that manufactures and integrates its own commercial products for a worldwide market. Throughout their 25 years they have concentrated in the area of laser radar (lidar) applications. Optech designs and manufactures custom scanning lidar systems that detect, measure and track the atmospheric elements listed below.

- Smoke effluents
- Man-made dust
- Volcanic eruptions
- Storms

They are currently concentrating on air- and space-based systems that provide global atmospheric monitoring

3.1.4 Discussion

From a review of the titles it is clear that although work has been done using Lidar-based techniques for evaluating fugitive dust there is actually very little real data available and presently there is merely discussion on the potential of the technique. The key is to establish dispersion models based on the lidar data so that both quantitative and qualitative data can be taken. It is clearly an area where there is interest in developing commercial applications.

Pertinent information summarized from the above references of the Lidar techniques are listed below with the appropriate reference.

1) That with the rapid profiling response times of the lidar, plume dynamics and PM10 fluxes can be described in detail. *(References (6), (7), (8) and (C1))*

2) It has also been shown that the lidar is capable of producing very detailed maps of PM distribution across an agricultural operation. *(References (6) and (7))*

3) Particulate matter directly emitted and re-suspended by vehicles traveling on both paved and unpaved roads has also been studied with some success. *(References (C1) and (C2))*

4) The lidar data together with detailed traffic counts and vehicle identification data can be employed with time series methods to investigate the relative contributions to ambient PM2.5 of cars and trucks. *(References (C1), (C2) and (C5))*

5) Direct-detection lidar has been demonstrated to be useful in locating probable sources of aerosol pollutants, and to some extent characterizing their density in a qualitative manner. *(References (11) and (12))*

6) To produce quantitative information of aerosol or fugitive dust measurements with lidar. the data must be combined with a dispersion model. This has been done for coal dust. *(Reference (11))*

7) Layers of smoke from upwind forest fires have been investigated using lidar techniques. *(References (C1) and (C4))*

8) Lidar observations from the Lidar-in Space Technology Experiment were used to examine the Saharan dust characteristics including its structure, evolution and optical depths over Western Africa and E. Atlantic regions. The lidar backscatter profiles revealed a complex structure of the dust layer but, in general, show a good agreement with the features depicted in the conceptual model of the dust plume. *(References (3) and (5))*

9) It has been shown that recently developed iterative procedures retrieve a plume dust concentration profile with a reasonable accuracy when applied to lidar-based data. *(References (12) and (15))*

10) Multi-wavelength lidar sounding across a stack plume has been computer simulated. The lidar data were then inverted using four different procedures resulting that these inversions were dependent on both: dust particle size dispersion and mass concentration. *(References (15))*

11) The passage of commercial and military aircraft through invisible fresh volcanic ash clouds has caused damage to many airplanes. The Defense Nuclear Agency is currently developing a compact and rugged lidar under the Aircraft Sensors Program to detect and estimate the mass density of nuclear-explosion produced dust clouds, high-explosive produced dust clouds, and fresh volcanic dust clouds at horizontal distances of up to 40 km from an aircraft. *(Reference (13))*

The INO (Institute National Optique of Quebec, Canada) has developed an Industrial Fiber Lidar (IFL). It enables the particulate pollution monitoring on industrial sites. More particularly, it has been used to take measurements of particulate concentration at Port Facilities of an aluminum plant during boat unloading. The lidar measurements have been compared to high volume samplers. Based on these comparisons, it has been established that the IFL is able to monitor the relative fluctuations of dust concentrations. It can be integrated to the process control of the industrial site for alarm generation when concentrations are above threshold. *(References (14))*

12) A relatively simple eye-safe compact GaAlAs lidar with solid state elements for the indoor/outdoor detection of aerosol/dust pollution layers and measuring its range and height has been developed and tested. In active operation mode the lidar produces the backscatter coefficient profiles within a hundred meters and estimates of atmosphere turbidity over the road. *(References (16))*

13) An application of lidar's data for the model tuning in situ is to predict heavy toxic aerosol plume spreading from low sources over the city building or the territory with complex terrain. *(References (12) and (16))*

14) Vertical profiles of optical extinction can be obtained in the through the troposphere using Raman lidar techniques. *(References (22) through (24))*

15) A lidar campaign for aerosol and smoke plume studies was carried out in collaboration with the Ministry of Environment of the Province of Ontario at the industrial complex in the city of Hamilton. The aim of the study was to apply lidar remote sensing to measure simultaneously emissions from different sources and determine the potential of lidar for tracking and differentiating plumes from various industrial processes. This study was carried out with the scanning lidar system of the Canadian Defense Research Establishment and was successful in mapping effluent plumes in 3-D from a range of over 5 km targeting major individual industrial sites. To understand the dynamic behavior of plumes, time series scans were required which are a key to determining sources of

Black Fallout and fugitive emissions that deposit particulate matter in the Hamilton area. *(References (17) and (C5))*

3.2 Pilot Study Results

3.2.1 Study Period

- Prestudy Background Meteorological Data

The background meteorological sensor was set up on 13 November 2000 at the location shown in Figure 2-3. Hourly data were collected at the site until approximately 0900 hours on 13 December 2000, when its data acquisition was switched to ten-second averaging time. Data were collected continuously at the background site until it was demobilized at 1300 hours on 18 December 2000.

- Pilot Study Dust Generation and Measurements

The dust generation and measurement instruments were set up on 13 December 2000. Measurements were made from 13 to 16 December 2000. Dust was generated and monitored for a total of 22 test periods. Ten-second average meteorological measurements, tracer gas releases and sampling, digital and video camera measurements, and lidar measurements were made during these test periods.

3.2.2 Dust Generation Tests

Dust was generated and monitored for a total of 22 test periods. These included 11 tests with sieved indigenous soil, 4 tests with the white paint pigment powder, 5 tests with vehicle-generated dust, and 2 tests with the fog generator. Table 3-5 summarizes the test activities and the time periods that those activities were performed. Appendix A gives a full description of events.

Table 3-5. Test activities log.

Event	Date	Start Time (hr:mn:sec)	Duration of Release (min:sec)	Release (Kg)	Dust Generation Material
1	12/13/2000	15:08:05	0:05	0.54	Sieved indigenous soil
2	12/13/2000	16:31:00	0:50	5.50	Sieved indigenous soil
3	12/14/2000	10:55:00	1:10	5.00	Sieved indigenous soil
4	12/14/2000	11:40:00	0:50	5.00	Sieved indigenous soil
5	12/14/2000	12:11:00	12:29	22.00	Sieved indigenous soil
6	12/14/2000	14:59:30	1:10	4.42	White paint pigment powder
7	12/14/2000	15:15:30	2:45	5.04	White paint pigment powder
8	12/14/2000	15:46:00	3:15	4.66	White paint pigment powder
9	12/14/2000	16:11:00	1:10	5.00	Sieved indigenous soil
10	12/14/2000	16:31:00	1:30	5.00	Sieved indigenous soil
11	12/14/2000	16:55:00	1:30	5.00	Sieved indigenous soil
12	12/14/2000	17:21:00	1:30	5.00	Sieved indigenous soil
13	12/14/2000	17:45:00	1:30	5.00	Sieved indigenous soil
14	12/15/2000	11:48:00	1:30	1.50	Sieved indigenous soil
15	12/15/2000	12:02:00	1:00	1.45	White paint pigment powder
16	12/15/2000	12:13:00	~20 sec		Suburban; drove around upwind of tower
17	12/15/2000	14:18:00	~20 sec		Suburban; 50 meter line source
18	12/15/2000	14:32:00	~20 sec		Suburban; down/back over 50 meter line (N-S)
19	12/15/2000	15:14:00	~20 sec		Suburban; 150 meter line (E->W)
20	12/15/2000	15:25:00	1:00		one minute "fog" release
21	12/15/2000	15:30:00	1:00		one minute "fog" release
22	12/16/2000	12:15:00	~20 sec		Suburban; N->S line release

Although the winds were out of the west, directing the plumes eastward from the fixed location dust generating station toward the downwind monitoring tower, minor variations in the wind direction resulted in very infrequent impacts of the dust plumes on the tower.

Test #2 on 12/13/2000 was a release of 5.5 kg of sieved indigenous soil over a 50-second period. The first set of particulate matter filter samples was collected during this event. Figure 3-1 presents the 10-second average DustTrak™ data and the mass concentration determined from the filter data for the period. Figure 3-1 shows no indication of plume impact on the downwind tower (which supported visual observations during the event).

The second set of filter samples was collected during Test #5 on 12/14/2000. During Test #5, 22 kg of sieved indigenous soil was steadily placed into the blower over an 18-minute period. The 10-second average DustTrak™ data and the mass concentration determined from the filter data for the period are presented in Figure 3-2 for this event. The DustTrak™ data show that there were about five periods, less than one minute each, when the plume impacted the downwind tower. The limited data set shown in Figure 3-2 indicates that the plume's maximum concentration was at 5 meters, followed by the 10-meter height, with a minor concentration change at the 2-meter height. These data also show a greater percentage of the particulate mass in the coarse size fraction (2.5- to 10-micron aerodynamic diameter) as opposed to the fine size fraction (i.e. $PM_{2.5}$).

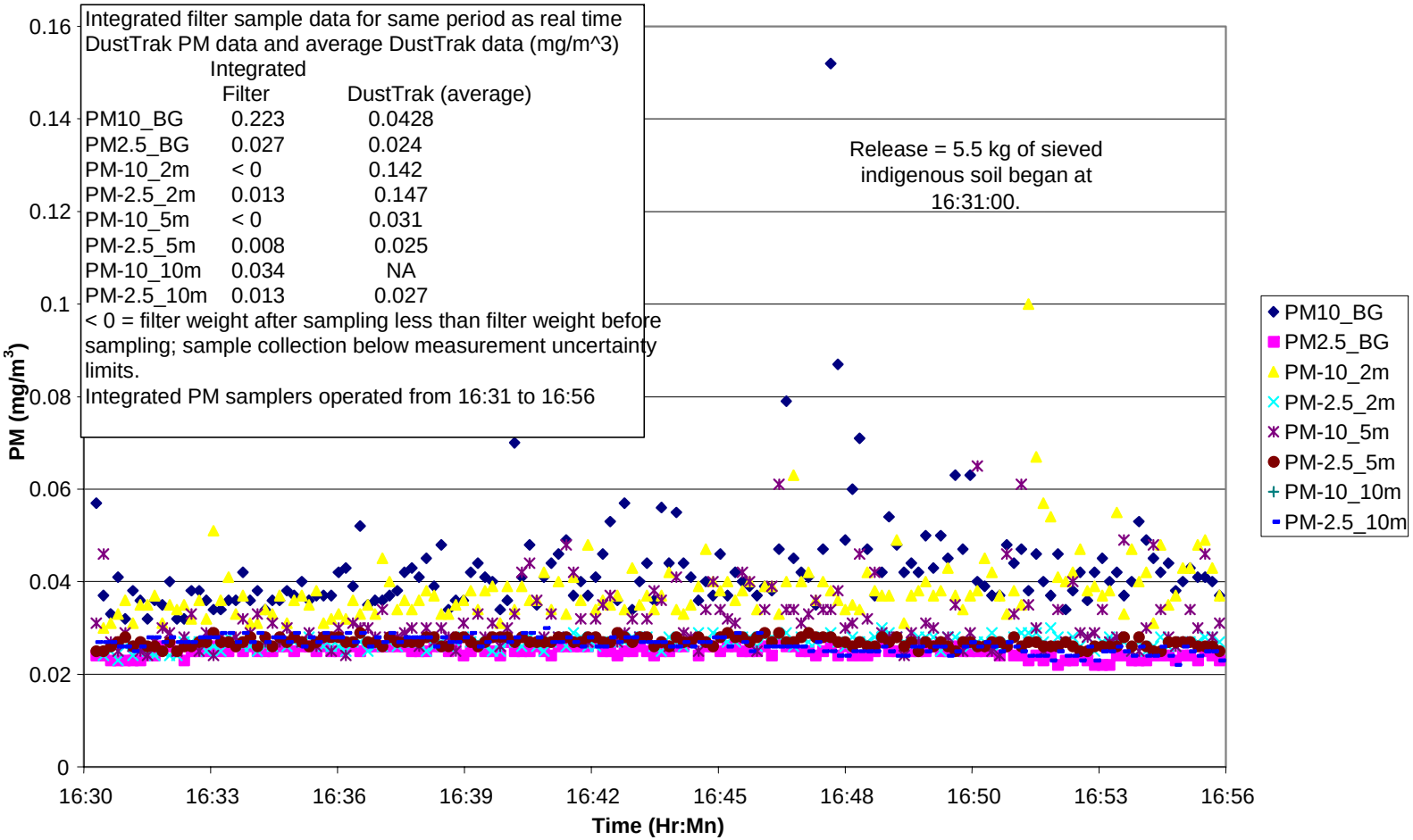

Figure 3-1. Time series plot of real time PM data and filter PM data for Test #2 on 12/13/2000.

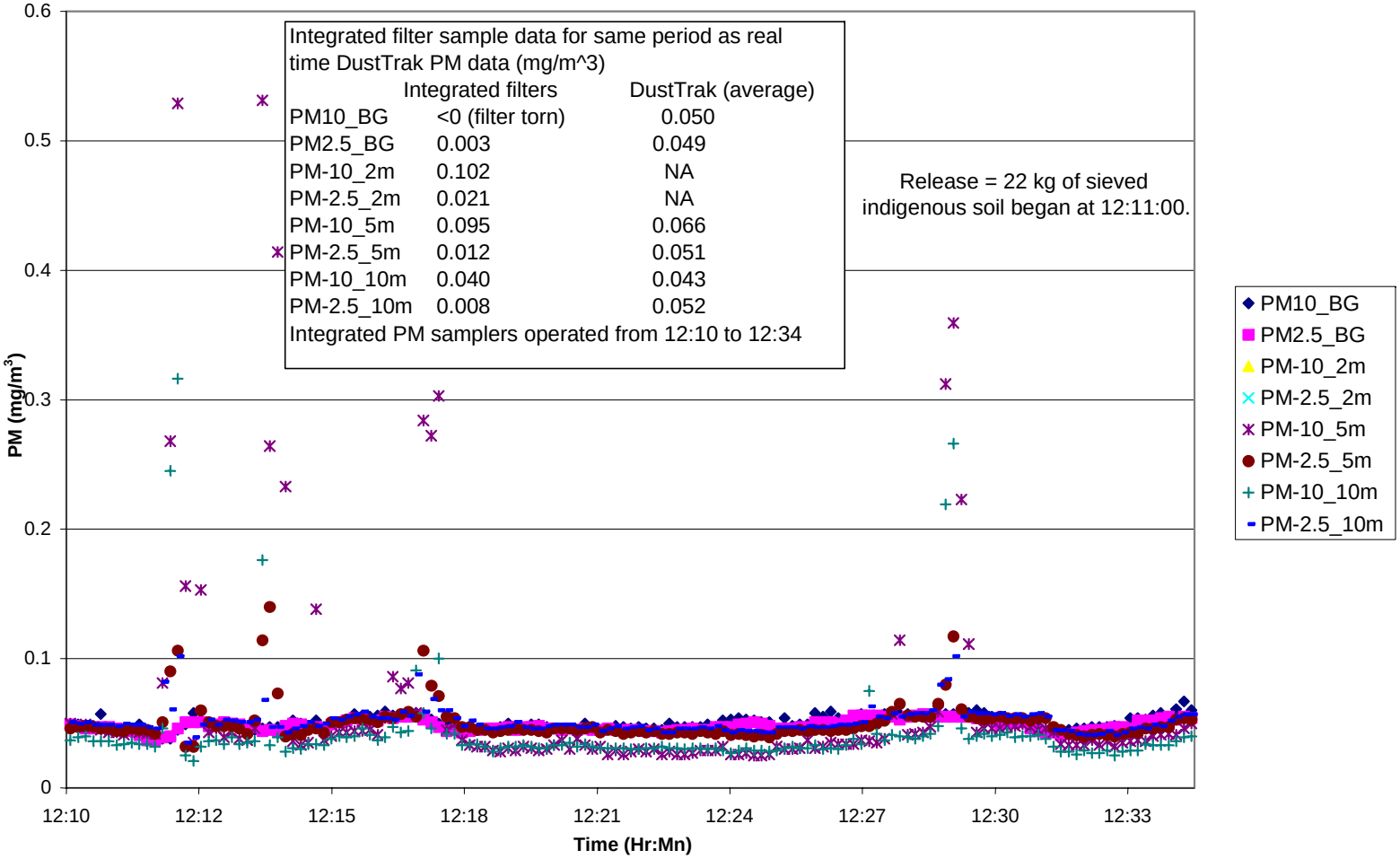

Figure 3-2. Time series plot of real time PM data and filter PM data for Test #5 on 12/14/2000.

The third and final set of filter samples was collected during Test #22 on 12/16/2000. For this event, the dust plume was generated from driving a vehicle on the field. An observer at the downwind tower directed the driver to a location that resulted in significant plume impact at the downwind site. Figure 3-3 presents the 10-second average DustTrak™ data and the mass concentration determined from the filter data for this event. The figure shows that the PM_{10} mass was significantly greater than the $PM_{2.5}$ mass for this event. It can also be seen in both the DustTrak™ and filter analysis data for this event that the highest impact was at the 2-meter height, followed by the 5- and 10-meter heights, respectively.

The validated 10-second DustTrak™ data for all 22-test periods, along with the meteorological and tracer gas data are contained in a single spreadsheet. A description of this spreadsheet data set is provided in Appendix B.

3.2.3 Hourly Meteorological Data

The ten-second meteorological data collected from the background (except for the wind direction fluctuation parameter, $\sigma\theta$, were averaged into hourly averages. These data were combined with the hourly average data collected from 11/13 to 12/13/2000. A description of these data is presented in Appendix C. Table 3-6 is a summary of the wind conditions for the approximately one month period that these data were collected:

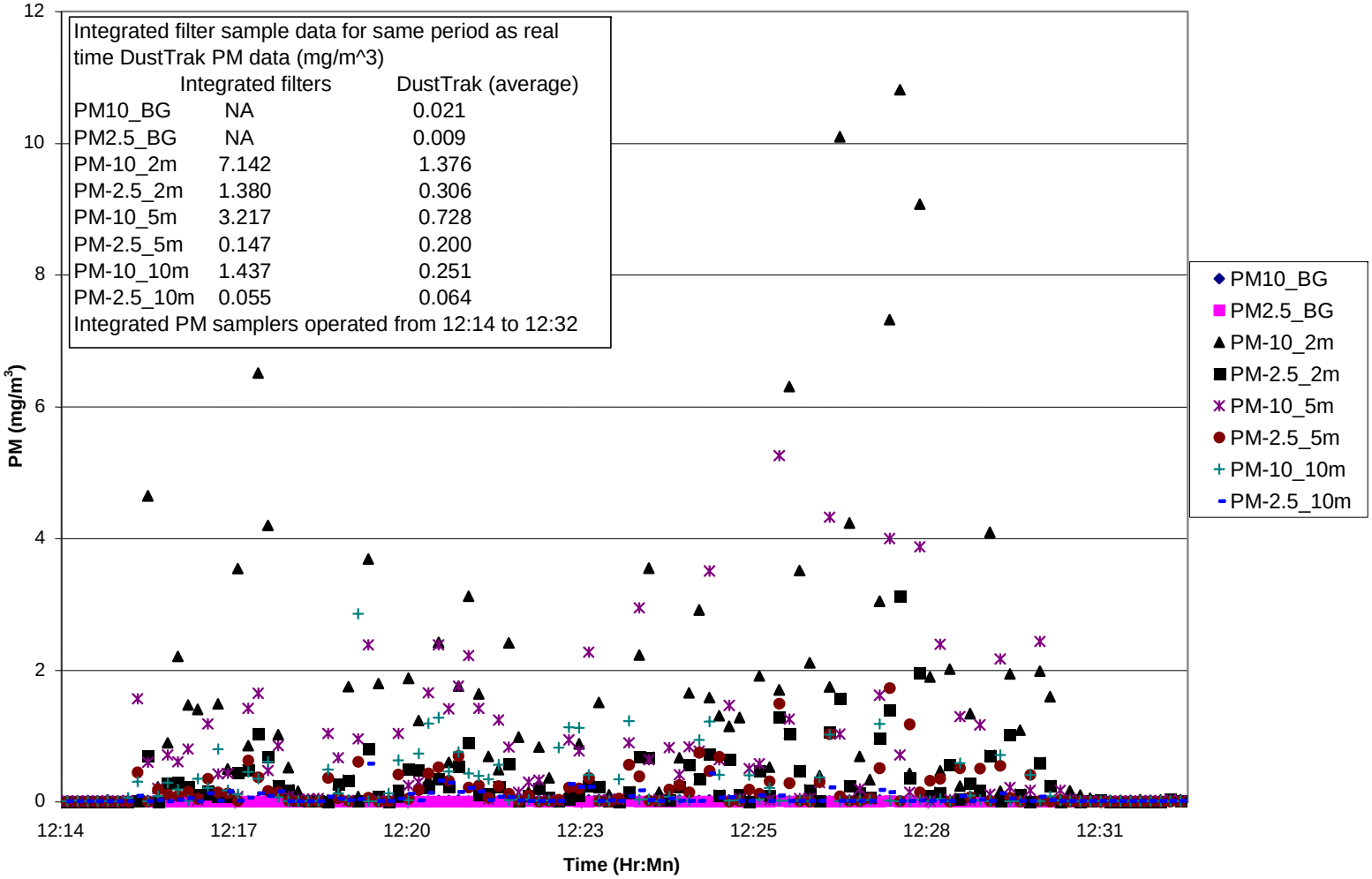

Figure 3-3. Time series plot of real time PM data and filter PM data for Test #22 on 12/16/2000.

Table 3-6. Summary of hourly meteorological data.

	WS (m/Sec)	WD (Deg)	σθ (Deg)	T (°C)	DP (°C)
Minimum	0.5	NA	5.6	0.3	-9.8
Maximum	8.6	NA	101.5	28.5	15.2
Average	2.0	West	42.9	13.8	4.5
Median	1.5	NA	38.5	13.6	5.0
No. of Hours	840	840	716	840	840

3.2.4 10-Second Meteorological, Particulate Matter, and Tracer Data.

The data loggers were programmed to collect data at a rate of 1 hertz and to process these data into 10-second averages for the four-day period of the pilot study that dust was generated. Data for all of the meteorological sensors, tracer gas analyzer, and the real time particulate samplers were collected at this sample rate during study. The data were processed, validated and output into a single spreadsheet. Appendix B presents a description of the spreadsheet format and data.

Figure 3-3 presents the 10-second data for one dust generation and monitoring Test #22. For this event, dust was generated via driving a vehicle in close proximity to the downwind monitoring tower. For this period the wind direction and speed appeared to be relatively constant. However, minor variations in the winds during this period did make it very difficult to direct the vehicle so that its plume impacted the downwind monitoring tower. As shown in Figure 3-3, the dust from the plume only sporadically impacted the tower during the several minutes that the dust was generated.

Tracer gas was released at a rate of 400 grams per hour on 12/14/2000 between 11:33 and 18:00. The tracer gas was released from the fixed dust generation location and monitored at a single point 2-meters in height 100 meters downwind on the main monitoring tower. Figure 3-4 is a time series plot of the 10-second average SF_6 concentration monitored at that location. These data, which were typical of all the study days (except when the Santa Ana winds were present), show the difficulty of trying to use a point source monitor to determine dispersion, dilution, or any other parameters about a point source release at the 100-meter "close range" distance in this study. (There were no usable tracer data obtained when the Santa Ana winds were present.)

The dilution factor, Ψ, where:

> Ψ = (μg/m^3 of SF_6 detected) / (g/sec of SF_6 released) at a monitoring location 100 meters from the release point

were calculated and also plotted on Figure 3-4 of the December 14, 2000 data. As can be seen on the plot, Ψ varied from 0.5 (reflective of the 10 ppt lower detection limit of the SF_6 analyzer) to over 1800 (reflective of the approximately 33,500 ppt upper detection limit of the SF_6 analyzer).

The tracer gas release rate was decreased to 200 grams per hour for subsequent study days to minimize or eliminate driving the tracer analyzer to full scale. However, the tracer data were still detected in the same sporadic manner on these subsequent study days.

3.2.5 Soil Sample Analysis

An aliquot from each of three sieved indigenous soil piles and one aliquot of the white paint pigment powder used for the dust generation were collected and analyzed for percent sand, silt and moisture. A sample of the "fine dust" found deposited on the rear bumper of the vehicle used for dust generation was also collected and analyzed. The results from these analyses are shown in Table 3-7. The analysis found about 3.5% moisture in the sieved indigenous soil, 1.5% moisture

in the fine powder that deposited on the rear bumper of the dust generation vehicle and no moisture present in the white paint pigment powder. The percentages of sand, silt and clay for the samples are also presented in the table.

Referring to the approximate particle diameters for sand (25-50 μm and larger), silt (2-30 μm) and clay (<2 μm) presented in Section 2.2.2.10, it can be seen that there was approximately the same potential amount (2-6%) of $PM_{2.5}$ mass in the sieved indigenous soil and white paint pigment. The white paint pigment had most of its mass in the 2-30 μm range. The mass of the sieved indigenous soil was split fairly even between the sand and silt size fractions.

Table 3-7. Analysis of soils used for dust generation.

Sample Identification Sample Date	Analysis Method	SOIL-1 12/13/2000	SOIL-2 12/14/2000	SOIL-3 12/14/2000	SOIL-4 12/14/2000	SOIL-5 12/15/2000
Sample Source/Description		Sample of sieved indigenous soil used for generation on 12/13	Sample of sieved indigenous soil used for generation for 12/14 morning runs	Sample of sieved indigenous soil used for generation for 12/14 late-morning runs	Sample of "white powder" (CaCO3 paint pigment) used for four dust generations on 12/14-15	Sample of silt deposited on rear bumper of vehicle after use of vehicle to generate dust on 12/15
		Percent	Percent	Percent	Percent	Percent
Total Solids	EPA 160.3	96.5	96.6	96.6	100.0	98.5
Soil Moisture	Drying	3.5	3.4	3.4	0.0	1.5
Sand	ASA 43-5	46.0	46.0	46.0	8.0	34.0
Silt	ASA 43-5	52.0	52.0	50.0	86.0	62.0
Clay	ASA 43-5	2.0	2.0	4.0	6.0	4.0

3.2.6 Collocated DustTrak Quality Control Procedures.

The eight DustTraks™ were collocated at the field site for two periods, 12/15/2000 10:00-11:00 and 12/16/2000 10:00-11:00. Time series plots for these two quality control runs are presented in Figures 3-5 and 3-6. To better identify differences, these quality control data were split into one set for the four PM_{10} samplers and a second for the four $PM_{2.5}$ samplers. Using the upwind PM_{10} and $PM_{2.5}$ samplers as the "reference" samplers, the normalized differences were calculated using the following equation for each size fraction:

$$\text{Normalized Difference} = [(\text{Downwind sampler})_i - (\text{Reference sampler})] / (\text{Reference sampler})$$

Plots of these differences for each 10-second averaging period are shown for the PM_{10} and $PM_{2.5}$ samplers in Figures 3-7 and 3-8, respectively.

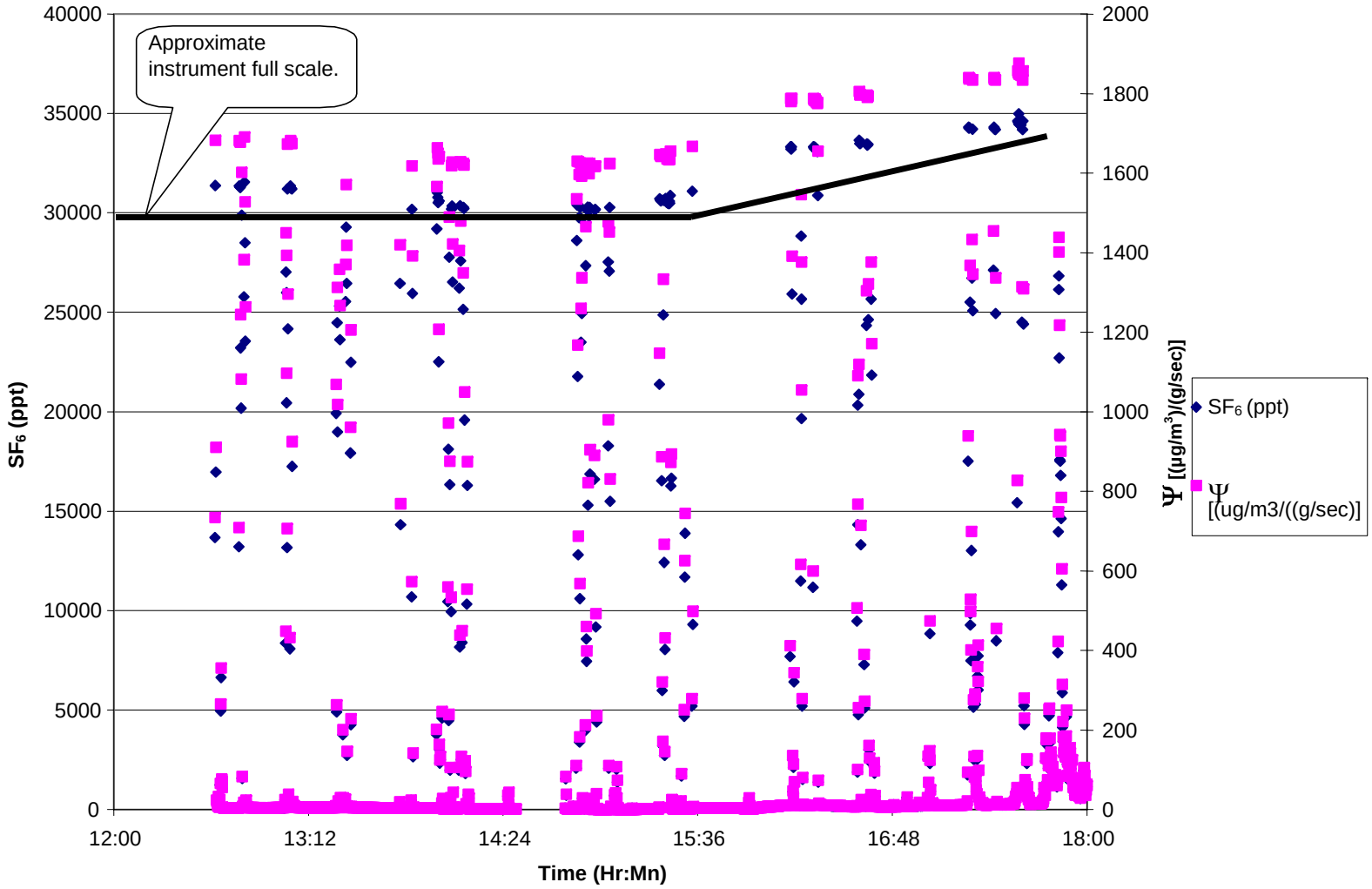

Figure 3-4. Time series of SF_6 tracer data for 12/14/2000.

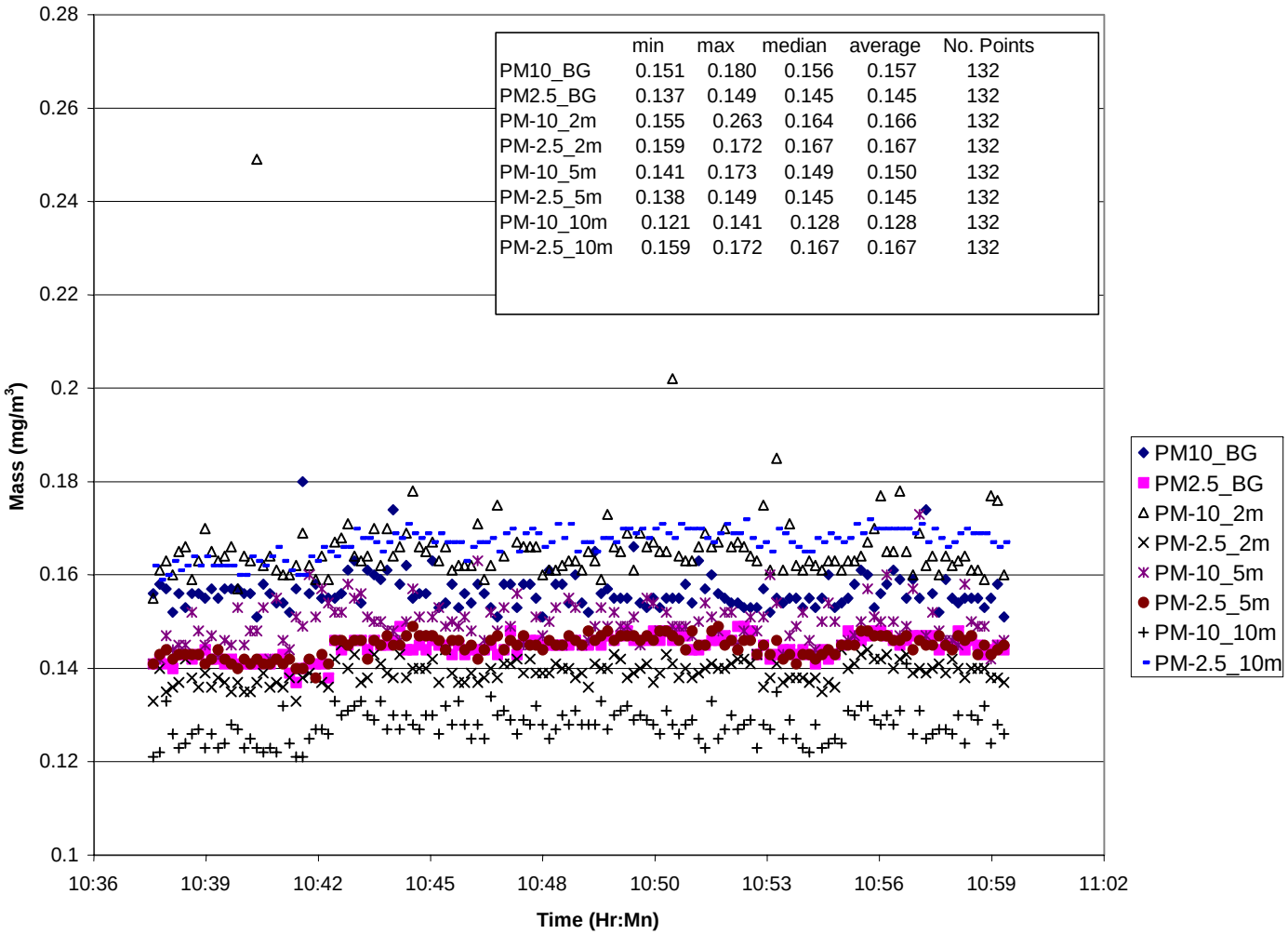

Figure 3-5. Time series of collocated DustTrak data obtained on 12/15/2000.

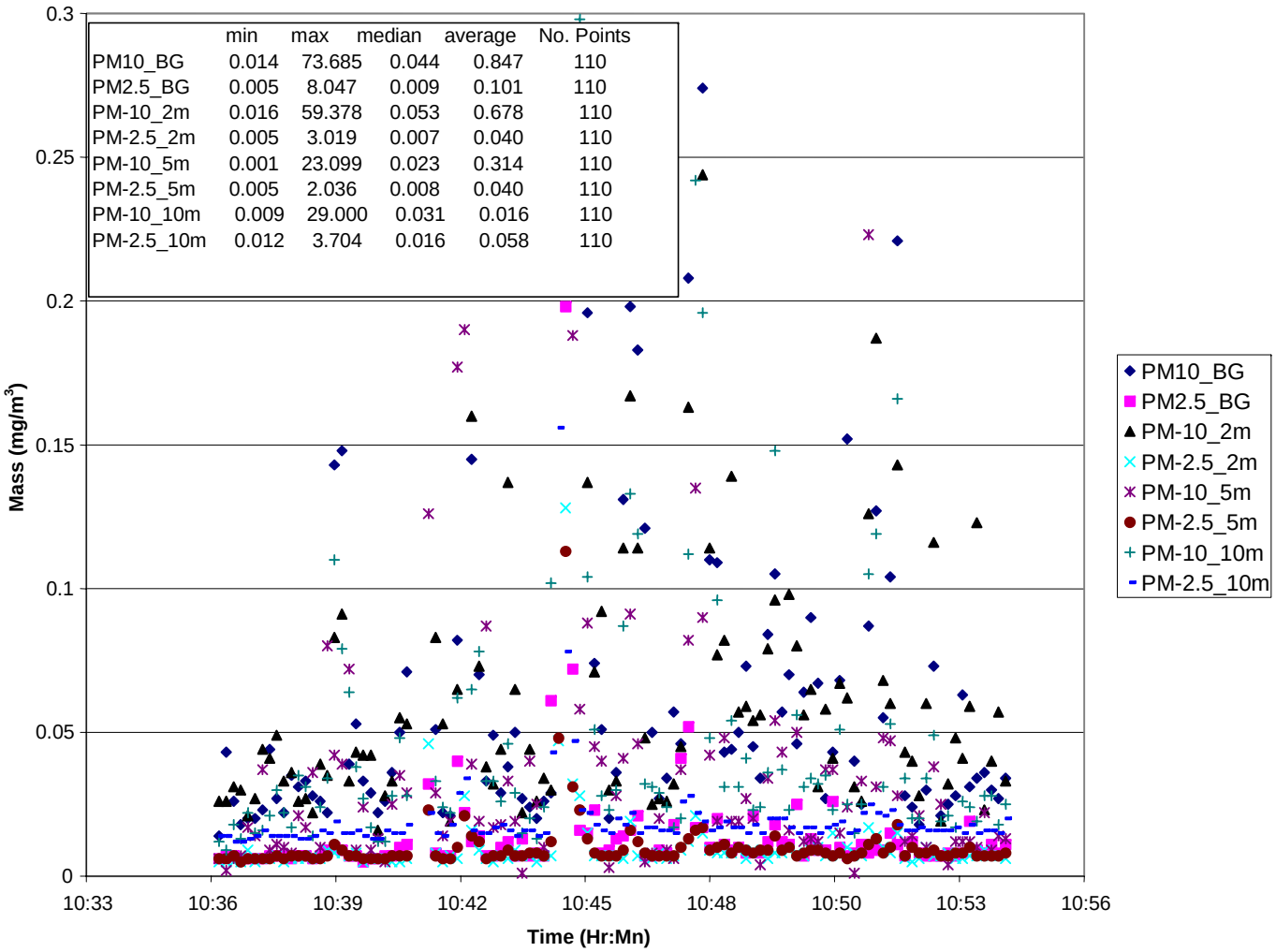

Figure 3-6. Time series of collocated DustTrak data obtained on 12/16/2000.

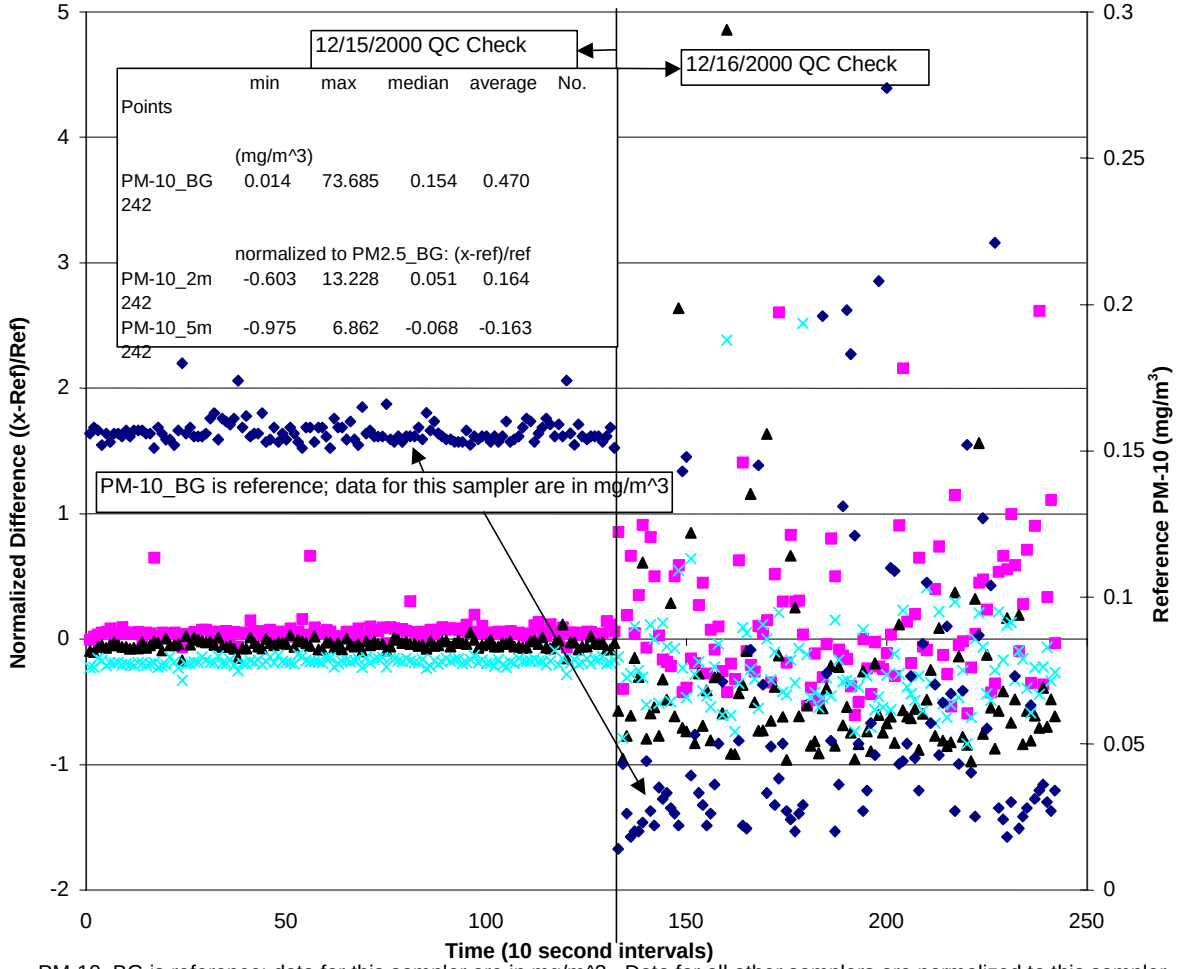

PM-10_BG is reference; data for this sampler are in mg/m^3. Data for all other samplers are normalized to this sampler.

Arbitrarily choosing the background PM_{10} sampler as the reference sampler, the normalized difference was calculated as:

Normalized Difference = [(Downwind sampler)I – (Reference sampler)] (Reference sampler)

This result (y-axis value) is plotted on the graph for each of the three downwind samplers for the ~130 ten-second sampling periods used for the 12/15 comparison and ~120 ten-second sampling periods used for the 12/16 comparison.

Figure 3-7. Plot of real time PM_{10} sampler QC data normalized to the background PM_{10} sampler.

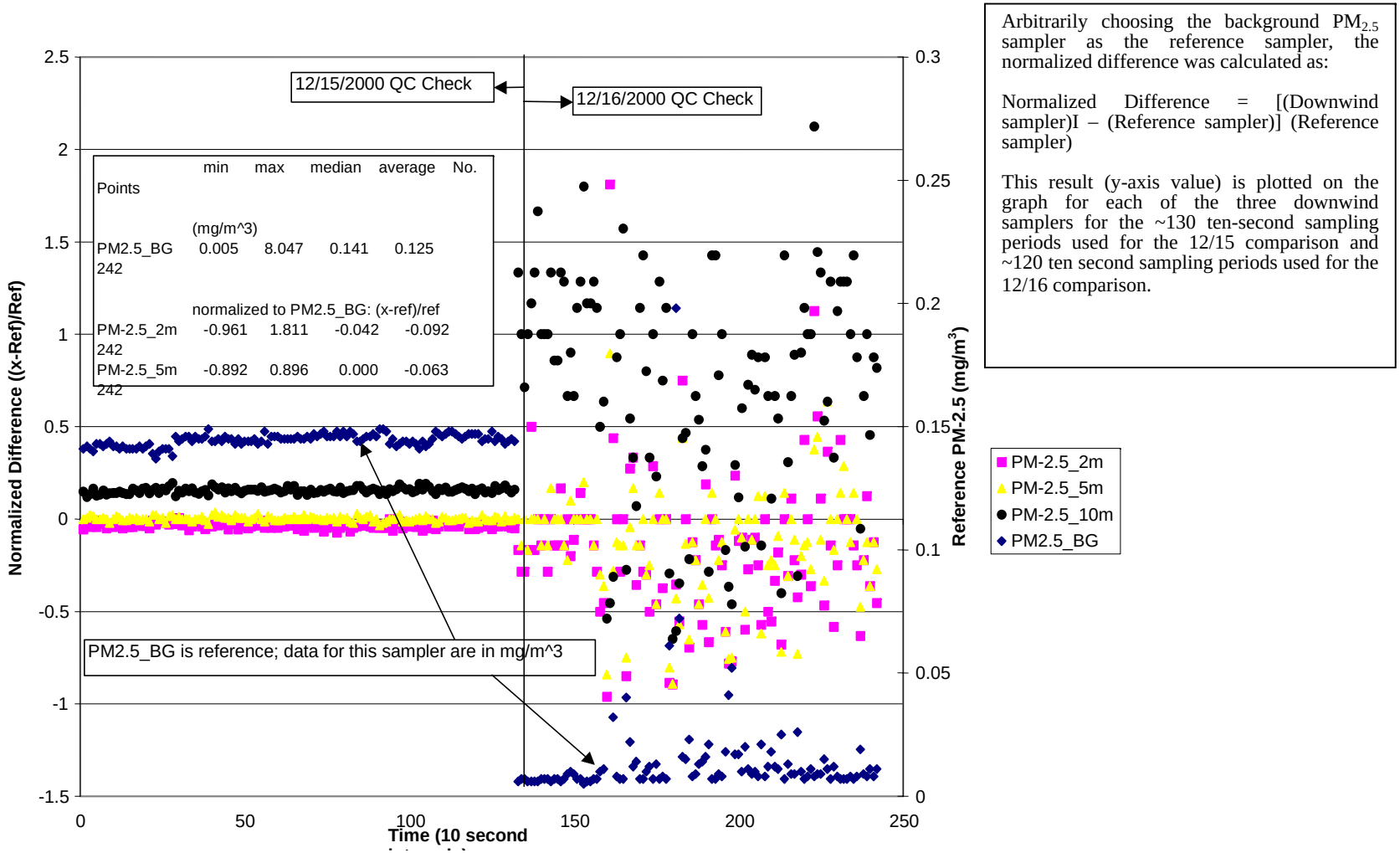

Figure 3-8. Plot of real time $PM_{2.5}$ sampler QC data normalized to the background $PM_{2.5}$ sampler.

The significant differences between the 12/15/2000 and 12/16/2000 testing was due to the differences in the prevailing ambient aerosol between the two days. On 12/15/2000, fairly steady one meter per second (m/s) west winds were present. On 12/16/2000, a Santa Ana condition had developed, resulting in strong and variable winds. During the 12/16/2000 collocated check, the average wind speed was 5.6 m/s out of the east. The average difference between the "reference" samplers and the other three samplers were 0.164 to 0.197 mg/m^3 and –0.092 to 0.408 mg/m^3 for the PM_{10} and $PM_{2.5}$ samplers respectively.

The significant differences in meteorological and airborne dust levels for the two collocated periods allowed both a check of the instruments relative response and errors (12/15/2000 QC check) and additional assessment of instrument uncertainties due to other variables, possibly including response times.

3.2.7 Lidar Results

The scanning lidar provides a unique opportunity to detect the distribution and evolution of airborne particulate matter. The optical signal from backscatter lidar is the most sensitive way of detecting the airborne particulates because the scattered signal has the optimum relationship between the wavelengths (ultraviolet, visible and near infrared) and the particle sizes of interest (0.1 – 20 μm). The Pilot Study ultimately lead to the formulation of an empirical model which were able to predict various characteristics of dust including the settling rate, dispersion and effect of prevailing meteorological conditions on the distribution and the airborne lifetime. The purpose of the pilot study is to obtain lidar data on locally generated dust to examine analysis techniques and to prepare measurement plan for the Main Study. Only a few examples are shown to show examples of the results obtained and for use in drawing some of the conclusions.

3.2.7.1 *Imaging Analysis of Dust Plumes*

Figure 3-9 shows the lidar instrument with the digital video camera mounted on top is observed in the foreground. The dust generation equipment is located about halfway between the lidar and the measurement tower, as shown in Figure 2-8. The lidar was used to automatically make horizontal scans of the test volume and the elevation angle could be adjusted manually. A total of 22 tests were conducted with lidar and digital charge-coupled device (CCD) data collected for each test.

The digital CCD camera provides a useful documentation of the sequence of events during a test period. Figure 3-10 shows the time sequence of CCD images at 30-second intervals for one of the tests. The documentation shows the early evolution of the cloud and provides an indication of the pointing position of the lidar. Information on the location and spatial extent of the dust cloud can be extracted from the images. In Figure 3-11, the result from use of scene extraction techniques is shown. The image obtained with a digital camera was analyzed by removing the background scene by subtracting, pixel by pixel, a background image obtained just before generating the dust plume. After scene extraction is applied, only the signal due to the dust plume is left. The spatial dimensions indicating growth or drift of the cloud can be extracted. It is also possible to determine the optical depth of the cloud relative to the background scene at times and locations where the path is not optically thick. This figure gives some indication of the way in which the digital images can be used to determine dispersion rates, but even then the question of whether the change in signal is primarily governed by changing size or by changing number is undetermined. Imaging measurements therefore have some general utility but it remains for the lidar techniques to separate the settling out of the larger particles from the changing density as the particles diffuse into a larger volume.

Figure 3-9. The lidar with digital camera observed in foreground scans dust cloud generated by a blower, a 10 m tower is located directly behind the generator and the target board can be seen in front of trees on the far left.

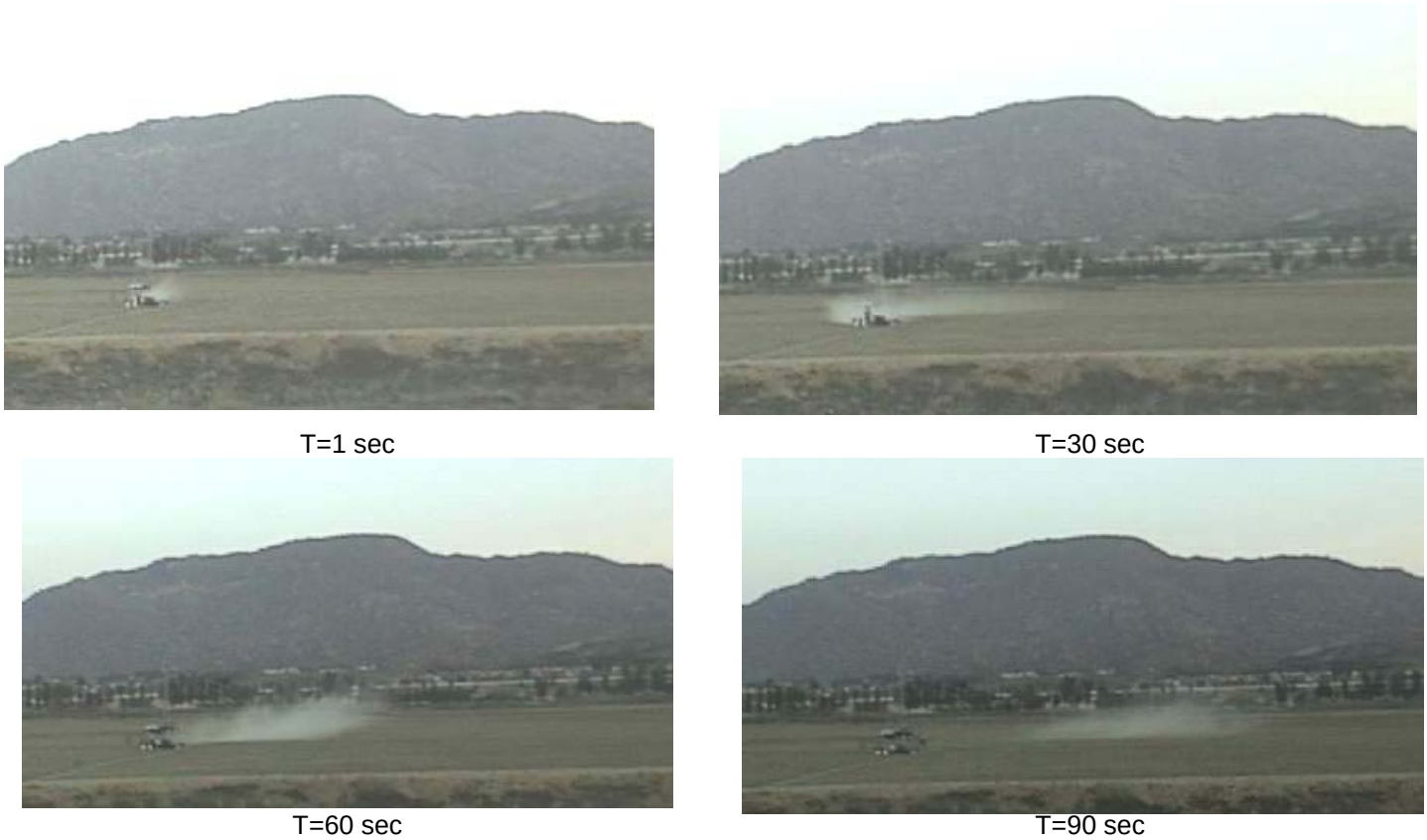

Figure 3-10. A set of the digital images selected from Test #2 to illustrate the growth of a dust cloud using the imaging data.

Figure 3-11. Test 18 (12/15/2000 14:30) generate dust with vehicle, this is time sequence of CCD images along with the corresponding background removed images. (a) 14:31:37 (b) 14:32:36 (c) 14:32:49 (d) 14:33:14

3.2.7.2 *Lidar Measurements of the Generation and Evolution of Dust Plumes*

The plumes were generally tracked with the lidar out to 1 km along the path and on radials, which were swept up to ±30º horizontally. The plumes probably could have been tracked much longer, at least along some radials, up to the lidar's maximum range of 20-30 km. Because it was more desirable to obtain data over shorter distances for the pilot study, tracking of plumes was stopped at about 1.5 km.

Figure 3-12 shows vertical profiles obtained for the visible and near infrared (NIR) channels when the instrument was pointed on an elevation angle of 70°. The data have been range-corrected for $1/R^2$ (where "R" is the distance from the lidar to the measured plume) dependence, but no other corrections have been applied. Therefore, the telescope form factor is quite noticeable. The top of the planetary boundary layer (PBL) is clearly evident in both the visible and NIR channels. The visible signal is large compared with the NIR signal, and we would expect that most of the contribution to the scattering is by small particles. The shape of the vertical scattering profile is that expected for a well-mixed atmosphere that is relatively clean. The increase in the signal versus altitude is due to two factors, the telescope form factor and the fact that the particles grow larger as the temperature decreases versus altitude. The increase in relative humidity as a function of altitude causes growth in the size of the particles, and since the optical scattering increases approximately with R^6 (where "R" is the radius of the particle) for small particles, we expect to observe more optical scattering toward the top of the boundary layer.

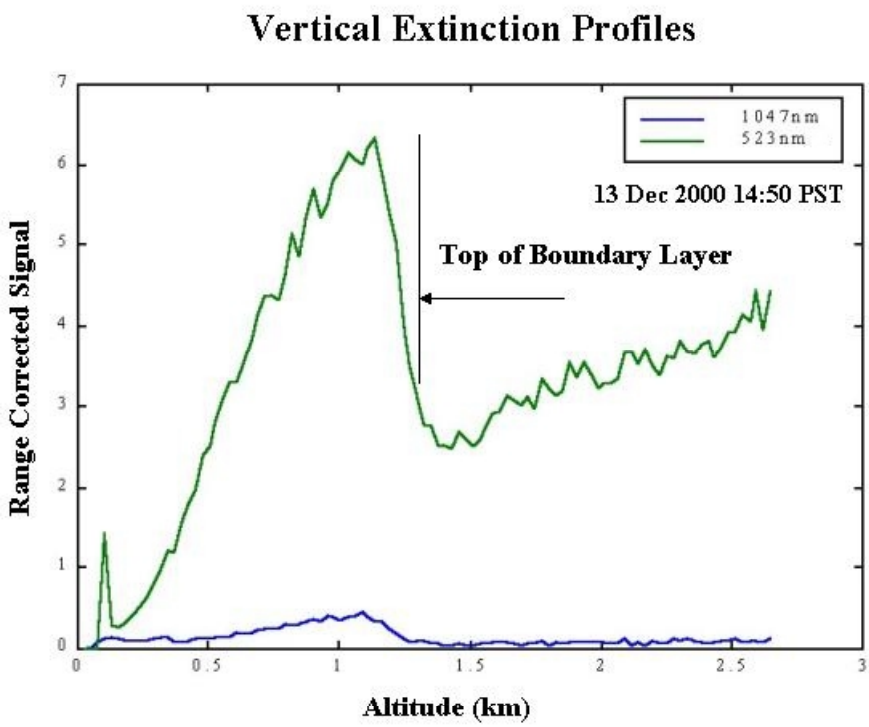

Figure 3-12. Vertical profile (elevation angle 70°) during period of afternoon convection shows the top of the boundary layer near 1300 m.

Figures 3-13 and 3-14 show examples of sequential lidar measurements at the two wavelengths as a function of time. In Figure 3-13, the signals measured are shown at intervals of one minute. In Figure 3-14 the measured profile before plume release is used to normalize the other times and so that the plot shows the backscatter and extinction due to the plume presence. This type of display is the one that was used to prepare the analysis and interpretation from the measurements. The results shown in Figure 3-13 display a time sequence of the backscatter and the extinction measured during Test #4 when 5 kilograms of local soil was used to generate a dust plume. The backscatter is larger for the red channel and the extinction is larger for the green channel. The fact that such striking differences exist provides a foundation for using the lidar data to describe and characterize the changes in the distribution of airborne particulate matter.

Figure 3-14 show the large range of changes in backscatter and extinction as the concentration of particles changes following the generation of a very dense cloud from a spinning tire of a vehicle moving along a 50 m long North-South line. The results are plotted relative to the profile immediately before the test to show the dust characteristics more clearly. During the 45-second generation period, the extinction increased and then rapidly decreased again as the larger particles settled quickly; the fine particle component is observed for a longer period of time. The small particle component is observed to continue to drift to longer range, while the larger particles which are responsible for most of the extinction have settled out of the plume.

Another of the analysis tools that was developed is shown in Figure 3-15. Here are shown the results from one scan (for both wavelengths) of the plume over a range out to one kilometer and from an azimuth of -5° to $+5^{o}$, relative to a centerline positioned on the meteorological tower, are shown for the two wavelengths. The left hand panel shows the map of the relative log-intensity and the right panel shows intensity contours from above the scene of the plume.

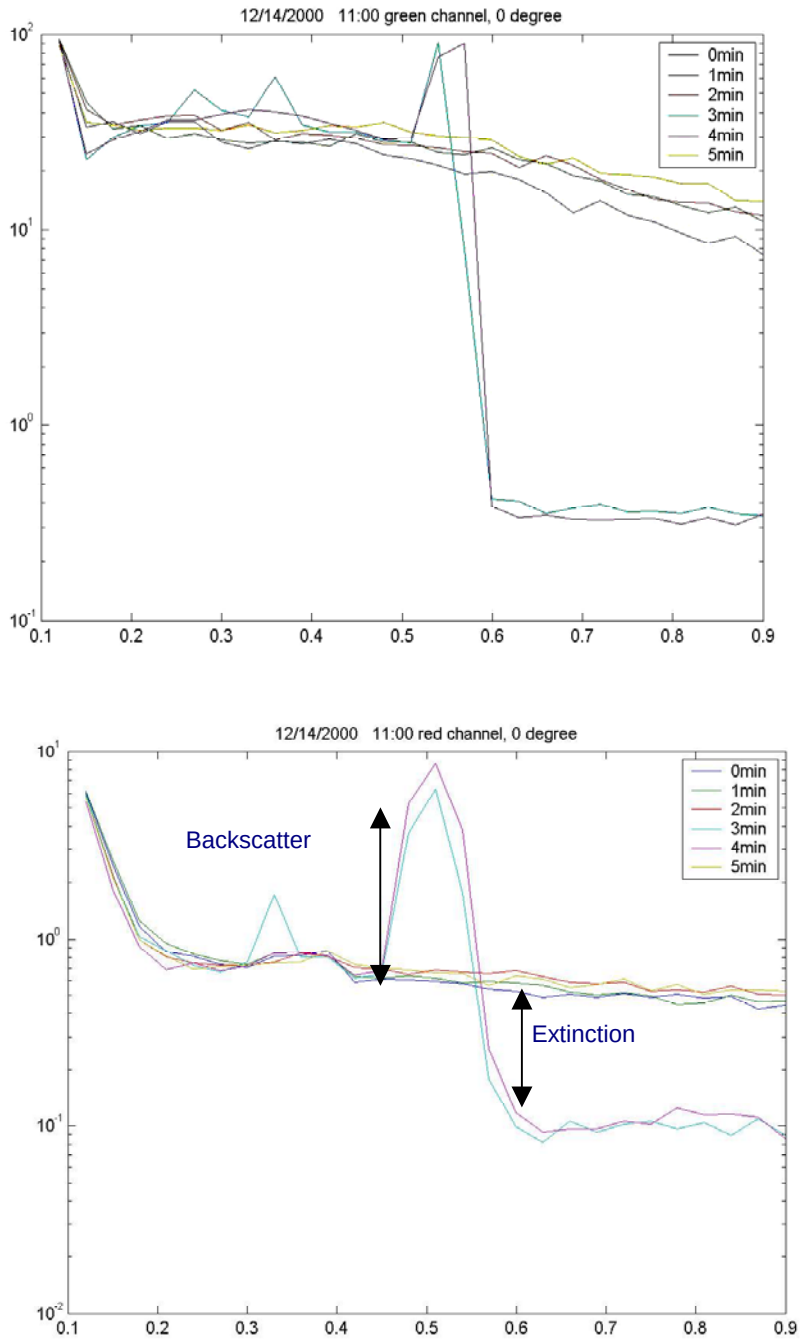

Figure 3-13. Examples of the raw data profiles from the lidar at the VIS and NIR wavelengths during Test #4 on 14 December 2000 show the variation in backscatter and extinction associated with a dust plume at a range of about 500 meters.

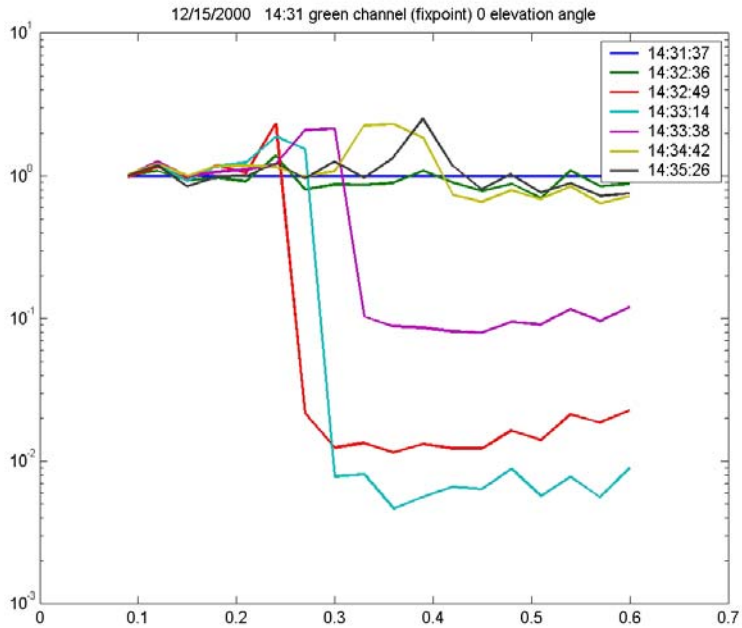

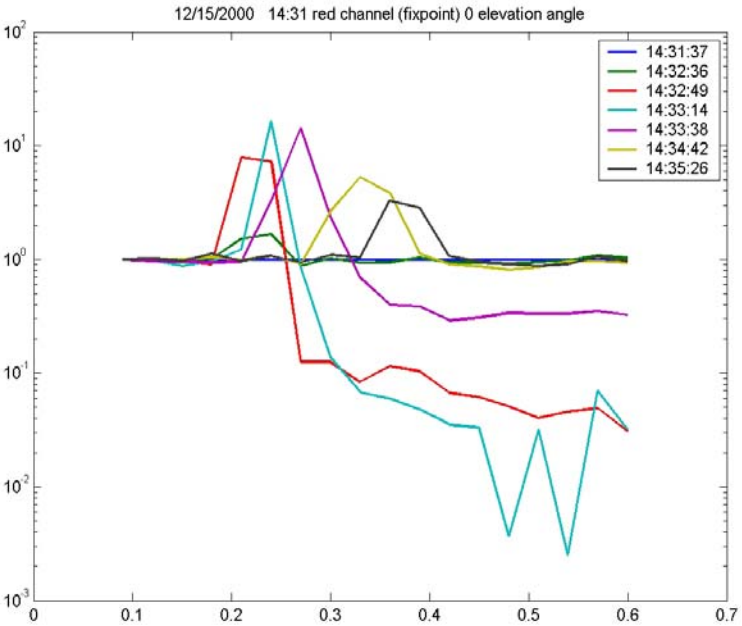

Figure 3-14. The backscatter and extinction for both visible and NIR wavelengths resulting from vehicle generated dust between 14:32:00 and 14:32:45 during Test #18 on 15 December 2000.

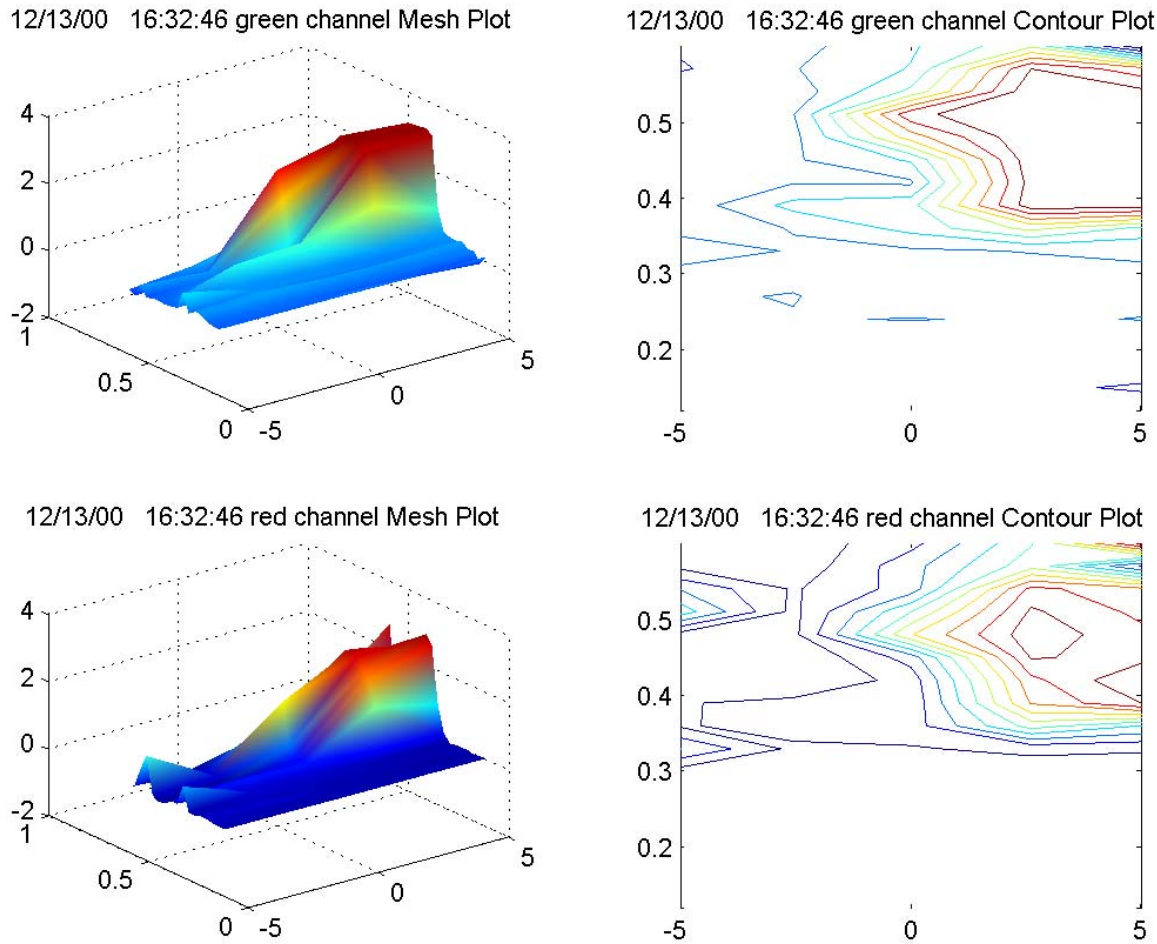

Figure 3-15. An example shows the mesh plot approach for display of the distribution of plume materials. Left frames show the log of the relative scatter intensity on the vertical axis for signal ranges to 1 km and angle scans of $\pm 5^{o}$. The right hand frames show the look down at contours of plume scattering intensity.

During the last two days of the testing period of Pilot Study, a Santa Ana windstorm developed. Figures 3-16 and 3-17 show the results from horizontal and vertical lidar profiles, respectively, obtained during the windstorm on December 18, 2000. Each sequential profile represents 2 seconds of averaged return signals. Both data sets show the NIR channel instrument problem with the data between 300 and 400 meters range. A decreasing signal intensity for ranges less than 800 meters is due to the telescope form factor is observed in Figure 3-17.

Figure 3.16 shows the effectiveness with which dust is being picked up by the wind shear near the surface and then distributed up to about 700 m altitude during this 7-minute time sequence. The NIR scattering from the region above 700 meters is negligible. Both the NIR and VIS data show that the plumes that carry most of the dust aloft occur when small vortices are formed and vertically transport the higher concentrations, and probably larger particles, upward to about 700 meters. The fact that the visible scattering signal is so much larger than the red signal indicates that much of the scattering is associated with particles smaller than 1 μm.

Figure 3-17 shows a 2 km horizontal path measurement of the ranged corrected lidar return signals at VIS (523 nm) and NIR (1047 nm) wavelengths. The data in Figure 3-17 were taken during a period of about 3 minutes when the instrument was staring horizontally. The effective motion and the location of the higher concentration plumes in the wind driven dust is easily observed.

The data from the dust storm serves to describe the effectiveness of wind shear for entrainment of dust particles. We found that digital imaging techniques currently available can be quite useful in describing the location distribution and evolution of plumes. However it is difficult to extract any quantitative information for describing the scattering particles, other than general information on the distribution of particles during the period while it could be observed visually (or photographically imaged). The lidar returns proved to be much more sensitive and the characteristics of the plume could be observed much longer than the plume was visible, probably due to the difference in contrast of the scene compared with the signal 'contrast' or signal-to-noise ratio within the measuring range bin. Examples are shown which demonstrate the way that backscatter and extinction can be obtained from the data. The obvious effects of the settling out of large particle components from the plume can be observed as time sequences are studied.

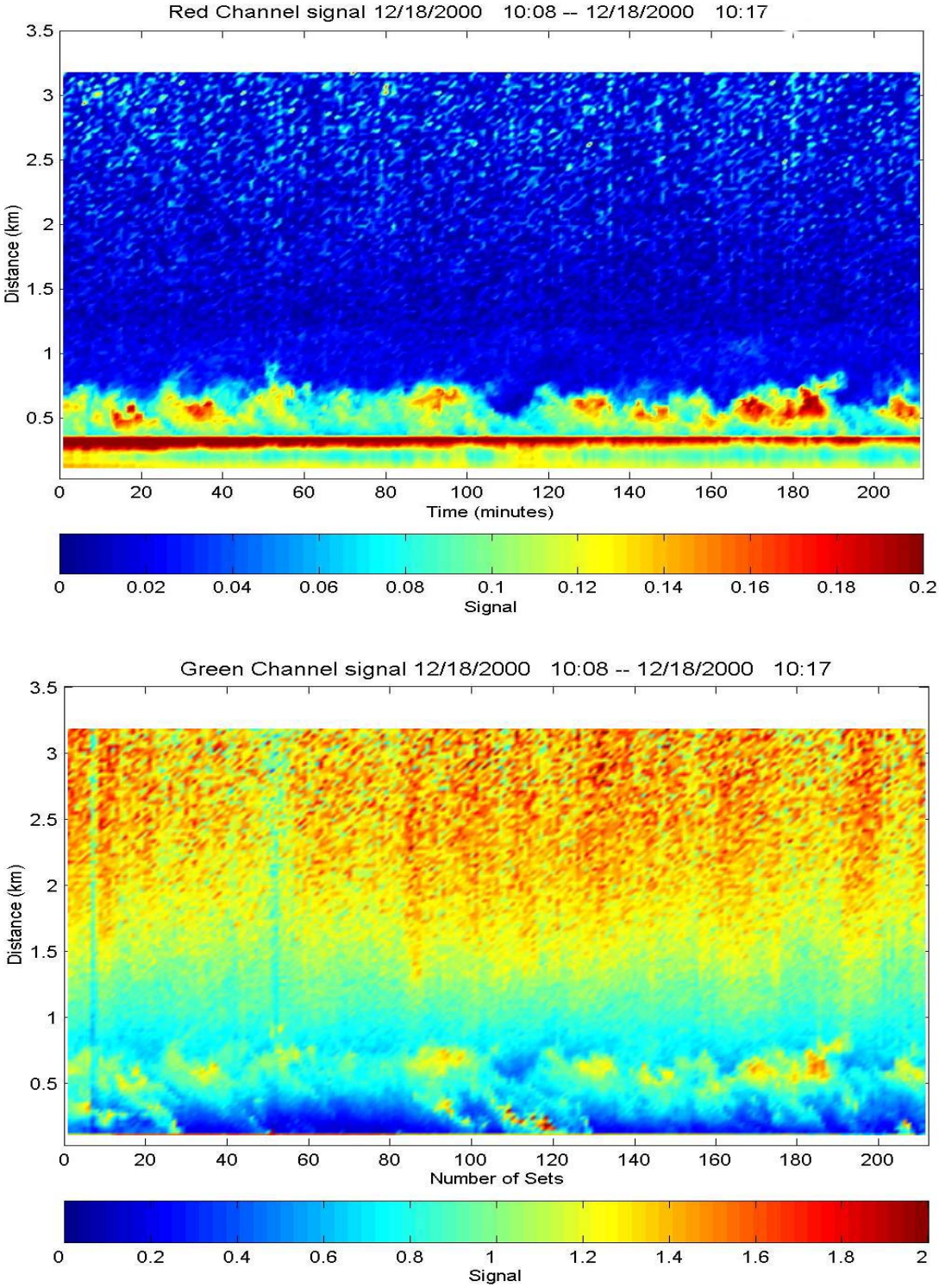

Figure 3-16 Vertical profiles show that most of the material in the dust plumes is distributed between surface and 700 m. The raw signals have only been range corrected (the red channel shows an instrument artifact near 300 m).

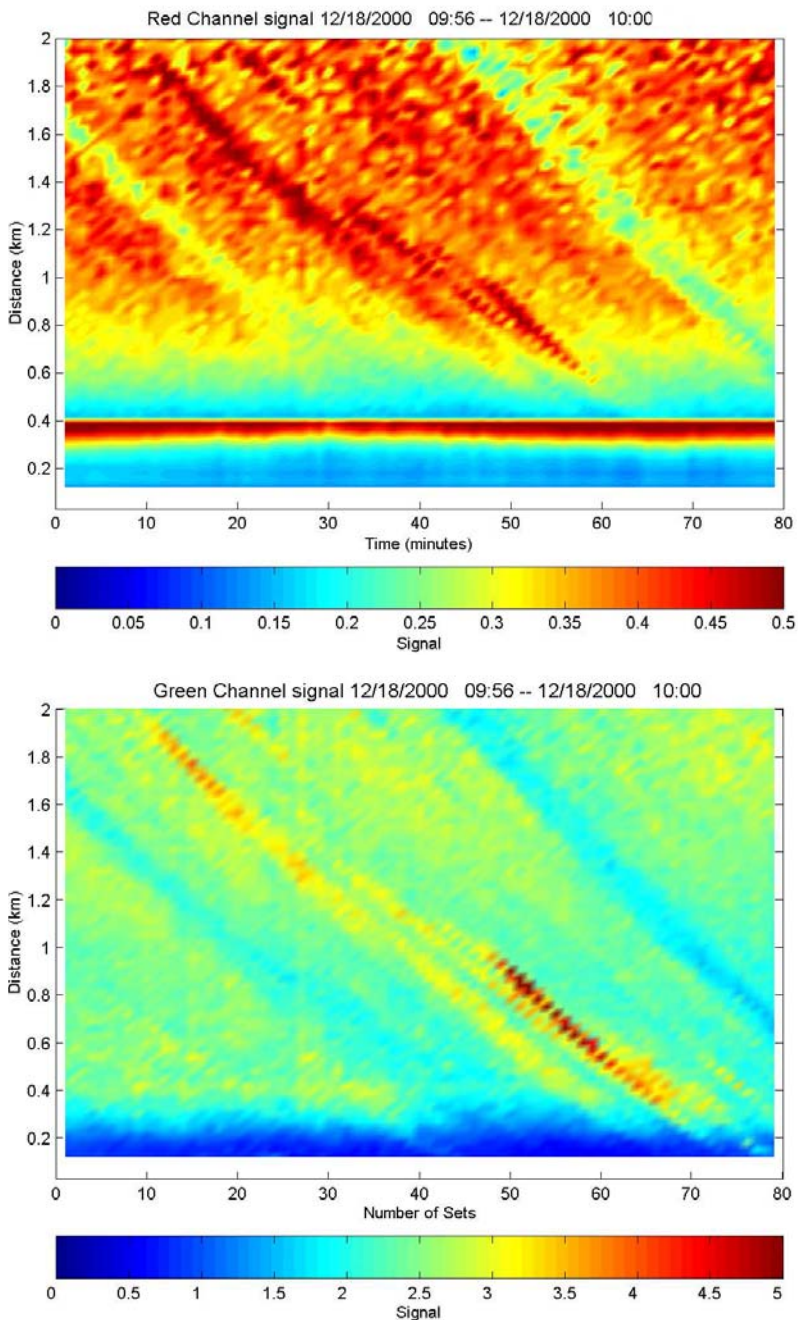

Figure 3-17 Horizontal scan profiles of raw data plots showing dust plumes were generated by the large wind shear at the surface during the Santa Ana on 18 Dec 2000.

3.2.7.3 *Lidar Model Simulations*

A simple model calculation based upon the scattering theory for spherical particles by Gustov Mie has been used to simulate first order effects observed. Mie theory calculations provide the scattering angle dependence for spherical particles with various indices of refraction. While the dust scattering studied in these experiments cannot be described as associated with spherical particles, it still provides a useful comparison of the scattering properties. In particular, the Mie theory results should provide accurate results for the smaller particles, where shape is less important, and the relationship between the forward and backward scatter intensities (extinction and backscatter) should make useful comparisons. The theory also provides insight to the variations in the absorption of the particles due to their complex index of refraction. The Mie scattering theory used for this investigation is a straightforward application of the scattering intensity in the two polarization planes that comes from electromagnetic theory, and all of the applications here use only the 0° and 180° scattering intensity.

Figures 3-18 and 3-19 show examples from the model calculations of visible and NIR backscatter and extinction for several particle concentrations and for a range of sizes of mono-disbursed particle diameters. These calculations for the two wavelengths correspond to particles for which the complex index of refraction is negligible. In general, the absorption associated with the complex index of refraction for crustal earth samples cannot be ignored and the calculations, which show that dependence, are included in the Appendices. The calculations in Figure 3-18 show the variations expected in backscatter and extinction signals as the number density of 10 μm particles changes while Figure 3-19 shows the variation as a function of particle size. These calculations simulate a 200-meter-thick uniform dust cloud and calculate values at 30-meter intervals (same as the bin size of the lidar result). The wider range of simulation results are presented in Appendix D.

It is important to notice that the extinction only depends on the concentration and size of particles and not on the wavelength, and the backscatter does depend strongly on the wavelength. The simulations demonstrate that the backscatter intensity and the extinction depend on the particle size. The relatively larger backscatter for the NIR wavelength is expected based upon the fact that the longer wavelength allows the particles to remain longer in the Rayleigh scattering range, where the cross-section dependence results in increased scattering. Increasing the particle size increases the backscatter up to the point where the scattering loss results in an optical thickness that reduces the backscatter signal. The value of using the results from the mono-disbursed distribution of particles depicted in Figures 3-18 and 3-19 is somewhat limited because real particle distributions always contain a significant range of particle sizes.

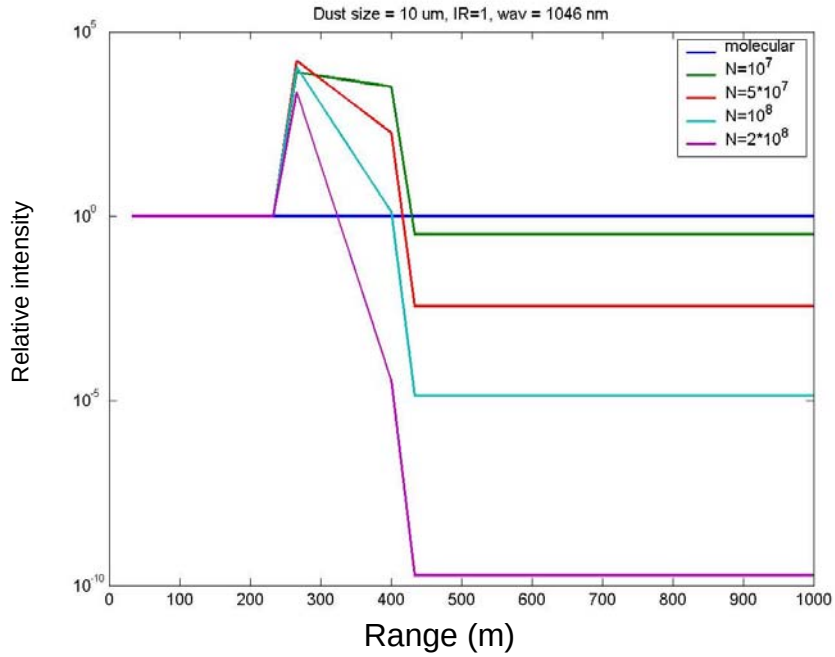

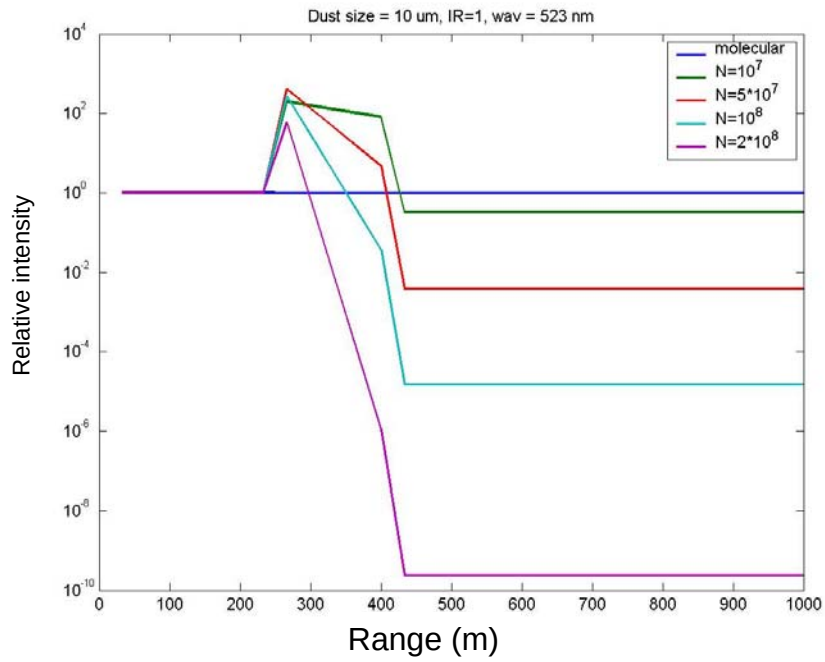

Figure 3-18 Simulation model of scattering intensity shows the difference between the two laser wavelengths and the scattering dependence on number density.

When examining the model simulations, we notice that the extinction only depends on the concentration of particles and not on the wavelength or absorption when the particles are large compared with the scattering wavelength. However, the backscatter does depend strongly on the wavelength and on the complex index of refraction, but it does not depend on the particle density except for the amount of extinction that occurs when the beam passes through the dust plumes.

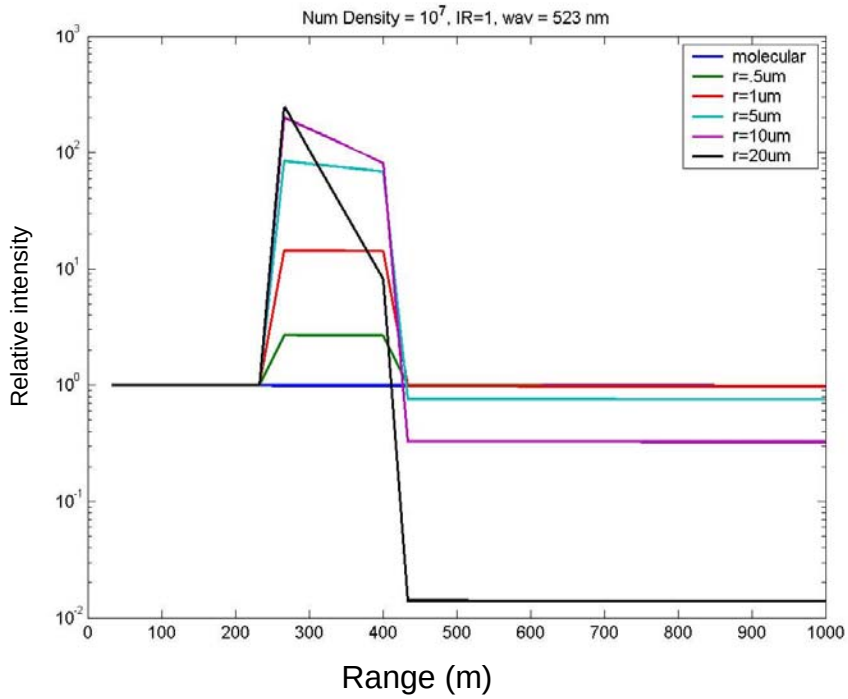

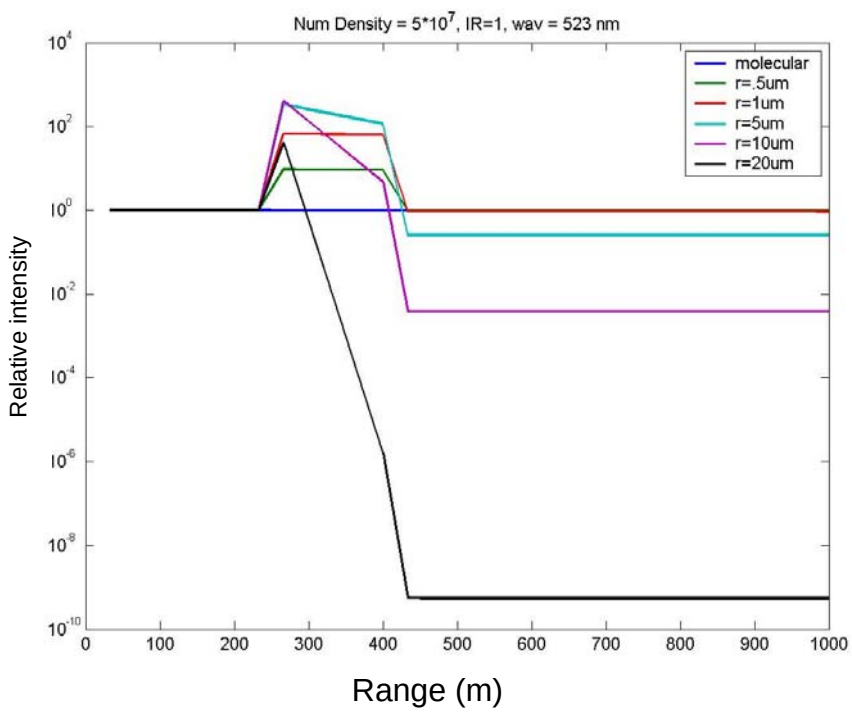

Figure 3-19. Model simulation of scattering intensity shows the difference between changing the particle density and scattering dependence on particle size.

By measuring the plumes as during these tests, it is possible to separate the changes that occur due to the changes in particle size and those due to changes in the number density of particles. The variation in the relationship between the backscatter and extinction signals for the two wavelengths provides a tool for analyzing the changes in the particle characteristics.

3.2.8 Conclusions and Recommendations from the Pilot Study

The measurements from lidar have been examined for each of the several tests, and some examples of the results have been presented here. The problems found in the data set included several features associated with the instrument, the experiment arrangement, and the operating approach. The major purpose in conducting the pilot study was to be able to identify these problems so that they can be avoided during the primary test period. The particular items that have been identified are:

1. The close proximity of the lidar to the dust generator (about 180 m) meant that the measurements were distorted by the telescope form factor. The overlap function extends to about 1 km, but the measurements can be made beyond 500 m during the primary test, then there will be a minimum error from that effect.
2. The lidar experienced a thermal drift in the background signal of the NIR channel. This drift causes significant variations in the profiles for ranges up to 500 m (particularly pronounced between 350 and 400 m). This effect was minimized by forming a ratio to describe the dust cloud observed relative to a background profile near the time of the test, but it still makes the analysis more difficult.
3. Attempts were made to reset the lidar to different elevation angles during several of the tests, and this leads to complications in analyzing the data. During subsequent tests, the elevation angles will be changed less frequently.
4. The scanning of the digital camera image makes it difficult to perform image background removal and to characterize the spatial evolution of a dust cloud. Since it is very useful to have a CCD mounted on the lidar to observe where it is pointing, a second camera should be obtained for future testing.
5. It is very important that the size distribution and refractive index of the dust used for several of the tests is determined by a measurement method independent of the lidar.
6. The spatial distributions for the dust clouds generated during these tests were very complicated. In particular, the dust generated by the vehicle driving through the soil to produce a dust cloud was complicated to analyze because the plume frequently folded over and produced several scattering regions. Those cases that will be most useful for understanding the evolution of the generated cloud appear to be smaller and short duration puffs.
7. The white paint pigment powder, although it appeared “finer” than the indigenous soil, did not have as much or any of the fine (~$PM_{2.5}$ and smaller) particle size fraction as the sieved indigenous soil. This was evident from the laboratory analysis of these samples and from the lidar field data.
8. In addition to using indigenous soil, some of the testing in the primary study should be performed with several different (approximately) monodisperse size particles covering a range of diameters.
9. Point source monitoring, such as the measurements that are performed at all ambient air quality sites, are a viable method for determining area-wide or regional sources. They are of limited or no value for determining emissions, or average levels from a point source at close range. This method of trying to “hit a bullet with a bullet” is not a viable approach. The pilot study had very little success when point emissions (fixed location dust generator and tracer gas release) were combined with point source monitors (filter samplers, DustTraks™ and

tracer gas analyzers). However, the lidar (a line source monitor) was able to track and obtain viable data from the point source releases.

10. Point source monitoring (integrated filter sampling, DustTraks™ and single point SF_6 monitoring) should not be included in the primary study (except possibly for use to calibrate the lidar) as they do not provide useful data for this type of field study.
11. When line source releases were used (vehicle driving a route to generate dust), the point source monitors were more successful at obtaining usable data.
12. All three dust generation methods (blower, driven vehicle and fog generator) provided valuable and complimentary data. The further work on the primary study should include all three dust-generation methods.
13. Performing calibrations and dust generation test with different size ranges of synthetic particles will provide useful data for correlating the soil test data to these monodisperse references and for developing models to predict dust fate based on the particle size composition of soils.
14. A controlled experimental volume is needed for evaluating the optical scattering from different sized particles.
15. A particle sizing instrument is needed to measure full size distributions of test aerosol in the controlled volume.

3.3 Main Study Results

The Main Study was planned to include several of the types of measurements carried out during the Pilot Study and combine them with additional measurements to help interpret the results. By having one year between the two field campaigns, it was possible to analyze the initial results and seek answers to the questions raised from those results. This gave time to evaluation of the Pilot Study results, develop the test plan, and obtain additional instruments for measurements in the Main Study.

3.3.1 Study Period

The detail list of the experiments conducted during the Main Study is contained in Appendix E. The field measurements included the following items:

- Pre-study Background Meteorological Data
  The meteorological monitoring system was set up on October 10, 2001,
  to collect hourly data. On December 8, 2001 the data logger program was changed to collect one-minute data until January 11, 2002.

- Lidar Set up
  The lidar was set up on December 8, 2001, and a number of preliminary scans were conducted to optimize the performance.

- Lidar Calibration
  The lidar was calibrated using the resuspension chamber starting December 16 and concluding on December 19, 2001. Most tests were conducted in the pre-dawn hours when the air was most stable.

- DustTrak Calibration
  The DustTraks were calibrated against PM_{10} filter samples on January 12, 2002.

- Dust Generation and Measurements
  The dust measurements using the chamber and open field were conducted beginning on December 11, and concluded on December 19, 2001.

3.3.2 Meteorological Data

Data validation showed only one problem, the solar radiometer showing sporadic negative values on December 14th and 21st. Values less than 6.5 watt/m^2 were removed from the data set. The total number of one-minute data removed was 1342. A description of these data is presented in Appendix B. Table 3-1 is a summary of the data during the field testing period, from December 8th to December 19th.

Table 3-8. Summary of meteorological conditions during the testing period.

Date	AVE WS m/s	MAX WS m/sec	AVE WD Deg	Min T Deg C	MAX T Deg C	AVE T Deg C	AVE SR watt/cm^2
8-Dec	6.7	10.3	53.0	12.3	21.9	16.5	137.1
9-Dec	3.6	7.3	148.6	4.9	18.3	11.5	136.7
10-Dec	1.9	5.7	111.6	0.6	11.6	6.2	97.3
11-Dec	2.8	9.9	176.9	-0.2	13.2	5.8	129.8
12-Dec	2.2	6.3	166.2	0.9	15.4	7.8	133.3
13-Dec	1.6	3.5	152.9	-2.3	15.2	6.0	132.0
14-Dec	1.9	4.5	136.9	1.4	8.8	5.2	ISD
15-Dec	2.5	6.8	118.2	0.1	12.5	5.3	140.5
17-Dec	1.6	5.0	176.0	-1.4	17.6	7.4	133.6
18-Dec	2.8	6.5	89.7	-2.0	20.6	9.5	139.1
19-Dec	1.6	2.7	119.1	0.1	22.2	9.5	137.5

ISD= Insufficient data to calculate an average

3.3.3 Resuspension Chamber Calibrations

The objective of the resuspension chamber was to measure PM_{10} concentrations with DustTraks and particle size distributions with an optical particle counter at the same time the lidar was used to characterize the PM in the chamber. To do this required calm and clean ambient air so that the generated dust would remain in the chamber for several minutes after the ends were removed so that lidar measurements could be made and that ambient PM did not interfere with the measurements. It was also necessary to do the experiments in the dark so that the lidar beam could be aimed through the chamber. For these reasons test were conducted a few hours before dawn. Since DustTraks are optical sensors whose output is dependent on particle size and composition it was also necessary to calibrate their response to the test soils while collecting PM_{10} on filters. In this two-step process, the lidar response can therefore be related to PM_{10} based on mass measurements.

All test soils were sieved with a 75um mesh screen and aliquots were weighed out prior to resuspension. The first day of testing was used to determine the optimum testing protocol. Tables E-3 and E-4 in Appendix E show the list of tests that were conducted on the next two days of testing, December 17th and 19th, respectively. The rightmost column of each table shows the average (of four instruments) DustTrak concentration for the full second minute of measurement; which is the first minute in which the chamber ends were opened to allow the lidar to make measurements.

3.3.3.1 DustTrak Calibration

On December 19th, the DustTraks were allowed to sample artificially generated aerosol in the chamber while all inlets were located at the same location; port B, of the resuspension chamber. One DustTrak failed to record data and was not included in the comparison. Two of the DustTrak responses (UCR #2 and UCR #3) were plotted against the third (UCR #1). The results are shown in Figure 3-20. The plot shows a bias between the responses of the analyzers. The least squares regressions of the scatter plots are also shown in Figure 3-20. There is nearly a 50% bias between UCR #2 and UCR #3 with the response of UCR #1 between these two.

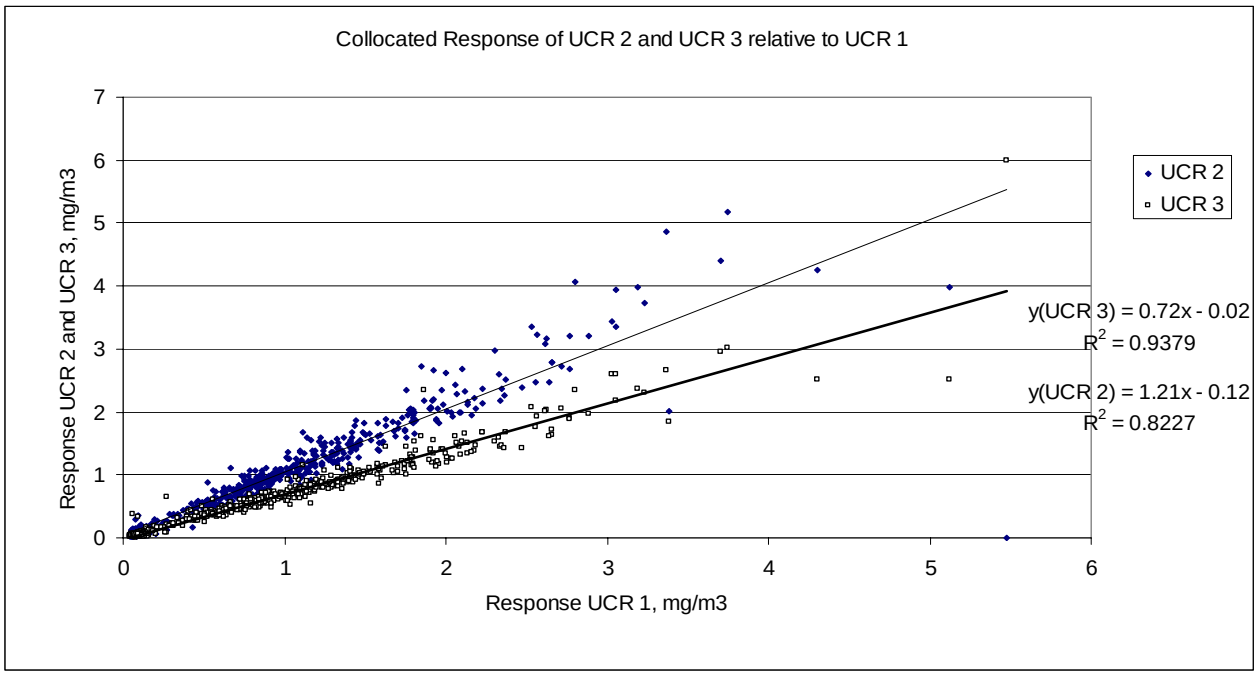

Figure 3-20. Scatter plots of the response of DustTraks UCR #2 and UCR #3 relative to UCR #1 during collocated sampling.

Table 3-9 summarizes the comparison of measurements obtained when filter samples were collected PM_{10}, while monitoring the concentration with the DustTrak analyzers. Consistent with the collocated sampling, the response of DustTrak #2 is higher than #1 or #3 and DustTrak #1 was generally higher than #3. Figure 3-21 shows a plot of the mean DustTrak response compared to the filter measured PM_{10}. The filter sample was nearly a factor of two higher than the DustTrak response, with a correlation coefficient of 0.93. The responses from all of the dust types tested fell along a straight line as shown in Figure 3-21, indicating that the type of soil had little effect on the comparison.

Table 3-9. Comparison of filter sampling with the DustTrak response

Dust Type	**Filter Conc**	**DT #1**	**DT#2**	**DT#3**	**DT#4**	**AV DT**
	µg/m3	**µg/m3**	**µg/m3**	**µg/m^3**	**µg/m3**	**µg/m3**
UCR< 75um	1421	411	770	460	331	493
Shafter < 75 um	2559/2218*	1431	1557	1051	714	1188
Kearney <75 um	2663	1630	1553	1262	928	1343
Westside <75 um	1775	1012	1183	760	551	877
AZ Road	5225	2839	3179	2274	2162	2614
UF CO3	1513	1151	1036	1431	814	1108

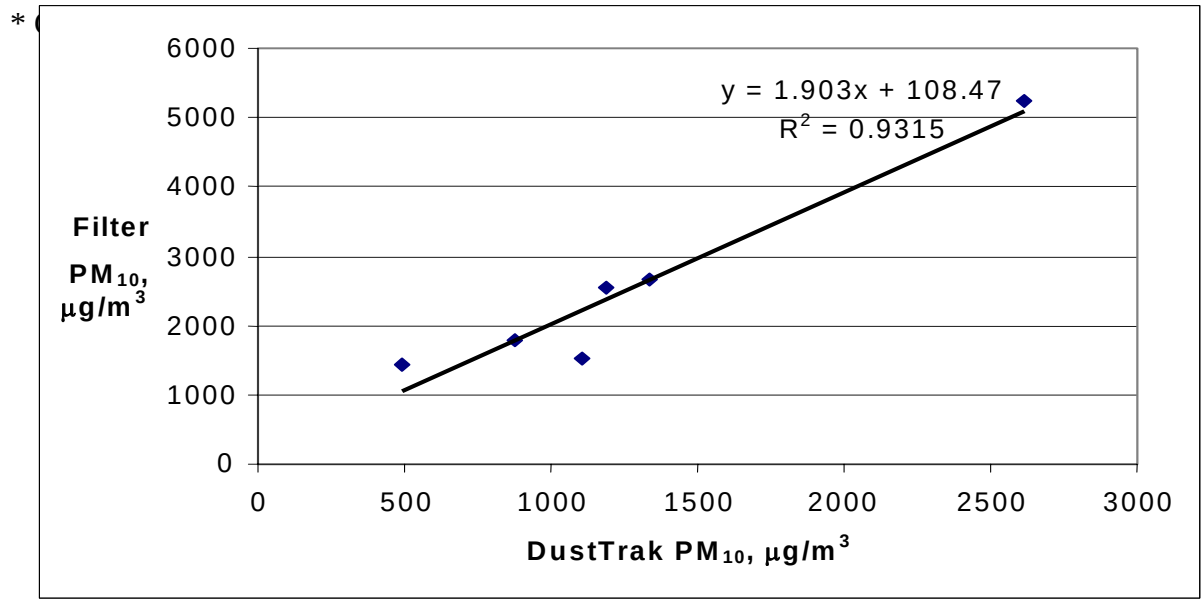

Figure 3-21. Plot of the filter mass concentration measurements compared to the mean DustTrak response (four-analyzer mean).

3.3.3.2 Lidar Calibration

The procedure for measurements in the chamber was to close the ends of the chamber, turn on the four fans located inside, and then inject the dust. After one minute, the ends of the chamber were opened, fans turned off, and the laser beam measurements commenced. Figure 3-22 shows the raw lidar returns from the chamber and the target board and the signals from the DustTrak for the 10µm $CaCO_3$ tests #10 (50 mg), #11 (200 mg) and #12 (800 mg) on 19 December 2001. The measurements in Figure 3-22 from the Lidar and DustTrak show the relationship between the change in signal level and the amount of material, 50, 200 and 800 mg.

The upper panel of Figure 3-22 shows the lidar signal return from the closed end on the chamber near 05:44, 05:50 and 05:55. When the chamber is opened, the lidar return from the dust in the chamber and the target board are observed. Since the chamber is only 10 meters in length (corresponding to only 1/3 of one range bin), the extinction signal is relatively weak and the hard target return is the only practical way to observe any extinction signal. Examination of the signals of the target board return shows that the extinction corresponding to the dust path can sometimes be detected, however the extinction signal from the target is not sufficient for a useful analysis.

The lower panel of Figure 3-22 shows the three DustTrak measurements (front, middle and back of chamber) together with the normalized lidar signal. The lidar signal has been normalized to "1" by forming a ratio to the signal measured on the clear atmospheric path before the test. The lidar signal in the chamber is high before opening due to the backscatter from a white card placed on the front of the chamber. The backscatter from the dust is observed in the lidar return when the path is open but the concentration within the chamber volume is not sufficient to observe any path extinction on the atmospheric path.

A comparison of these three tests (#10 - #12) shows some difference in the settling rate of the dust. The increase in signals with increasing sample size is easily observed. During a measurement period when the Climet particle size spectrum was obtained (1 minute scan), the DustTrak data (two second step) was averaged and compared with the integrated value of particles less than 10 µm reported by the Climet instrument. These compared quite well. The size range of particle spectrometer instrument includes most of the range for particles

contributing to the optical properties, since heavier particles settle quickly and the scattering cross-section for particles less than 0.1 µm is quite small. The instruments are capable of measuring particles less than 20 µm (Climet) and 10 µm (DustTrak) respectively, and therefore the concentrations of particles larger than that were not characterized.

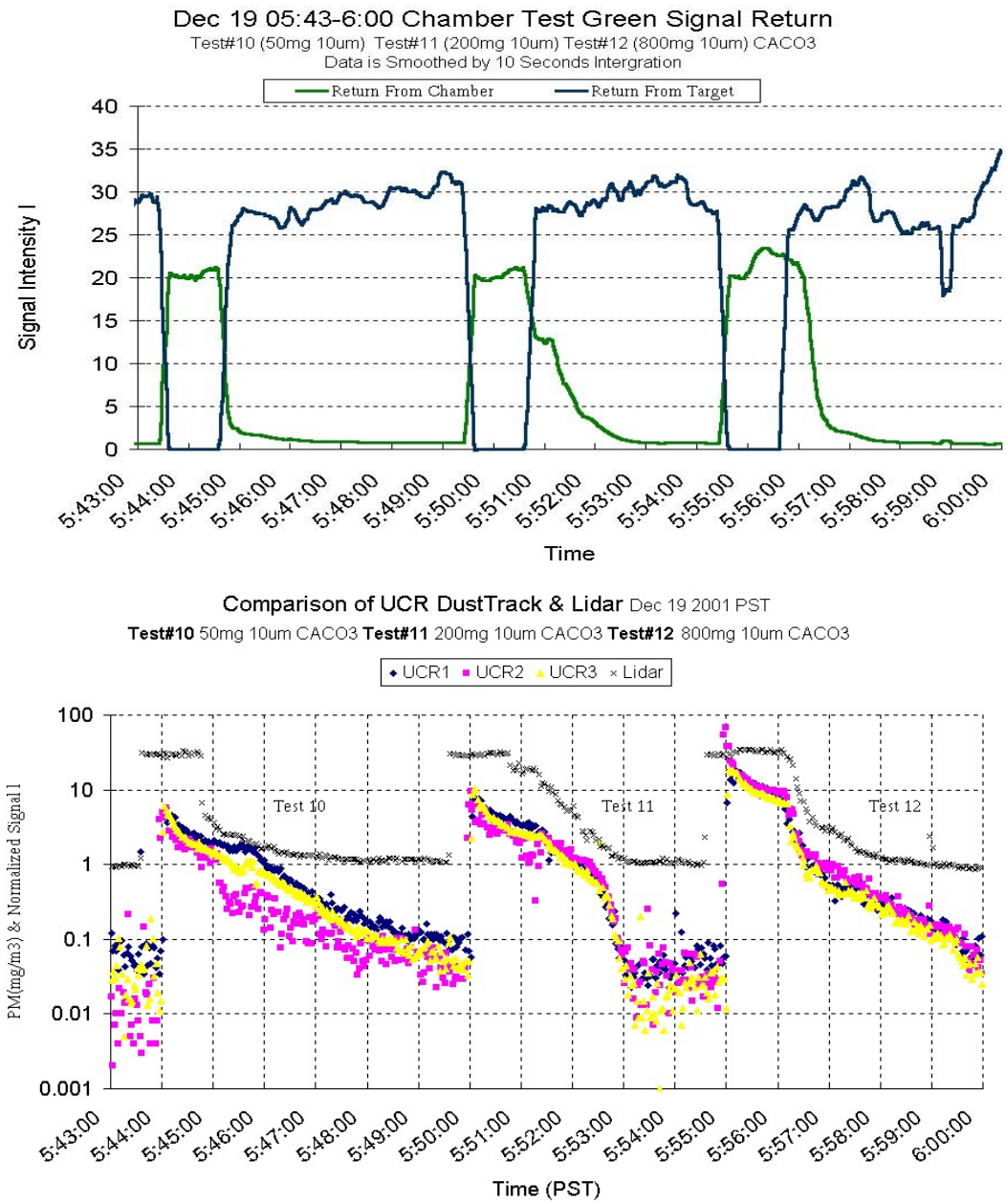

Figure 3-22. The chamber test measurements from Tests #10, #11 and #12 on 19 December 2001 are shown. The upper panel shows the raw signal returns from the lidar at the range intervals corresponding to the chamber and the target board. The lower panel shows the signal from the DustTrak instruments and the normalized lidar return on a logarithmic scale.

Figure 3-23 shows the particle size spectrum from the Climet instrument of the 0.7 µm $CaCO_3$ sample. In the figure a two component log-normal distribution has been fit to the measured

spectrum. Figure 3-24 shows the particle size spectra of the various $CaCO_3$ samples measured on 19 December 2001 from the tests using the 200 mg samples. The variations between these curves are small on a log scale, however, the observed variation agrees with expected changes. It is apparent that the 0.7 µm sample is anonymously low compared with the other samples. The lower particle concentration observed in the 0.7 µm tests may be due to poor disbursal during injection, or may be lost because of the particles adhering to the plywood sides of the chamber. Examination of Figure 3-24 shows that the relative signals change as expected for the other size distributions measured.

The Climet instrument measurements of the 0.7 µm sample, that are shown in Figure 3-24, are presented as mass density and number density in Figure 3-25. We used the particle spectrum shown in Figure 3-25 to calculate the expected optical signal expected for the lidar and examine the expected variations when the larger particle sizes are removed from the distribution; this analysis is described at the end of this report.

The results shown in Figure 3-26 provide the Climet particle spectra for the several types of soils measured during the chamber tests. Soil samples included local sifted field soil and soil samples from several California sites, including Shafter, Westside and Kearney locations. In addition, the results from 2 and 10 µm samples of $CaCO_3$ and a standard of Arizona Road Dust were measured and the results are shown in Figure 3-26. It is obvious that the $CaCO_3$ samples contain a larger relative concentration of the smaller particles than do the soil samples. Also the Arizona Road Dust contains a larger fraction of small particles than any of the soil samples.

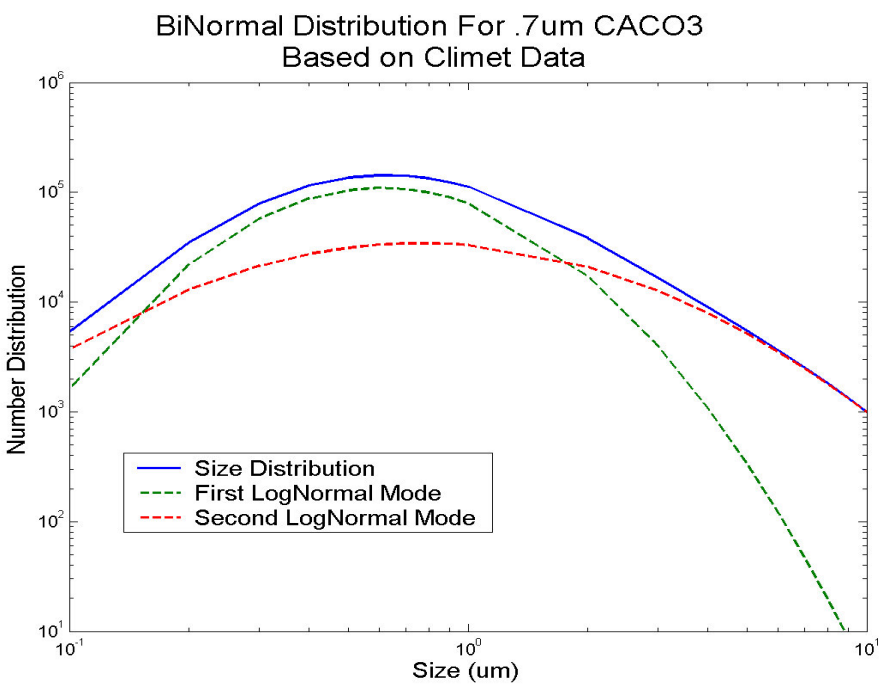

Figure 3-23. The log-normal distributions for a two components are fit to the Climet instrument measured curve for the 0.7 :m sample of $CaCO_3$.

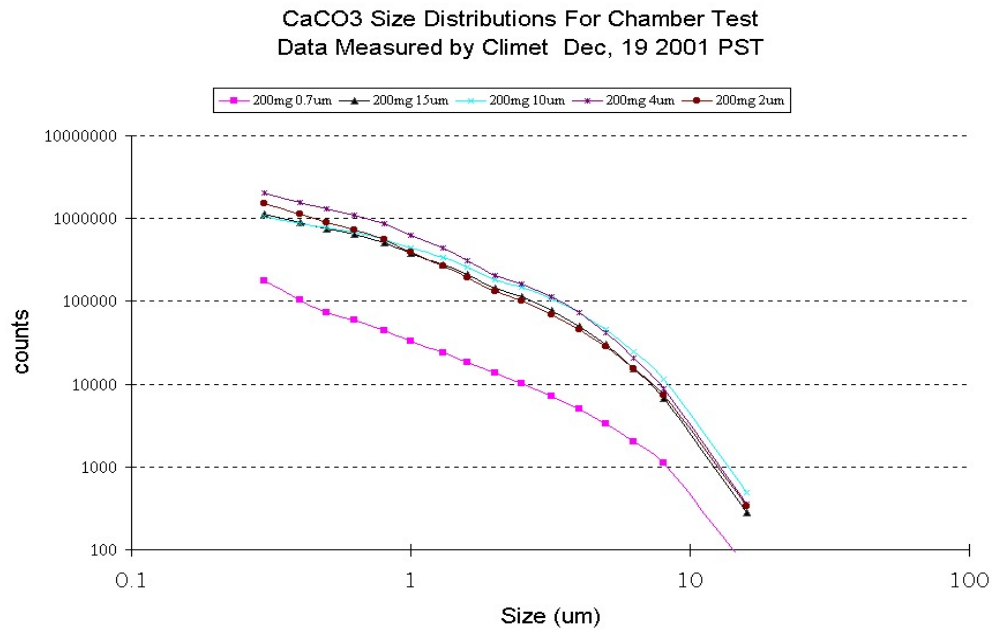

Figure 3-24. The Climet spectrum of the particle counts versus particle size for the several samples of $CaCO_3$ power that were used during the testing. Notice that the 0.7 µm case is an anomaly (see text), however the other samples do show changes that generally agree with the increasing size of the samples.

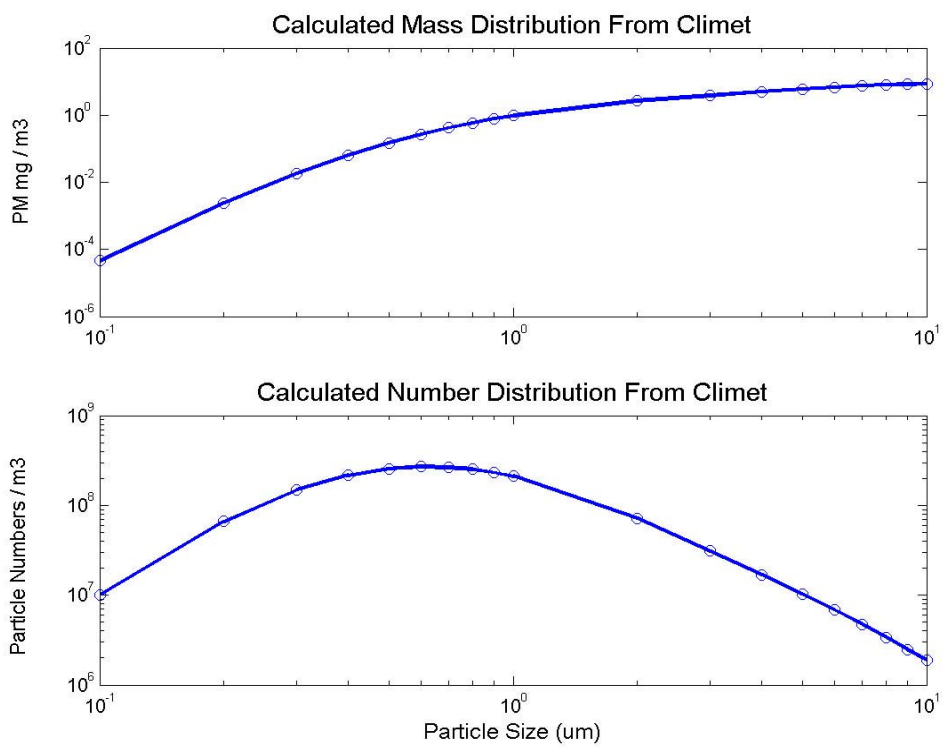

Figure 3-25. The Climet spectrum for the 0.7 µm sample of the $CaCO_3$ dust is shown for the measurements in Figure 4-9 converted to number density and to mass density

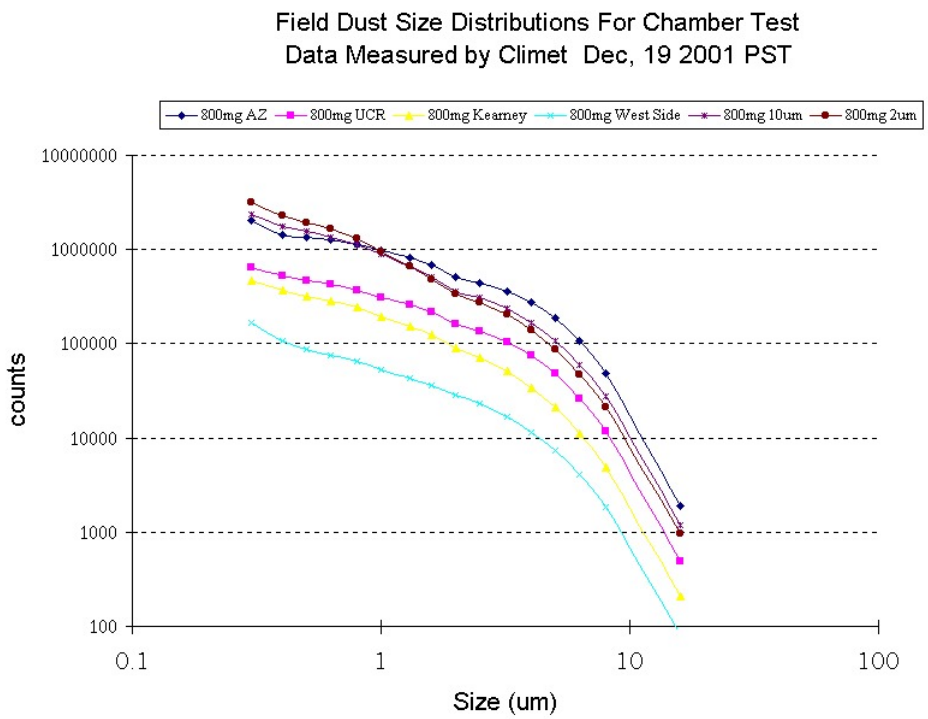

Figure 3-26. The Climet particle size spectra for the several different types of soil and powder used during the test are compared.

3.3.4 Soil Sample Analysis

Table 3-10 summarizes the sieve measurements of the dust types tested. The soil at the UCR site was the finest and moistest of the actual soils. The three San Joaquin Valley soils were collected during the early fall, prior to any rainfall, and therefore were very dry. The UCR sample was collected during the testing in December. The 2um $CaCO_3$ composition was, as expected, split between clay and silt at 2µm.

Table 3-10. Particle size analysis of various soil types used.

	Shafter	Kearney	Westside	UCR	2µm $CaCO_3$
Sieve No. 20	100	100	100	100	
Sieve No. 40	99.5	99.8	99.1	99.9	
Sieve No. 60	85.2	91	91	99.2	
Sieve No. 100	69.3	78.3	72.5	94.5	
Sieve No. 200	45.4	60.7	37.7	79.4	100
Gravel %	0	0	0	0	0
Sand %	55	39	62	21	0
Silt %	31	53	28	58	52
Clay (<0.002 mm) %	14	8	10	21	48
Moisture (%)	1.6	1.5	1.3	8.8	0.3

3.3.5 Lidar Field Measurements

Due to the vast amount of lidar data generated only a small sample of the results obtained can be included in this report. We have chosen to use one test day during the field-testing program as an example of the type on measurements obtained.

The open field tests of these samples were conducted by generating sample puffs using the blower generator. In Figure 3-27, the time sequences of the lidar measured backscatter peak values and the integrated extinction through the cloud are shown for Test #44, which is a 600 g sample of 0.7 µm $CaCO_3$. This plot shows the ratio of the signals relative to the background atmospheric path prior to the test. Note is that the backscatter signal remains high for quite a long time after the extinction signal has returned to pretest levels. That there is such a large difference in the residence time for particles in the size range between 1 and 10 µm is recognized from the expected settling velocity shown in Figure 3-28.[8]

Figure 3-29 shows a typical experiment depicting the generation of a dust cloud generated with the blower unit as observed by the digital video camera mounted on top of the lidar instrument. The dust generation equipment was located at ranges from 150 to 800 meters in various test scenarios. The lidar was used to either point at the center of the plume, as presented in Figure 3-27, or was scanned automatically to make a horizontal slice through the test volume, and the elevation angle could be adjusted manually. Using the scanning lidar, the plumes were generally tracked out to 1.5 km along the path and on radials, which were set to sweep up to ±30º horizontally. The plumes probably could have been tracked much longer, at least along some radials (up to the lidar's maximum range of 20-30 km). Because it was more desirable to obtain data over shorter ranges, plume tracking generally stopped when the plume drifted to ranges greater than about 1.5 km.

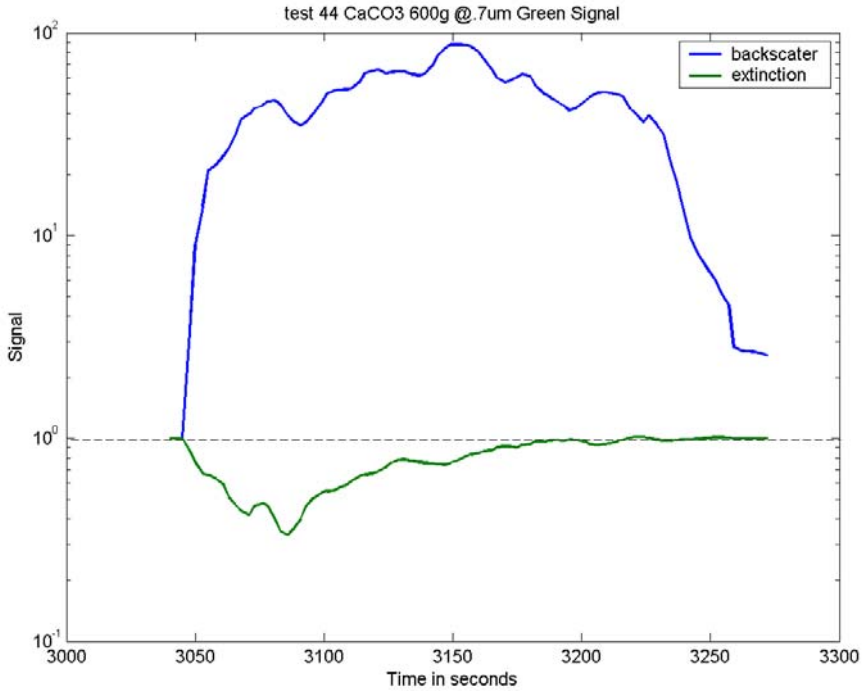

Figure 3-27. The open-air measurement sequence shows the lidar backscatter peak values and extinction values for profiles during Test #44 on 19 December 2001 that used a 0.7 µm $CaCO_3$ 600 g sample.

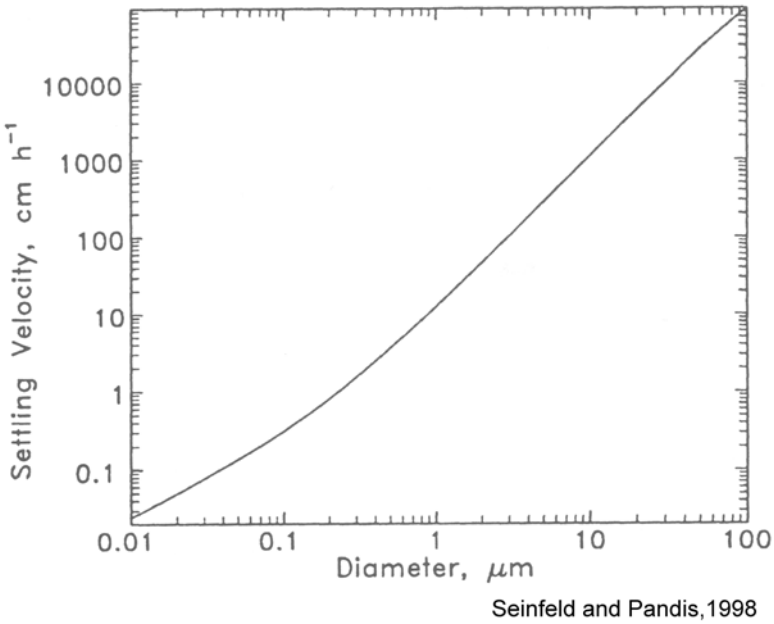

Figure 3-28. The expected settling velocity versus particle diameter from standard text (Seinfeld and Pandis[8]).

Figure 3-29. Sequence of pictures shows a puff plume of local soil that was tracked by scanning lidar.

3.3.6 Model Simulations of Plumes

Figures 3-18 and 3-19 from the Pilot Study showed examples from the model calculations of visible and NIR backscatter and extinction for several particle concentrations and for a range of sizes of mono-disbursed particle diameters. The wider range of simulation results are presented in Appendix D. These calculations simulate a 200-meter-thick uniform dust cloud and calculate values at 30-meter intervals (same as the bin size of the lidar result). The figures show the differences in backscatter and extinction signals as the density and size of particles is changed. It is important to notice that the extinction only depends on the concentration and size of particles and not on the wavelength, and the backscatter does depend strongly on the wavelength. The simulations demonstrate that the backscatter intensity and the extinction depend on the particle size.

The relatively larger backscatter for the NIR wavelength is expected based upon the fact that the longer wavelength allows the particles to remain longer in the Rayleigh scattering range, where the cross-section dependence results in increased scattering. Increasing the particle size increases the backscatter up to the point where the scattering loss results in an optical thickness that reduces the backscatter signal. The value of using the results from the mono-disbursed distribution of particles depicted in Figures 3-18 and 3-19 is somewhat limited because real particle distributions always contain a significant range of particle sizes.

When examining the model simulations, we notice that the extinction only depends on the concentration of particles and not on the wavelength or absorption when the particles are large compared with the scattering wavelength. However, the backscatter does depend strongly on the wavelength and on the complex index of refraction, but it does not depend on the particle density except for the amount of extinction that occurs when the beam passes through the dust plumes. However the same calculations can be carried out for a range of particles sizes, as shown in the following example.

The lidar backscatter signals and extinction from passing through the dust cloud that was generated by the blower unit are shown in Figure 3-30. These curves are obtained by comparing with the backscatter signal before the dust was generated; the signal strength starts increasing at the front edge of dust plume and forms a peak in the center of cloud. The backscatter coefficient can be estimated from the signal magnitude. After the laser beam passes through the cloud, there is a sudden drop of backscatter signal due to the attenuation of the laser beam. The extinction coefficient can be estimated by the attenuation amount, which is the signal drop after the laser signal passing through the dust plume. If we assume the dust particles inside the cloud are uniform and spherical, a certain relationship should exist between the values of backscatter and extinction coefficients that correspond to a dust plume with given set of particle sizes. This will allow us to simulate the laser backscatter profile passing through the cloud and specify the dust particle size and density from the analysis of the simulation.

Figure 3-30 shows one example from the 19 December 2001 test (#44) for the case of 0.7 µm calcium carbonate cloud containing 600 grams of material. Notice that the magnitude of the backscatter and extinction are similar to the values that would be expected from the simulation shown in Figure 3-30 and 3-17. Figures 3-30 and 3-17 show that after release, the backscatter signal does not change very much during the next two minutes (4 profiles in Figure 3-30) while the extinction is observed to recover. The small particles in the sample material are sufficiently small that the settling time is slow, however the rapid recovery of the extinction is observed as the larger dust particles settle out of the sample.

The model calculations, shown in Figure 3-31, depict the backscatter and extinction, which would be expected for the sample of 0.7 µm $CaCO_3$ particles represented in Figure 3-25, which shows the particle size spectrum for this material. The calculations shown in Figure 3-31 represent the changes, which are expected to occur as the particles larger than a certain size are removed. The particle distribution shown in Figure 3-25 is truncated for particles greater than selected sizes to calculate the optical properties. The calculation is intended to represent the changes that would be expected for the case of larger particles settling from the distribution. It is interesting to see that this simple calculation does have many similarities to the results shown in Figure 3-30. The magnitude of the backscatter and extinction calculated from the particle size spectrum does agree well with the measured lidar profiles. The changes in the backscatter and extinction calculated from truncating the particle spectrum agree quite well with the time sequence of measured profiles. These comparisons show that the relative changes in the backscatter and extinction profiles are representative of the settling of larger particles from the airborne sample.

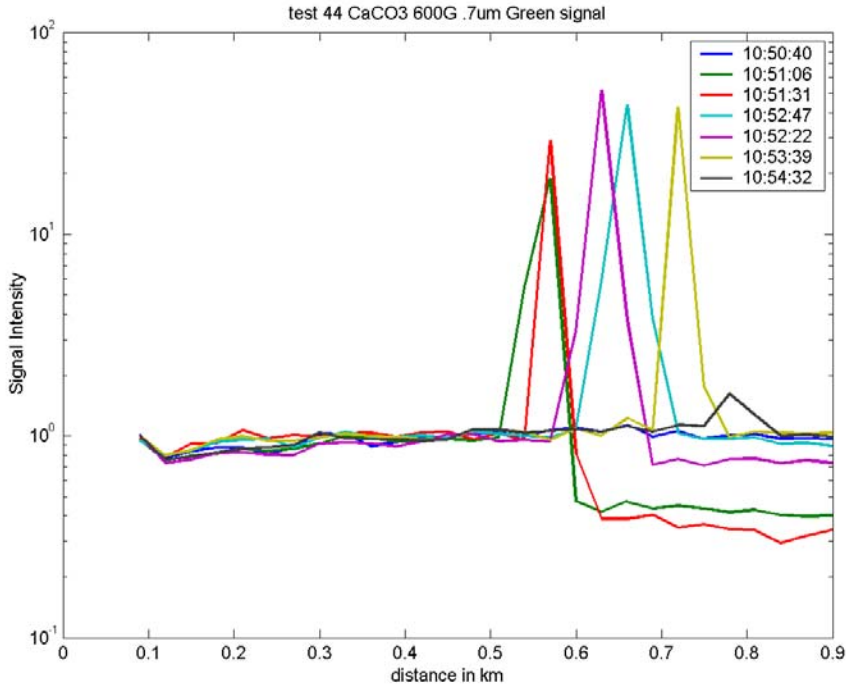

Figure 3-30. The results from Test #44 on 19 December 2001 show several of the lidar profiles that show the time variation in the backscatter and the extinction measured by the lidar. These range profiles are from the same data set that is shown in Figure 4-25.

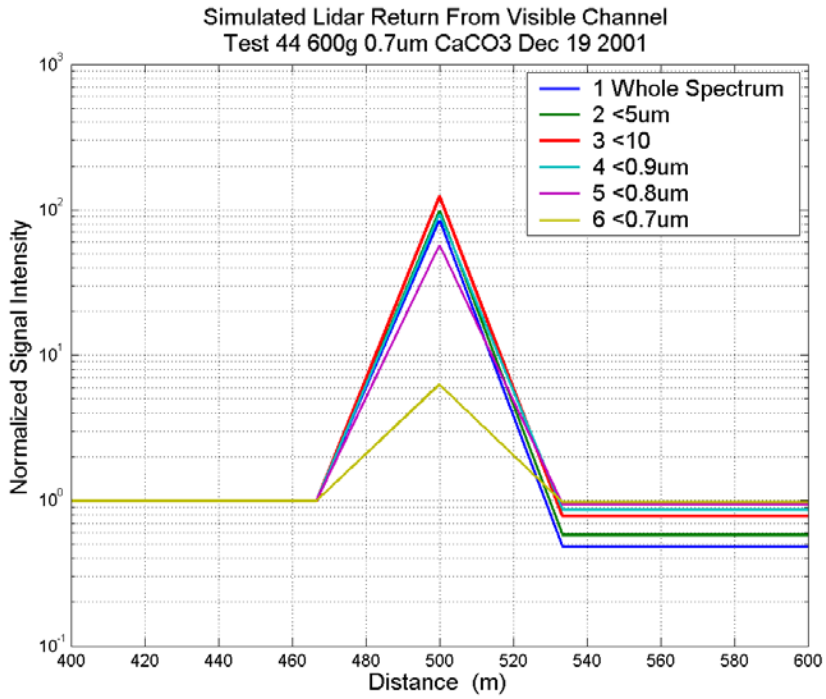

Figure 3-31. The results from a calculation of the backscatter and extinction expected when one sequentially removes the larger end of the spectrum of the scattering particles. The calculation is performed for the spectrum shown in Figure 3-26 and corresponds to the measurements shown in Figure 3-31.

4.0 Conclusions

The overall objective of this project was to characterize the fate (deposition and transport) of PM emissions originating from mechanical disturbance of the soil (see Watson and Chow[5]). The results from the measurements were to be used to estimate the validity of the algorithms used to determine emission inventories from such sources. The study focused on PM from unpaved roads and agricultural tilling. The tests also include artificially generated dust clouds of material of known size distribution to provide a validation of the analysis of the optical scattering properties and the algorithms for deposition of airborne particulate matter.

The Pilot Study was very useful in determining the effectiveness of our original approach and changes to improve our approach. It was clear that it is very difficult to obtain useful information about dust cloud characteristics from point sampling. Plumes, even from line sources, meandered about and it was not possible to keep sampling equipment positioned in a plume for a long enough period to obtain a representative sample. This made the reliance on the lidar all the more important to characterize the dust plume. While the lidar responds to changes in concentration and size distribution, it is of a relative nature. To go a step further, we developed a resuspension chamber in which we could record the optical characteristics of dust clouds while simultaneously measuring the PM concentration and size distribution.

While a considerable amount of data was collected during the Main Study, only a limited amount of data was analyzed. The reason for this was that it appeared that the two-wavelength lidar did not provide sufficient particle size resolution to characterize the size distribution by other than qualitative characteristics. The basic finding is that by combining measurements of the backscatter and extinction from the lidar with simple models demonstrated that the larger particles settled out of a dust plume rapidly indicated by a rapid decrease in optical extinction. Since these larger particles contain most of the mass, the PM_{10} concentration is therefore expected to drop rapidly also. The small particle fraction provides most of the optical backscatter and thus a plume carrying a relatively small amount of mass showed considerable backscatter for some time. Backscatter alone therefore can be misleading and can lead to an incorrect conclusion that the particle mass remains suspended for longer and is transported further than is actually the case. The simultaneous measurements of backscatter and extinction gave us information about particle size that can be modeled based on light scattering principles.

We were unable, however, to answer was how fast particles of a specific size range settled. The test aerosols were expected to be relatively monodisperse, and probably were for the liquid solutions in which they were size-segregated, but measurements of size distribution of the particles dispersed in the air showed a broad size cut. These standards were therefore not very useful in calibrating the lidar. Future studies should use a calibration chamber with monodisperse particle generators typically used to study aerosols. There will be a challenge in developing a generator with sufficient output to reach sizeable concentrations in a large, opened outdoor test chamber. A multi-wavelength lidar would also give better size resolution of the optical properties of particles

The particle settling velocities in standard texts indicate longer residence times than those found in these experiments, and the results raise questions about what factors may contribute to a faster settling rate for the larger particles. The effective Stokes velocity is changed by turbulent motions and increases the migration for particles in a range of aerodynamic sizes. Gravitational effects dominate motion of heavy particles and very light particles are controlled by diffusion. In the normal surface layer, turbulence cells are present from generation by wind shears and by turbulent convection from surface heating.

This study, although not conclusive in meeting its objective, has extended the study of lidar in measuring fugitive dust plumes. The results were presented at four conferences. Appendix F contains the text prepared for these meetings. A great deal of data was generated and more useful information could be obtained by a detailed analysis of the optical properties and comparison with particle scattering theory. Such a detailed analysis was beyond the scope of this study; the approach was far more complex than originally envisioned.

5.0 References

1. Fitz, D., D. Pankratz, R. Philbrick, and G. Li: "Evaluation of the Transport and Deposition of Fugitive Dust Using Lidar," Proc. Environmental Protection Agency's 11th Annual Emission Inventory Conference: Emission Inventories-Partnering for the Future, Atlanta GA (2002)
2. Magari, S.R., R. Hauser, J. Schwartz, P.L. Williams, T.J. Smith, and D.C. Christiani: "Association of Heart Rate Variability with Occupational and Environmental Exposure to Particulate Air Pollution," *Circulation* 104, 986-991, 2001.
3. Peters, A., D.W. Dockery, J.E. Muller, and M.A. Mittleman: "Increased Particulate Air Pollution and the Triggering of Myocardial Infarction," *Circulation* 103, 2810-2815, 2001.
4. Mauderly, J., L. Neas, and R. Schlesinger: "PM Monitoring Needs Related to Health Effects," *Proc. PM Measurements Workshop*, EPA Report No. 2, Chapel Hill, NC, pp 9-14, July 1998.
5. Watson, J.G., J.C. and Chow: "Reconciling Urban Fugitive Dust Emissions Inventory and Ambient Source Contribution Estimates: Summary of Current Knowledge and Needed Research," Document No. 61110.4D2, Desert Research Institute, Reno NV, September 3, 1999.
6. Li, G., S.N. Kizhakkemadam, and C.R. Philbrick: "Optical Scattering by Airborne Dust Particles," Proc. Air Force Optical Transmission Meeting, Hanscom AFB, MA, June 2001.
7. Li, Guangkun, Sachin J. Verghese, C. Russell Philbrick, Dennis Fitz and David Pankratz: "Airborne Dust and Aerosols Description Using Lidar Backscatter," 25th Annual Conference on Atmospheric Transmission and Radiance Models, Lexington, MA, June 2002.
8. Seinfeld, J.H and S.N, Pandis: *Atmospheric Chemistry and Physics: From Air Pollution to Climate Change*, Wiley-Interscience, 1998.